

UNIVERSITY OF SOUTHAMPTON

**SAMPLING AND STRENGTH TESTING AN
UNBONDED LOCKED SAND**

by

Andrew Cresswell

A dissertation submitted for the degree of Doctor of
Philosophy

Department of Civil and Environmental Engineering

June 1999

UNIVERSITY OF SOUTHAMPTON

ABSTRACT

FACULTY OF ENGINEERING AND APPLIED SCIENCE

DEPARTMENT OF CIVIL AND ENVIRONMENTAL ENGINEERING

Doctor of Philosophy

SAMPLING AND STRENGTH TESTING AN UNBONDED LOCKED SAND

by Andrew Cresswell

This study examines a material on the sand /sandstone borderline where the behaviour is not dominated by bonding between grains but by the shape of the grains and how they are fitted together. This has been termed fabric structure and produces a locked sand. How these sands are formed and how they are classified is explored and the relevant areas of the large body of work which investigates the mechanics of sands is reviewed.

Fabric structure poses a problem in that it cannot be created artificially and so intact material must be tested. New sampling and specimen preparation techniques are described that allow the intact testing of locked sands with negligible grain bonding

The high density of the intact material cannot be reproduced by recompacting the disaggregated grains, and any comparison has to be between the intact material and recompacted material at a lower density. This density should be as high as possible; an improved slow pouring method and an investigation into the fundamental mechanism by which the high densities are achieved are described.

As expected uniaxial testing showed that the material was stiffer and more brittle than a dense sand without fabric structure. In the direct shear apparatus the material produced stress induced structures, in the form of columns supporting the applied load, and large peak friction angles ($\phi' = 65^\circ$) and dilation. At normal loads above 100kPa these were suppressed and a bilinear failure envelope formed. Normal loads of 10MPa and above produced more rock like behaviour; peak strength was not suppressed and plumose structures were formed.

The triaxial tests did not produce a bilinear failure envelope, although changes in the failure mechanism were noted. The peak friction angles were similar to those for direct shear above normal loads of 100kPa. The differences between the observed behaviour in the two forms of test are due to the boundary interactions of the stress induced structures and the final orientation of the very narrow ultimate shear band compared to the applied stresses. The results from both testing methods indicated that the peak strength of these materials is due to their fabric structure. Dilation occurred after the peak as a consequence of the disintegration of the dense fabric structure.

The applicability of other work on sands and structured soils is investigated. The term *dense fabric structure* is introduced to make the distinction between the fabric of unbonded sands that will display abrupt yield and contractile behaviour, and the fabric of unbonded sands that will not behave in this manner even at the highest envisaged engineering loads. A comparison is made between the behaviour produced by fabric rather than bonded structure and whether the behaviour of a sand with a dense fabric structure assists the concept of a continuous geotechnical spectrum. A conceptual model of the behaviour of a soil with a high fabric strength is developed by considering the material as individual grains with a particular contact morphology. Mechanisms other than that of dilation within a continuum are postulated to explain the peak strength of soils with a dense fabric structure and also all dense granular materials.

ACKNOWLEDGEMENTS

Dr. M. E. Barton supervised both the research contained within this thesis and the writing of it. I am grateful for his help throughout and also his thoughtfulness when introducing new and complex topics. Conversations with William Powrie and extensive conversations with Richard Harkness have been enlightening, they were often of a highly dialectic nature, and have influenced both the content and direction of the research.

Harvey Skinner made suggestions for apparatus modification and was responsible for the digital data capture equipment, including the high accuracy obtained from the displacement transducers. Technical assistance and advice was provided by Stephen Wake and Deryk Taylor.

Dave Jeffries and John Sedman of A.R.C. generously allowed block sampling of the Reigate Silver Sand in Park Pit Reigate.

Funding was provided by the Department of Civil and Environmental Engineering.

LIST OF CONTENTS

Abstract	
Acknowledgements	
List of contents	
List of figures	
List of tables	
Notation	
INTRODUCTION	Page 1
CHAPTER 1: GEOLOGICAL AND GEOTECHNICAL BACKGROUND	4
1.1 Arenaceous materials on the soil-rock borderline	4
1.1.1 Classification systems	4
1.1.2 Nomenclature of the sand/sandstone borderline materials	4
1.1.3 Sandstone cementation and silica mobility	5
1.1.4 Compaction of sands	6
1.1.5 Ageing of sands	9
1.1.6 Locked sands	10
1.2 The mechanics of arenaceous materials on the soil-rock borderline	14
1.2.1 Friction	14
1.2.2 Adhesion within granular materials - Inter-particle forces	16
1.2.3 Cohesion of granular materials	16
1.2.4 Grain interlocking	17
1.2.4 Grain bonding	17
1.2.5 Apparent cohesion	19
1.2.6 Water and sandstone strength	20
1.2.7 Water and sandstone strength - discussion	21
1.2.8 Effective stress	21
1.2.9 Mohr - Coulomb and critical state	23
1.2.10 The effect of structure on the shear strength of sands	23
CHAPTER 2: FIELD SAMPLING, SAMPLE PREPARATION and IMPREGNATION	25
2.1 Block sampling	25
2.1.1 Introduction	25
2.1.2 Wide set scraper saw	27
2.1.3 Cord and washer saw	27
2.1.4 Extractive method	27
2.2 Hard shell	29
2.2.1 Introduction	29

2.2.2 Hairspray	29
2.3 Pluviated sample preparation	30
2.3.1 Introduction	30
2.3.2 Why this investigation was instigated	30
2.3.3 Past studies	32
2.3.4 Observations of slow pouring	32
2.3.5 Fundamentals of deposition during pluviation	33
2.3.6 Modifications to the slow pour apparatus	36
2.3.7 The experimental method	38
2.3.8 Results	39
2.3.9 Conclusions and discussion	40
2.3.10 Consequences for uniform sand bed preparation	41
2.3.11 Development of insitu density	42
2.4 Impregnation methods	43
2.4.1 Introduction	43
2.4.2 Direct shear sample impregnation	43
2.4.3 Method of impregnating direct shear samples	45
2.4.4 Results and recommendations	45
 CHAPTER 3: THE TESTED MATERIAL - REIGATE SILVER SAND, AND QUARRY STABILITY	 46
3.1 Reigate Silver Sand	46
3.1.1 Stratigraphical position	46
3.1.2 The Silver Sand - A2 and A3 - location and characteristics	48
3.1.3 A2 and A3 - description and index tests	49
3.1.4 A2 and A3 - grain mineralogy and morphology	50
3.1.5 Grain surface texture	54
3.1.6 A2 and A3 grain contacts	57
3.1.7 Spicules	59
3.1.8 Fabric - discussion and conclusions	60
3.2 Wetting of Reigate Silver Sand	61
3.2.1 Introduction	61
3.2.2 Methods and results - with vacuum	61
3.2.3 Method and results - no vacuum	62
3.2.4 Observations, discussion and conclusions	62
3.3 Park Pit - dark crust and banding	63
3.3.1 Dark crust	63
3.3.2 Banding	66
3.3.3 Mechanism of formation	66
3.4 Park pit slope stability	66
3.4.1 Mohr - Coulomb analysis	66

CHAPTER 4: INTRODUCTION TO TESTING AND DIRECT SHEAR**TESTS 69****4.1 Introduction to testing 69**

4.1.2 Difficulties 69

4.1.2 The program of testing 69

4.1.3 The squeeze test 70

4.2 Apparatus and methods 71

4.2.1 Apparatus 71

4.2.2 Method 72

4.2.3 Intact sample preparation 73

4.2.4 Pluviated sample preparation 75

4.3 Results of Shearing A2 76

4.3.1 Introduction 76

4.3.2 Pluviated samples 76

4.3.3 Intact samples 81

4.3.4 Proving ring/loadcell results 81

4.3.5 Shear surface morphology 82

4.3.6 The shear zone and shear induced structures of intact blocks 85

4.3.7 Dilation during shearing 91

4.4 Observations and Discussion 93

4.4.1 Friction angles of arenaceous materials 93

4.4.2 Shear zone width and testing methods 93

4.4.3 Pluviated sample strength envelope 95

4.4.4 Intact sample strength envelope 96

4.4.5 The intact peak strength envelope 98

4.4.6 Rock joint models 100

4.4.7 Failure modes of closely jointed rock masses 101

4.4.8 Intercept - cohesion in A2 103

4.4.9 Post peak undulations 104

4.4.10 Mode of failure of A2 105

4.4.11 Mode of failure - high pressure tests 105

4.4.12 Mode of failure - medium pressure tests 106

4.4.13 Mode of failure - low pressure tests 107

4.4.14 Crack formation 107

4.4.15 Columns 108

4.4.16 Dilation at low normal loads 108

4.4.17 Column spacing 110

4.4.18 Column orientation, formation and shearing 110

4.5 A3 direct shear tests 112

4.5.1 Introduction and methods 112

4.5.2	A3 results	112
4.5.3	A3 tests observations and discussion	117
4.5.4	A2 and A3 compared	118
4.6	Direct shear - conclusions	121
 CHAPTER 5: TRIAXIAL TESTS		
5.1	Methods	123
5.1.1	The hard shell	123
5.1.2	Sample preparation	123
5.1.3	Testing method	125
5.2	Results	126
5.2.1	Introduction	126
5.2.2	Mobilised ϕ' and volumetric strain vs. axial strain plots.	126
5.2.3	Extended peak and dilation	129
5.2.4	Strength envelope	132
5.2.5	Failure Mode	133
5.2.6	Long and short samples	134
5.3	Observations and discussion	136
5.3.1	Sample uniformity	136
5.3.2	Extended peak	136
5.3.3	Dilation angles	337
5.3.4	Triaxial strain or plane strain	138
5.3.5	Fabric structure and the failure mechanism	138
5.3.6	Softening, dilation and soil mechanics	140
5.3.7	A3 triaxial behaviour compared to that of rock	141
5.4	Conclusions - triaxial testing	141
 CHAPTER 6: UNIAXIAL TESTS		
6.1	Methods	143
6.1.1	Introduction	143
6.1.2	Sample preparation	143
6.1.3	Apparatus	144
6.2	Results	147
6.2.1	Introduction	147
6.2.2	LVDTs	147
6.2.3	Stress at failure and failure mode	148
6.2.4	Stress strain plots	152
6.2.5	Stiffness	153
6.2.6	U5 - reload loops	155
6.3	Observations and discussion	157

6.3.1 Local LVDTs and divergence	157
6.3.2 Local LVDTs and expansion	157
6.3.3 Local LVDTs and stiffness	158
6.3.4 Stiffness at small strains	158
6.3.5 Stiffness variation	159
6.3.6 Peak strengths	160
6.3.7 Failure type	160
6.3.8 Reload loop test	161
6.4 Conclusions - uniaxial testing	162
 CHAPTER 7: GENERAL DISCUSSION	 163
7.1 General discussion	163
7.1.1 Introduction	163
7.1.2 Comparison of strength test results	163
7.1.3 Peak strength and dilation	165
7.1.4 Dense fabric structure	166
7.1.5 Locked - bonded	166
7.1.6 A continuous geotechnical spectrum?	170
 7.2 Modelling and implications	 171
7.2.1 Conceptual/physical modelling of dense fabric structure.	171
7.2.2 Implications for soil models	173
 CHAPTER 8: CONCLUSIONS AND RECOMMENDATIONS FOR FURTHER WORK	 176
8.1 Conclusions	176
8.1.1 Sampling improvements	176
8.1.2 Disaggregated sample preparation	176
8.1.3 Strength testing	176
8.1.4 Stability of locked sands	179
8.1.5 Modelling and Implications	179
 7.2 Recommendations for further work	 180
8.2.1 Strength testing	180
8.2.2 Sampling	182
8.2.3 Pluviation	182
8.2.4 Formation of the interlocked fabric	182
8.2.5 The dark crust	183
8.2.6 Modelling	183
 References	 184

LIST OF TABLES

Table 3.1	Stratigraphical position of the Folkstone Beds.
Table 3.2	Summary of wetting results.
Table 4.1	Dilation totals.
Table 4.2	Comparison of A2 and A3.
Table 6.1	The failure stress and failure mode of all tests.
Table 6.2	Values of Young's modulus for the linear regions of tests U2, U3 and U4.

LIST OF FIGURES

Figure 1.1	Locked sand classification diagram (Barton et. al., 1993).
Figure 2.1	The two saws developed for extracting intact samples of a highly dilatant locked sand with very little cohesion.
Figure 2.2a	The wide set scraper saw in use.
Figure 2.2b	The washer saw in use.
Figure 2.3a	The original pouring apparatus.
Figure 2.3b	Slow pouring with a concentrated central stream.
Figure 2.4a	Photograph of deposition during slow pouring with the development of an energetic layer.
Figure 2.4b	Deposition during slow pouring with the development of an energetic layer.
Figure 2.5	Modified pouring apparatus showing details of the spreader meshes.
Figure 2.6	Grain size distribution for Reigate silver sand and Leighton Buzzard sand.
Figure 2.7	Density vs time of pour plot.
Figure 2.8	Comparison of pluviation and pouring for Leighton Buzzard sand.
Figure 2.9	Explanation of the layering produced by the moving curtain method.
Figure 2.10	Impregnation of shearbox sample using reservoir.
Figure 3.1	Particle size curves for A2 and A3.
Figure 3.2	Freshly disaggregated A2.
Figure 3.3	Freshly disaggregated A2.
Figure 3.4	Thin section of A2. PPL.
Figure 3.5	Thin section of A2. XP.
Figure 3.6	Angular, highly non-spherical grains with embayments and fractures.
Figure 3.7	Grains with long noses or necks.
Figure 3.8	Fines clustered at grain contacts.
Figure 3.9	Freshly disaggregated A3.
Figure 3.10	Freshly disaggregated A3.
Figure 3.11	Thin section of A3. PPL.
Figure 3.12	Thin section of A3. XP.

- Figure 3.13 Thin section of A3 showing iron oxide and clay minerals at grain contacts. PPL.
- Figure 3.14 Thin section showing grain contacts dominated by long/straight and concavo-convex contacts.
- Figure 3.15 Interpenetration and micro-suturing at grain contacts.
- Figure 3.16 A thread-like form, possibly a sponge spicule, in A2.
- Figure 3.17 Thin section showing the dark crust. XP.
- Figure 3.18 Thin section showing the dark crust. PPL.
- Figure 3.19 Thin section of the dark crust. PPL.
- Figure 3.20 Thin section of a heavily cemented area of the dark crust. PPL.
- Figure 3.21 Typical section of the Park Pit Reigate. Reproduced from Barton and Cresswell (1998).
-
- Figure 4.1. Comparison of the two apparatuses used for direct shear testing.
- Figure 4.2 A2 sample with hard shell.
- Figure 4.3 A2 sample stuck to the shearbox bottom platen, note the rounded top corners and the hard layer adjacent to the platen.
- Figure 4.4 A2 at 50kPa vertical stress. Pluviated dense (1.67Mg/m^3).
- Figure 4.5 A2 at 50 kPa vertical stress. Poured loose (1.43Mg/m^3).
- Figure 4.6 A2 at 750kPa normal stress. Density between minimum and intact.
- Figure 4.7 Strength envelope for pluviated and intact samples at normal loads below 1250kPa. The data points for the pluviated samples are averages.
- Figure 4.8 Strength envelope for pluviated and intact samples at normal loads up to 11MPa.
- Figure 4.10 Shear surface of intact A2 sheared at 100kPa. The steps are opposing the shear direction.
- Figure 4.11 Generalised morphology of the steps produced on the intact samples of A2 at low normal load. Note the sharpness of the corners. Arrows show the shear direction.
- Figure 4.12. The shear surface of intact A2 sheared at a normal stress of 750kPa.
- Figure 4.13 The shear surface of intact A2 sheared at a normal stress of 10MPa.
- Figure 4.14. Thin section investigation results showing the development of shear zone during a 100kPa normal load test.
- Figure 4.15 Photomicrograph of thin section C figure 4.14 showing the shear zone and high void ratio area. Field of view 13mm.
- Figure 4.16. Development of the low pressure shear plane.
- Figure 4.17 The surface of A2 after shearing at 1MPa. Note the abundance of fines compared to the surface of unsheared material (fig 4.18). Scale bar 1mm.
- Figure 4.18 The surface of unsheared A2. Scale bar 1mm.
- Figure 4.19 Thin section of a test carried out at 10MPa normal stress. Note the convex up shear zone.
- Figure 4.20 Detail at location A of figure 4.19. Obvious grain crushing. Field of view 6mm.
- Figure 4.21 Detail at location A of figure 4.19. Obvious grain crushing. Field of view 3mm, XP.
- Figure 4.22 Detail at location B of figure 4.19. The shear zone is represented by a macrovoid with less evident grain crushing. Field of view 2.6mm.

- Figure 4.23 Comparison of the shear zones in sand, A2 and rock.
- Figure 4.24 Detail of high and low normal load apparatus results at overlap.
- Figure 4.25 Patton's rock joint model giving an abrupt change of slope in the failure envelope.
- Figure 4.26a A3 shear surface after testing at 25kPa normal stress.
- Figure 4.26b A3 shear surface after testing at 100kPa normal stress.
- Figure 4.26c A3 shear surface after testing at 750kPa normal stress.
- Figure 4.27 Front wedge type of failure seen in A3.
- Figure 4.29 Shear strength vs. normal load plot for A3.
- Figure 4.30a Envelope for intact A2 and A3 at normal stresses of 100kPa and below.
- Figure 4.30b Envelope for intact A2 and A3.
- Figure 5.1 Method of applying the vacuum and flushing the sample.
- Figure 5.2 Mobilised friction angles vs axial strain.
- Figure 5.3a The average length of the extended peak (as axial strain) plotted against confining pressure. Note the change between 50 and 100kPa.
- Figure 5.3b The average volume change plotted against confining pressure. Note the change between 50 and 100kPa.
- Figure 5.4 The length of the extended peak plotted against the total volume change. The arrows show the two short and the one long sample corrected to a nominal axial strain value using a length of 76mm.
- Figure 5.5 The dilation angle calculated for triaxial strain and plain strain plotted against the confining pressure.
- Figure 5.6 Peak strength s'_t plot for all the triaxial results.
- Figure 5.7 Comparison of the shear plane orientation and morphology. A) The shear plane in the 2:1 samples at pressures at 50kPa and over was from corner to corner. B) The shear plane at confining pressures below 50 kPa contained a central step. C) and D) Both the long and short samples produced shear planes at the same angles as the 2:1 samples (60 to 64 degrees).
- Figure 5.8 Mobilised friction angles vs axial strain for the long and short samples.
- Figure 5.9 The influence of fabric structure on the failure mechanism.
- Figure 6.1 The Uniaxial apparatus.
- Figure 6.2 Stress strain plot for test U3. The strain is calculated from the closing gap between the platens.
- Figure 6.3 Stress strain plot for test U3. The strain is calculated from the LVDTs acting over the middle half of the sample.
- Figure 6.4 Failure mode of U2 and U3. A) Intact vertical columns with 40° to 60° shears between them. B) Plan of A. C) Intact cone left after U3.
- Figure 6.5 Photograph of uniaxial sample U2 toward the end of the test.
- Figure 6.6 Photograph of U5 after removal of the rubber membrane showing lines on the surface of the sample.
- Figure 6.7 Details of the lines on the surface of U5.
- Figure 6.8a Stress strain plot for test U2.
- Figure 6.8b Stress strain plot for test U3.
- Figure 6.8c Stress strain plot for test U4.
- Figure 6.9 The stress strain plot of U2 for small strains showing the initial flat zone followed by a linear zone with $E = 400\text{MPa}$.

- Figure 6.10 · The stress strain plot for U5 showing the reload loops.
- Figure 6.11a The stress strain plot for U5 showing the reload loops. Strain is calculated as an average of the two LVDTs. The boxed numbers are the E values for the adjacent linear zone calculated from the average strain.
- Figure 11b Detail of the stress strain plot for U5 showing the final reload loop with the strain increasing even though the stress is declining.
- Figure 6.12 Idealised model of failure typified by U3.
- Figure 7.1 Comparison of the strength envelopes for sand with bonded and dense fabric structures.
- Figure 7.2 Conceptual modelling of grain fabric using stacked and heaped bricks.
- Figure 7.3 Two dimensional modelling of a locked sand.
- Figure 7.4 Conceptualisation of dilation and peak strength as due to the rotation and collapse of stress induced structures.

NOTATION

D_r	Relative density = $(\rho_{d \text{ intact}} - \rho_{d \text{ min}}) / (\rho_{d \text{ max}} - \rho_{d \text{ min}}) \times (\rho_{d \text{ max}} / \rho_{d \text{ intact}})$
E	Youngs modulus
s'	Centre of effective stress circle on an Mohr Coulomb plot = $(\sigma'_1 + \sigma'_3) / 2$
t	Height of stress circle on a Mohr coulomb plot = $(\sigma_1 - \sigma_3) / 2$
α	Angle of inclination of maximum stress ratio to the horizontal in the direct shear apparatus
γ	Engineering shear strain
ε	Nominal strain = $\delta l / l_0$
ε_a	Axial strain in the triaxial test
ε_r	Radial strain in the triaxial test
ε_v	Nominal volumetric strain = $\delta v / v_0$
θ	Angle of inclination of maximum stress ratio to the horizontal in the triaxial apparatus
μ	Coefficient of friction
ρ_d	Dry density
$\rho_{d \text{ intact}}$	Dry density of intact block samples
$\rho_{d \text{ max}}$	Maximum dry density
$\rho_{d \text{ min}}$	Minimum dry density
σ, σ'	Total stress, Effective stress. Subscripts denote directions (or major, intermediate and minor: 1, 2 and 3)
τ	Shear stress
τ_{peak}	Peak shear stress
τ_{ult}	Ultimate shear stress
ϕ'	Angle of shearing resistance
ϕ'_u	Friction angle of grains on a flat plate of the same material
ϕ'_{cv}	Critical state friction angle
ϕ'_{peak}	Peak friction angle
ϕ'_{ult}	Ultimate friction angle
ψ	Dilation angle

INTRODUCTION

The transitional materials between sands and sandstones form a neglected group compared to the equivalent materials in the argillaceous spectrum. This study examines a material on the sand /sandstone borderline where the behaviour is not dominated by bonding between grains but by the shape of the grains and how they are fitted together. Sands, over geological time, may develop strength that is not due to adhesion between grains. These have been termed locked sands. How these sands are formed and how they are classified is explored in the first half of chapter one.

The second part of chapter one reviews the relevant areas of the large body of work which investigates the mechanics of sands. Cemented sands have recently received attention along with micro-structure in soils and weak rocks. Structure has been divided into bonding between grains (bonded structure) and interlocking between grains (fabric structure). Bonded structure can be investigated by artificially cementing sand; reportedly producing a brittle failure mode at low confining pressures with a transition to ductile failure at higher confining pressures. This is explained by brittle failure of the bonds controlling the overall behaviour at low loads giving way to domination by the frictional component at higher loads.

Fabric structure poses a problem in that it cannot be created artificially and so intact material must be tested. The small cohesion created by fabric structure alone is very prone to disturbance and hence intact sampling and testing is rarely carried out. This has led most workers to test sands with a mix of fabric and bonded structure; resulting in a confused understanding of the mechanisms occurring. Chapter two describes the developments in sampling and specimen preparation techniques that were necessary to allow the intact testing of locked sands with negligible grain bonding and also the impregnation methods used to allow thin sections of the shear zones to be made.

The results of tests carried out on an intact sand will show a component of strength due to the structure but will also show a component of strength due to the shape and

friction properties of the disaggregated sand grains. Intact tests must therefore be compared with those carried out on the disaggregated material. The high density of the intact material cannot be reproduced by recompacting the disaggregated grains, and any comparison has to be between the intact material and recompacted material at a lower density. This density should be as high as possible; chapter two section three describes an improved slow pouring method and an investigation into the fundamental mechanism by which the high densities are achieved.

Two examples of Reigate Silver Sand (RSS) from particular locations within the A.R.C. Park Pit Quarry (designated A2 and A3) were chosen for this study because they fulfilled the following criteria:

1. Zero matrix and cement for A2, trace cement for A3
2. A ϕ' of 65 degrees at low normal loads
3. Isotropic and homogeneous (according to Richards, 1992)
4. Block sampling is possible with care

Chapter 3 locates A2 and A3 stratigraphically and describes them using both standard index tests and a microfabric investigation. The formation of the interlocked fabric is discussed. The behaviour of A2 and A3 when wetted is explored, and this, combined with the effect of a dark crust formed on the walls of the Park Pit, are discussed and considered in relation to the stability of the 70° quarry walls.

Chapter 4 introduces the testing program and contains the extensive direct shear tests. These tests (including the use of glass sided shearboxes and impregnation followed by thin-sectioning) showed that these sands behave, at low normal loads, superficially like a highly dilatant soil but with the development of “columns” supporting the principal stress. These columns were seen, at the end of the test, as a stepped failure surface with the steps opposing the shear direction. At high normal loads, the sands displayed a brittle, rock - like manner during shear. This was

observed as a narrow shear zone with plumose structures. The results demonstrate that sand with fabric structure has different phases at different normal loads.

Chapter 5 describes the triaxial tests. These have also produced novel results: an extended peak is present that is accompanied by a uniform dilation. The dilation rate is not compatible with triaxial strain interpretation; this is thought due to plain strain failure occurring early in the test before localisation begins. From considerations of the grain contact morphology a failure mechanism that explains the extended peak and the biaxial strain is proposed.

The trace of cement present in A3 produced enough cohesion for uniaxial (unconfined) tests (chapter 6). The results show strain weakening after 0.01% strain followed by a small amount of strain hardening and brittle failure at strains of less than 0.5%. A3 was found to be both stiffer and more brittle than a ‘normal’ dense sand.

Chapter 7 brings together the test results. The applicability of other work on sands and structured soils is investigated. The term *dense fabric structure* is introduced to make the distinction between the fabric of unbonded sands that will display abrupt yield and contractile behaviour, and the fabric of unbonded sands that will not behave in this manner even at the highest envisaged engineering loads. A comparison is made between the behaviour produced by fabric rather than bonded structure and whether the behaviour of a sand with a dense fabric structure assists the concept of a continuous geotechnical spectrum. A conceptual model of the behaviour of a soil with a high fabric strength is developed by considering the material as individual grains with a particular contact morphology. Mechanisms other than that of dilation within a continuum are postulated to explain the peak strength of soils with a dense fabric structure and also all dense granular materials.

General conclusions and recommendations for further work are given in chapter 8.

CHAPTER 1: GEOLOGICAL AND GEOTECHNICAL BACKGROUND

1.1 Arenaceous materials on the soil-rock borderline

1.1.1 Classification systems

Classification systems that rely on material strength such as the International Society of Rock Mechanics (1978), the Geological Society of London (1970) and the British Standard 5930 (1981) show good agreement in the categories strong, very strong and extremely strong rock but less agreement when defining weak rock. Generally definitions become more problematic as the soil / rock borderline is reached and materials on the sand / sandstone borderline have received less attention than their argillaceous counterparts. Barnes and Dusseault (1982) produced a qualitative scheme for sands and sandstones that correlated the increase in shear strength with the degree of diagenetic alteration. Dobereiner and DeFreitas (1986) suggested that the definition that separates sand from sandstones must rely on strength alone and defined weak sandstone as having a saturated unconfined compressive strength of 0.5 to 20.0 MPa. They also showed that the saturated moisture content maybe used as a practical index parameter for assessing the strength and deformability of weak sandstones.

A “rule of thumb” definition for positioning the soil/rock boundary (quoted by Dobereiner and DeFreitas, 1986) is that soils disintegrate when immersed in water whereas rocks do not. Unlike argillaceous sediments, however, weak sandstones only exhibit limited softening; when immersed they either disintegrate or remain intact with little change to their strength.

1.1.2 Nomenclature of the sand/sandstone borderline materials

The nomenclature of the sand/sandstone borderline materials is derived from sedimentary geology, engineering geology, soil physics and geotechnical engineering. Terms are often used in a inconsistent manner or even to represent an opposite meaning. The engineering classifications are more material behaviour based whilst

the geological ones are more likely to be based on the materials' genesis. Especially relevant to this study are the terms structure and fabric. These terms are misused in the literature to the extent that they have become almost interchangeable. Here they will be used in the geotechnical sense as defined below.

The geological term “structure” refers to the relationship between different parts of the rock. Examples of “structures” are bedding, jointing and cleavage. Soil physicists use “soil structure” as indicating the shape, size and degree of aggregation between primary soil grains and the spatial arrangements between them. A highly structured soil is one with a large degree of aggregation between grains resulting in the formation of soil peds (Hodgson, 1976). Geotechnically, when discussing sands, “structure” is now used to represent anything that increases the strength parameters of intact samples above those of the disaggregated material. It is divided into fabric and bonding (Barton et al 1993; Cuccovillo and Coop, 1997).

“Fabric” is commonly used by geologists as a term that includes all the features of texture and structure, ranging from the arrangement of individual grains to a regional joint system. In a sedimentary rock the term grain fabric refers to the orientation and packing of the grains, and to the nature of the contacts between them (Tucker, 1991). This is not quite synonymous with the term microfabric which includes the arrangement of all material composing the sediment including any matrix. Many geotechnical authors when discussing soils use the terms fabric, grain fabric and microfabric interchangeably. Here the term fabric will be used to describe that part of the structure not associated with bonding of grains; it includes the orientation and packing of the grains, the morphology of the contacts between them and the influence of any matrix.

1.1.3 Sandstone cementation and silica mobility

Cementation is a chemical process of diagenesis resulting in the precipitation of minerals in the pore spaces. Cement may either be active or passive; active cement adheres firmly to the grains and provides a bond between them, passive cement

simply fills the pore space or creates a rim around the grains without any bonding of grains occurring.

The usual cementing materials in sandstones are the carbonates, iron oxide, and quartz, the latter often in the form of syntaxial overgrowths. Silica may also be present in the form of microquartz, megaquartz, chalcedonic quartz and opaline silica (Tucker, 1991). The controls over quartz cement in sandstones are reviewed by McBride (1989). They are summarised as: framework composition, residence time in the “silica mobility window”, the pore fluid composition, flow volume and available pathways.

Sources of silica for cementation are thought to include other beds within the depositional basin, including deeper rocks undergoing low grade metamorphism. The relative importance of sources however is not known. The sources of silica in unmetamorphosed quartzitic sandstones are most likely to be from pressure solution of detrital quartz grains at grain contacts and at stylolites. The dissolution of opal skeletal grains is more often considered a source of silica in unmetamorphosed shales (McBride, 1989). The mechanisms of silica diagenesis are given by Williams and Crerar (1985) and solubility controls by Williams et al (1985).

1.1.4 Compaction of sands

Compaction of arenaceous sediments is a poorly understood geological process even though it has received much attention due to their being reservoir rocks. Porosity reduction with depth is widely reported but there is debate over how much can be attributed to the rotation, slipping and fracturing of grains into tighter packing arrangements, termed physical compaction, and chemical compaction due to pressure solution and stylolitization.

Taylor (1950) investigated sandstone samples from depths between 1500m and 5000m from two deep wells in Wyoming, varying from Cretaceous to Jurassic in age, and also an experimentally compacted sand. Three types of pore space reduction were recognised:

1. Simple pore filling.
2. Solid flow.
3. Solution followed by re-deposition or removal of the dissolved material.

Thin section point counting techniques were used to look at contact types and cement and how they change with depth. A relationship between contact type and depth was established, but no relationship between depth and cementation/replacement was found. Contact types were classified as; floating, tangential, long, concavo-convex and sutured. The list is in order of increasing numbers of that contact type found with increasing pressure/depth. The contacts “show a progressive change with depth from those resulting from original packing to those resulting from pressure”. Taylor (1950) also point counted an experimentally compacted sand, finding no c/c or sutured contacts present.

Houseknecht (1987) used the figure 40% for the original porosity of well sorted sand, quoting the extensive data for natural sands produced by Prior (1973). He divided porosity loss under the following headings;

- a) Mechanical compaction - reorientation and repacking of brittle, competent grains with little fracture and cleavage occurring. Porosity may be reduced to 30%.
- b) Chemical compaction - intergranular pressure solution and possibly with some stylolitization. Porosity may be reduced to 0%.
- c) Cementation. Porosity may be reduced to 0%

The importance of compactional processes (a and b above) were compared with cementation (c) in reducing porosity by using a graph of intergranular volume (minus cement porosity) against cement. Mechanical compaction and intergranular pressure solution were found to be more important than cementation in reducing porosity.

However, doubts exist as to the possibility of reducing the intergranular volume of a sand below 40% by mechanical compaction. The problem is that the intergranular volume would have to be temporarily increased to allow grains enough space to

manoeuvre into tighter packing arrangements; this requires a source of negative entropy. Seismic activity including minor earth movements has been proposed as a possible provider of energy to overcome this (Taylor, 1959).

The nomenclature used by Houseknecht (1987) is confusing: terms such as intergranular volume, intergranular porosity, minus cement porosity and porosity have to be interpreted with care. His method of calculating compactional porosity loss was criticised in several papers (Pate 1989, Ehrenberg 1989), and also the estimation of original porosity as 40% for all sandstones was criticised, the suggestion being that a sorting coefficient should be used. Sorting may not affect the porosity of compacted sandstones but it will influence the determination of original porosity (Pate 1989). Houseknecht (1989) replied that our understanding of the original porosity of sand is often derived from laboratory experiments and packing models. Whilst these show that poorer sorting does result in lower porosity, Prior's (1973) data reveals significantly higher porosities in natural sands and that they show only a "subtle" relationship between porosity and sorting.

Lundegard (1992) used a large data base to compare compaction (both physical and chemical) vs. cementation porosity loss and suggested that using an original porosity of 40 to 45% will give little error for a clean sandstone. Problems in estimating how much porosity loss is due to either compaction or cementation are due to;

- a) Original porosity estimation errors,
- b) Amount of local grain dissolution - underestimation will cause an underestimate of the significance of compaction,
- c) Errors in the method of calculating porosity loss due to compaction;

Houseknecht (1987) did not take into account bulk volume loss resulting in an underestimation of compactional porosity loss.

Lundegard (1992) concludes that compactional porosity loss has in the past been underestimated and is probably the dominant mechanism of porosity loss in most sandstones. Porosity loss due to compaction is related to grain composition and basin thermal structure.

Pressure dissolution at grain contacts is prevented by early cementation or by large amounts of matrix (Tucker 1991). A combination of mechanical and chemical compaction has been suggested as the mechanism for the large reductions in porosity recorded for sands that have undergone shallow burial; only small amounts of morphological change at grain asperities would be required to allow grain movement (Houseknecht, 1989). Stephenson et al (1992) suggests that movement of quartz crystals in the solid state is possible and solid state diffusion may be more important in some sandstones than pressure dissolution and recrystallisation.

Shallow shelf sands that have zero or trace cement and no matrix are therefore likely to have undergone compaction by morphological change at grain boundaries. If no evidence of solution and deposition of silica is evident (in the form of solution pits and overgrowth) then the morphological change is due to solid state diffusion.

1.1.5 Ageing of sands

An increased stiffness of sand occurring over laboratory, engineering and historical time scales, not necessarily accompanied by any increase in density, has been reported by various workers (see Mitchell and Solymar 1984). Denisov and Reltov (1961) explained this behaviour in sands as well as clays as being controlled by the presence of silicic acid gels and soluble compounds on the surface of grains. These are formed as a result of the hydrolysis of the superficial silicate layer, they have negligible solubility and remain on the surface as a very thin film firmly adhering to the surface of the grain. The gel films are elastic and have cementing properties enabling them to form strong bonds between particles of different sizes. When dehydrated the films become brittle but they retain a cementing capacity over large variations in humidity. Experimental evidence was put forward by Denisov and Reltov (1961) to confirm the presence of bonds between quartz grains due to the presence of silicic acid gel films and that these are developed within laboratory time scales. They suggested that it is these bonds that cause the gradual strengthening of sands in hydraulically placed embankments.

There is however a reluctance to accept the presence of silica gel films as causing time dependant strength gain in freshly deposited sand (see Mitchell et. al. 1984).

The work of Lee (1979) showed that with quartzose sands, no adhesion bonds formed during triaxial tests at 14MPa confining pressure. However a “sand” containing 35% feldspar and 15% *amphibole or pyroxene* minerals did show bonding. Authors often quote Lee (1979) ambiguously, suggesting that quartzose sands will show cohesion (and presumably a measurable tensile strength) due to cold welding or solution/deposition of silica at grain contacts over laboratory and engineering time scales (see Mitchell et. al. 1984).

Increased strength in sands is currently thought to be due to a combination of secondary consolidation and the development of micro interlocking of grain asperities. Mesri et al (1990) use the terms “geometrical particle interference through more efficient packing” and “interlocking of particle surface roughness”. This gives rise to what is termed an aged sand. Frictional rather than cohesive effects are considered to produce the increased stiffness (Schmertmann 1991). Arguments against “invisible” cement bonds at grain contacts rely on the observation that there are uncemented natural sand deposits (Mesri et al 1990). No direct evidence has been put forward to show that the small scale interlocking is occurring.

1.1.6 Locked sands

Dusseault and Morgenstern (1979) described a new category of geomaterials which they termed locked sands. The strata to which this new term was applied were North American Athabasca Oil Sand and Swan River Sandstone of the Lower Cretaceous and St Peter Sandstone of the Ordovician. These occur in steep natural slopes and are able to support large loads with only small deformations. The slopes do not fail by deep seated shear but by surface erosion and shear along discontinuities. Block samples disintegrate when placed in water but the confining pressures on the insitu material result in it remaining strong and capable of supporting considerable loads. Dusseault and Morgenstern (1979) considered that the characteristic high strength

and friction angles of locked sands (see below) was due to the dilation they displayed on shearing.

Barton et al (1986) investigated two Hampshire Tertiary sand beds (Bagshot and Barton Sands) to discover whether or not they could be placed within this new category. They organised the characteristics of the locked sands as defined by Dusseault and Morgenstern into the five sets outlined below.

1. The sand is quartzose, with little or no cement. Disaggregation can be achieved by rubbing between fingers and intact samples for laboratory testing can be produced only if care is taken. Disaggregation occurs on immersion.
2. The microfabric shows large interpenetrative grain contacts with no intergranular cementing. The grains have a rugose surface. These features are thought to occur from the solution and recrystallisation of quartz without any cementing of the grains occurring.
3. The porosity is lower than that of a dense sand and relative density measurements are in excess of 100% with a commensurate low compressibility.
4. In shear tests locked sand shows brittle behaviour, high peak shear strength, curved failure envelopes, small strains to failure, very large dilation rates, no cohesion, and residual strength between 30 and 35 degrees.
5. Natural slopes in locked sands are steep with angles in excess of the measured values of ϕ' . The angle of slope is height dependent but even the largest slopes (60m) are between 50° and 55°.

Barton et al (1986) concluded that the two Hampshire sands corresponded to the criteria in respect of a lack of cement, an insitu relative density greater than 100% and enough cohesion to be sampled as intact blocks. However they showed less strength and a higher porosity than the North American sands and would be better described as partially or weakly locked sands.

The application of the term locked sand caused confusion in regard to the boundaries of the category of materials to which it applied. To resolve this problem a tripartate

system of classification, which can be applied to the whole spectrum of arenaceous materials, was developed (Barton et. al., 1993) as shown in figure 1.1.

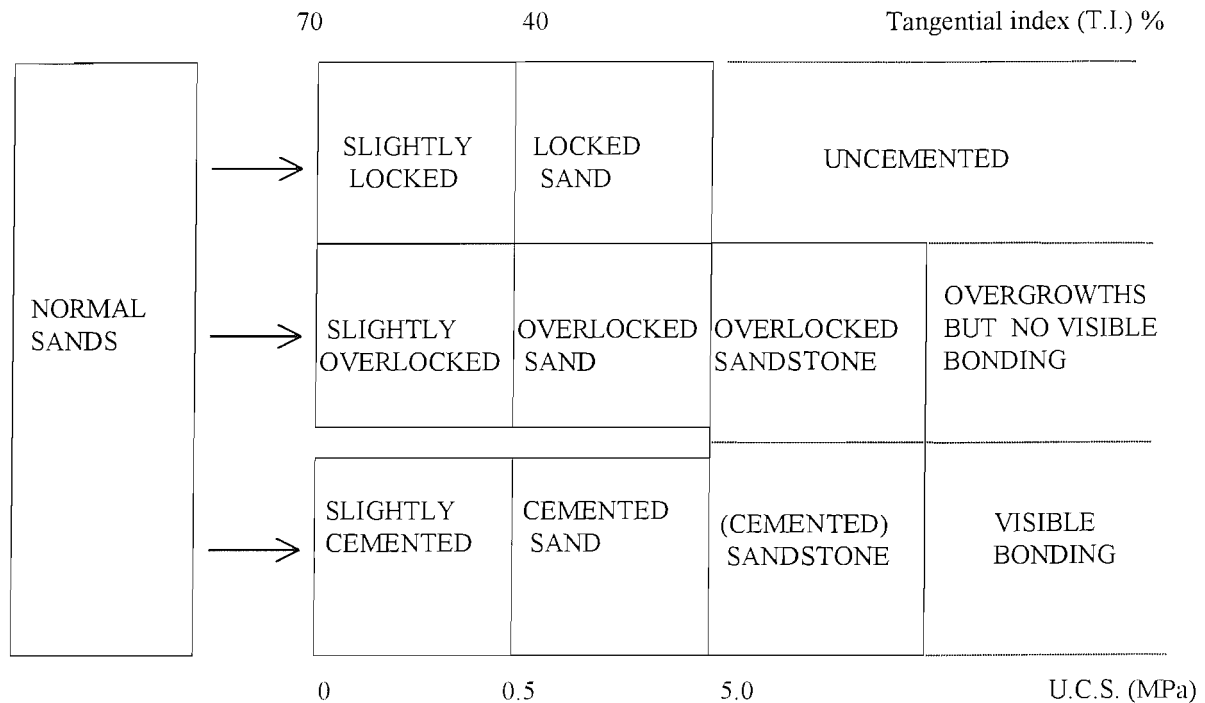


Figure 1.1 Locked sand classification diagram (Barton et. al., 1993)

This differentiates between interlocking and overlocking fabrics, the former having no crystal overgrowths but the latter having overgrowths formed by authigenic silica or from silica liberated by pressure solution. In this system the sands described by Dusseault and Morgenstern (1979) would be placed in the overlocked category. This is not now thought to answer the problem as it shows no overlap between slightly locked and slightly cemented sands; which are by far the most numerous group of transitional arenaceous materials.

The term cohesive sand was therefore re-introduced, this was placed between aged sands and sandstones (Barton, 1993b) as shown below and then divided into categories depending upon the cause of the cohesion. The materials in the cohesive sand category receive their strength from either “interlock cohesion” or bonding by authigenic cement, although in many, if not most, cases from both.

deposit	ageing	mild diagenesis	induration
sand	aged sand	cohesive sand	sandstone

The author suggests that the problem with this classification is that some recently investigated sands, have a negligible tensile strength and yet display friction angles, measured in the direct shear test, of up to 65 degrees (Richards, 1992; Richards and Barton, 1999). A name for these materials that includes the term cohesion will always cause confusion. Barnes and Dusseault (1982) used the term fabric cohesion, this being cohesion on a Mohr-Coulomb plot and not necessarily measurable as a tensile strength.

1.2 The mechanics of arenaceous materials on the soil-rock borderline

1.2.1 Friction

There are two basic laws of friction; firstly that friction is independent of the area of contact between the solids and secondly that friction is proportional to the load between surfaces. These were described by Leonardo da Vinci and rediscovered by Amontons, a French engineer at the end of the seventeenth century, they are often referred to as Amontons laws. The second law can be restated that the ratio of friction over load is constant, this constant is called the “coefficient of friction”.

Coulomb in the eighteenth century verified Amontons observations and made a distinction between static and kinetic friction. Kinetic friction was shown to be often lower than static friction and was believed to be independent of the speed of sliding.

The Coulomb model describes the sliding of one block over another. The forces are resolved into two components, N perpendicular to the surface and F parallel to it. The blocks slide when the ratio F/N exceeds a certain limiting value μ . If F_{\max} is the limiting frictional force then:

$$F_{\max} = \mu N \quad 1.1$$

Where μ does not depend upon the area in contact.

Also:

$$\mu = \tan \phi \quad 1.2$$

Where $\tan \phi = F_{\max} / N$. The angle ϕ is therefore the largest angle of inclination of a force to a slip surface and ϕ is also equal to the tilt of the slip surface to the horizontal if the load is applied vertically. When used as a soil failure model the Coulomb friction model implicitly incorporates the interlocking of grains on the shear surface and the friction angle μ is identical to the soils angle of repose.

Friction is now explained by molecular adhesion between surfaces (Bowden and Tabor 1967). This was considered by Coulomb but rejected as it seemed to suggest that friction should be proportional to the area of the sliding bodies. He came to the conclusion that friction was due to the interlocking of surface asperities and consisted partly of the work done in lifting the load over these. A distinction is now made between real (or true) and apparent (or superficial) areas of contact. The true area of contact, which consists of the tips of surface asperities, is proportional to the normal force N . Intimate contact occurs at these positions and adhesion takes place. Coulomb's friction law can then be derived.

By far the largest group of materials investigated as to their friction characteristics are the metals. These follow the laws of friction because they deform plastically and their junctions formed at asperity contacts have a constant specific shear strength. If either of these criteria is not obeyed, for example an extremely hard material such as diamond or very elastic material such as rubber, then Amonton's laws cease to apply. However a large variety of materials approximately conform to the friction laws even though, like rock forming minerals, they are brittle rather than plastic when tested on the macro scale. Bowden and Tabor (1967) suggest that this is due to the large confining pressures in the region of the asperity contacts suppressing any brittle behaviour.

This explanation of friction, requiring strong adhesion, would imply that a strong normal adhesion was also produced. Normal adhesion, however, is not generally observed for the following reasons;

- Friction is measured during sliding and contaminant films will be rubbed off. These will not be removed by pressing two surfaces together.
- Adhesion, unlike friction, is measured after the normal load has been removed. Elastic stresses around the junctions will be released as the normal load is removed causing strains in the material. The junctions will be brittle due to the work done to them and will fail (be stripped apart) due to tensile strains provided by the release of the elastic stresses.

1.2.2 Adhesion within granular materials - Interparticle forces

The strength behaviour of soil is in reasonable conformity with the adhesion theory of friction and this shows that interatomic bonding between particles must be occurring. However Mitchell (1976) suggests the absence of cohesion in overconsolidated silts and sands argues against this. The interparticle contact stresses are calculated as being many orders of magnitude greater in these soils than those in overconsolidated clays which have true cohesion. The higher contact stresses in the silts and sands should have produced more cohesion than that observed in the overconsolidated clays. However this argument takes no account of the fact that adhesion is not generally observed after the normal load is removed (see above).

1.2.3 Cohesion of granular materials

Cohesion in soil mechanics is often defined by an intercept on a shear strength versus normal stress diagram (see section on the strength of granular materials). This value may be an extrapolation from test results using normal stress levels greater than zero. To avoid confusion it is better to define a cohesive soil as one possessing a certain amount of tensile strength (Barton 1993).

The cohesion exhibited by bulk samples of granular materials is not simply the sum of the adhesive forces between grains. Cohesion in sands can come from two sources:

1. Grain interlocking
2. Grain bonding

1.2.4 Grain interlocking

Though micro interlocking of grain asperities may possibly produce stiffness and shear strength (Sitar 1983), significant cohesion is only produced after pressure solution and overgrowths have resulted in macro interlocking of grains (Barnes and Dusseault 1982). This is termed interlock cohesion (Barton et. al. 1993) or fabric cohesion (Barnes and Dusseault 1982).

1.2.4 Grain bonding

Grain bonding may be due to; cement, matrix cohesion or intergranular welding.

Cementation (due to active cement) requires a chemical bond between the grain and the cement. Cohesion increases with the effectiveness of the bonding and varies with the type of cement (Barton 1993). Problems occur in trying to measure the proportion of cement that results in bonding, i.e. that which is adhering to the grains, rather than passive cement. In extreme cases large amounts of passive cement may produce interlock cohesion whereas only small quantities of bonding cement are required at grain contacts to produce a rock.

Matrix cohesion is due to presence of fines, usually clay; these are often in the form of bridges between grains and may be measurable only as trace by weight yet impart some cohesion. Numerous authors show electron micrographs of these bridges (Richards 1992, Mitchell 1976). The sands studied here have been chosen for a zero or trace level of matrix.

The creation of bonding by the forcing together of materials is termed cold welding. In granular materials cold welding forms adhesive bonds that are due to ionic or covalent atomic bonds at grain contacts. There is doubt that this mechanism is occurring in sediments subject to mild diagenesis (Barton 1993).

1.2.5 Apparent cohesion

This has been a confusing term. It is used both for the cohesion caused by the presence of an amount of water causing unsaturated conditions, and for the extrapolated intercept on a τ vs. σ_n plot. The former actually exists, it is real, and though small it is measurable. The latter does not exist as the material is not necessarily cohesive and using it can cause problems of overestimating the strength of a granular material at low normal loads.

The desiccation of a soil increases the tension in the pore water (from zero to a value $-u_w$), this produces an effective all-round pressure (Terzaghi and Peck 1948), or in more modern terms, tension given as;

$$p_k = -u_w \quad 1.3$$

And the shearing resistance of the soil is increased by;

$$d\tau = p_k \tan\phi \quad 1.4$$

However when the shrinkage limit is reached air enters the soil, the soil moisture ceases to be continuous and the equations above cease to hold. Also $-u_w$ is measured by the difficulty of removing the remaining water, and it does not represent p_k acting to pull the grains together.

When cohesion is due to negative pore water pressures which is lost when the soil is immersed it is referred to as apparent cohesion (Terzaghi and Peck 1948). This term has caused confusion; the addition of the word ‘apparent’ led some to believe it was not ‘real’ and therefore not actually there (Bolton 1991). However as pointed out by Barton (1993) the tension of water films in partly saturated sands is a definite source of cohesion and he terms it suction cohesion.

The importance of negative pore water pressures in influencing the engineering strength of silts and clays is widely accepted. But, however, the situation with sands is ambiguous. Bolton (1991) states that “damp sand might even be prepared to stand vertically if the suction due to the surface tension were strong enough”. What is strange is that given the availability of sand and water the experiment has not been carried out to remove the word “might”.

Sandcastles have long been used as an example of the engineering significance of suction cohesion. However the present author considers they show that with sands the opposite is the case. Sand ‘castles’, if they are constructed from sand, display vertical walls of less than 300mm and to gain overall heights greater than this the vertical walls are interspaced with near horizontal benches. The overall slope angle being only slightly above

the friction angle of the wet sand. The reason why sand 'castles' are constructed on the beach and not sand 'men' is that the available cohesion only allows a small vertical face to be constructed; ideal for modelling 13th century castles, whereas a sand 'man' would fall down.

By wetting samples of loess with different liquids Denisov and Reltov (1961) established that the drop in strength and degree of disintegration have no relationship to changes in capillary forces and that the weakening effect of liquids on soils depends upon their dielectric constant. They concluded that water was not providing suction cohesion to these materials but that the strength was due to surface forces bonding the small, high surface area, particles. The drop in strength was caused by the fluids destroying these surface forces and this depended upon their dielectric constant. The implication for sands, where negative pore water pressures will have less effect than silts, is that negative pore water pressures do not provide significant cohesion.

1.2.6 Water and sandstone strength

It is widely accepted that as moisture content increases the compressive strength of sandstone decreases (Colback and Wiid 1965, Hasizadeh and Law 1991, Hawkins and McConnell 1992). The commonly suggested mechanism at low (i.e. geotechnical engineering) temperatures is that weakening is due to a reduction in surface free energy allowing stress corrosion; the strained Si-O bonds react more readily in a moist environment. Other mechanisms of strength reduction have been suggested: capillary tension decrease (see West 1994), pore pressure increase, reduction in friction and chemical and physical deterioration.

Colback and Wiid (1965) reported that quartzose sandstone under saturated conditions loses 50% of its compressive strength. From the observation that the Mohr fracture envelope of the rock is displaced in a parallel fashion they conclude that the reduction in strength with increasing moisture content is caused by a reduction in tensile strength which in turn is a function of molecular cohesive strength of the material.

Hasizadeh and Law (1991) investigated water weakening at various stress and strain rates. They tested two rocks; a quartzite (98% quartz) and a sandstone (50% quartz,

25% feldspars and lithic fragments, 25% clay matrix). They found that the water saturated quartzite remained as strong as the dry rock with only probable weakening beginning to appear at stress rates less than 10^{-2} MPa/sec (slower than 10^{-6} /sec strain rate). They interpret this as indicating that microfabric, particularly the quantity of clayey matrix, is a significant factor in how water physiochemically changes the strength of a rock.

Hawkins and McConnell (1992) tested 35 sandstones and also concluded that the degree of sensitivity to moisture content is influenced primarily by the proportion of clay matrix and to a lesser extent the microfabric. Of note was an U.C.S. loss in siliceous sandstone of 8% compared to a loss of 78% in a clay rich sandstone. The saturated U.C.S. was not found to be dependent upon the initial dry U.C.S. or the porosity. The development of pore water pressures during loading was negligible and they suggest it plays no part in strength reduction. Moisture contents as low as 1% had a marked effect on strength and deformability and with the exception of clay rich sandstones negligible loss of strength occurred when the moisture content was increased from 1% to saturation.

1.2.7 Water and sandstone strength - discussion

Wetting is reported as reducing the strength of sandstones by a very variable and sometimes very large value; in general the more quartz the less effect moisture content has. No consensus for the complete explanation of this phenomena has been reached. It is possible that many mechanisms are occurring and that these may be in conflict; some sandstones are even reported to increase their strength on immersion. Richards and Barton (in press QJEG) when investigating the strength of Folkestone sands (locked/cohesive geologically aged sands) suggest that capillary forces are neither the sole nor major factor producing the observed cohesion in those aged sands. They give the reasons as:

- Some room dry samples had negligible cohesion, their small water content should have produced microscopic moisture films under tension causing suction cohesion.
- The 17 different sands when room dry showed a wide variation in cohesion.
- Significant cohesion was retained by some samples on wetting.

1.2.8 Effective stress

The well known concept of effective stress, developed by Terzaghi and resulting in the equation

$$\sigma' = \sigma - u \quad 1.5$$

is described in all soil mechanics texts (see Bolton 1987, Craig 1992, Powrie 1997).

The pore water supports none of the shear load which must be carried by the soil skeleton. Changes in shearing resistance are due to changes in effective stress. The sands tested here have a high permeability which, combined with the strain rates chosen, allowed fully drained triaxial and direct shear tests to be carried out. The pore water pressure remained hydrostatic with a zero or minimal head resulting in all stresses derived from external measurements being effective stresses. Effective stress parameters are denoted by a prime.

1.2.9 Mohr - Coulomb and critical state

The shear strength (τ) developed on a plane within a granular material or a rock discontinuity can be represented by Coulomb's equation;

$$\tau = c + \sigma_n \tan \phi \quad 1.6$$

where ϕ is now described as the angle of shearing resistance and c is the cohesion intercept (possibly due to apparent cohesion) which is independent of the normal pressure σ_n . When a liquid phase (usually water) is present in a soil or rock the shear strength is expressed as a function of effective normal stress;

$$\tau = c' + \sigma'_n \tan \phi' \quad 1.7$$

The above is used in the interpretation (often graphical) of direct shear tests. It is not a satisfactory peak strength criterion for a geomaterial (see Brady and Brown, 1993) due to:

1. It is not always the case that a major shear fracture exists at peak strength
2. The implied direction of shear may not be that which is observed
3. Peak strength envelopes are often curved

The shear strength of a soil or rock in the triaxial test can be expressed in terms of σ'_1 and σ'_3 ;

$$\sigma'_1 = \sigma'_3 \tan^2(45 + \frac{1}{2}\phi') + 2c \tan(45 + \frac{1}{2}\phi') \quad 1.8$$

This is referred to as the Mohr - Coulomb failure criterion, a graphical construction may be used to produce the failure envelope of the geomaterial. A failure plane at an angle of θ to the major principal stress is predicted, where:

$$\theta = 45 + \phi'/2 \quad 1.9$$

Soil mechanics has attempted to develop failure criteria that are related to the basic soil properties of grain mineralogy and texture, and the primary state variables which are void ratio and stress. The above criterion makes no allowance for volume change, the suggestion being that the grains slide with no change in volume in the same manner as blocks in a simple friction test. However, dilation of dense soils and contraction of loose soils is a feature of shear. This was demonstrated by Casagrande, Terzaghi, Peck and Taylor (see Rowe 1962). Roscoe, Schofield and Wroth (1958) showed that grains reach a critical state void ratio specific to a certain normal pressure and this is independent of the initial void ratio.

Dilation is now held to be responsible for the peak strength of granular soils (see Bolton 1991, Schofield 1998). Cohesion intercepts are considered to be due to extrapolation from a curved envelope. It is the secant ϕ' values that are important not the tangent ϕ' values; the conventional tangent parameters (c' and ϕ') are able to describe the full range of a soils strength only if both are allowed to vary with density and stress. Bolton (1986) correlated the increased angle of shear of dense sand with its dilation rate. This allowed the construction of a dilatancy index derived from the sands relative density and the

mean effective stress applied to it. Powrie (1997) gives details of why the peak strength criterion should not be used in design with soils.

Traditional strength theories cannot be applied to rock due to the concave down nature of the τ vs σ_n envelopes. Highly empirical criteria are used usually with a power law (Brady and Brown 1993) such as;

$$\sigma_1 / \sigma_c = 1 + A(\sigma_3 / \sigma_c)^k \quad 1.10$$

Fissured rock may be significantly strengthened by small confinement pressures which equations such as 1.8 may not be able to predict. Increases in strength of 10 times the amount of a small confining stress have been reported (Goodman, 1989)

1.2.10 The effect of structure on the shear strength of sands

As already discussed, sands develop both bonded and fabric structure over both engineering and geological time scales. At some point on the spectrum from normal sand to a sandstone both the cohesive intercept and the peak strength must be incorporated in design. Although bonded structure, often in the form of artificially cemented sand samples, has been extensively investigated (Clough et al 1981; Coop and Atkinson 1993) fabric structure has been neglected until very recently. Clough et al (1981) concluded that a weakly cemented sand shows a brittle failure mode at low confining pressures with a transition to ductile failure at higher confining pressures.

Leroueil and Vaughan (1990) reviewed the effect of structure on sands concentrating on the effects of bonded structure. They demonstrated that the effect of structure is as important as the initial void ratio and stress history. DeFreitas (1993) reported that geotechnical studies appeared to demonstrate that the mechanical behaviour of structured sands was dominated by bonding between grains and influenced by grain mineralogy.

Dobereiner and deFreitas (1986) whilst investigating weak sandstones concluded that samples with a saturated unconfined compressive strength of less than 20MPa failed by the rolling of clasts. The confining pressure was important; without it they were weak.

Cuccovillo and Coop (1998 and in press) investigated the effects of both fabric and bonding structure by comparing the behaviour of two sands; one with a natural carbonate cement and the other with an interlocked fabric. The latter sand however needed a rubber pestle to disaggregate it and would therefore have had a large amount of cohesion when tested as an intact material. It would also not fit into the category of a locked sand as defined by Dusseault and Morgenstern (1979). Cuccovillo and Coop (in press) concluded that sands in which the structure arises predominately from an interlocking fabric and in which bonding is weak would have a shear behaviour that is largely frictional. They also suggested that this behaviour cannot be described by a conventional soil mechanics framework based on the behaviour of recompacted materials or by a framework used to describe bonded sands. A sand with fabric structure was shown to dilate more than a disaggregated sand even if an adjustment was made for the difference in density.

Apart from the work of Barton et al (1986) and Richards and Barton (1999) no tests appear to have been carried out on a sand with no, or minimal, grain bonding but with a degree of fabric strength.

CHAPTER 2: FIELD SAMPLING, SAMPLE PREPARATION and IMPREGNATION

2.1 Block sampling

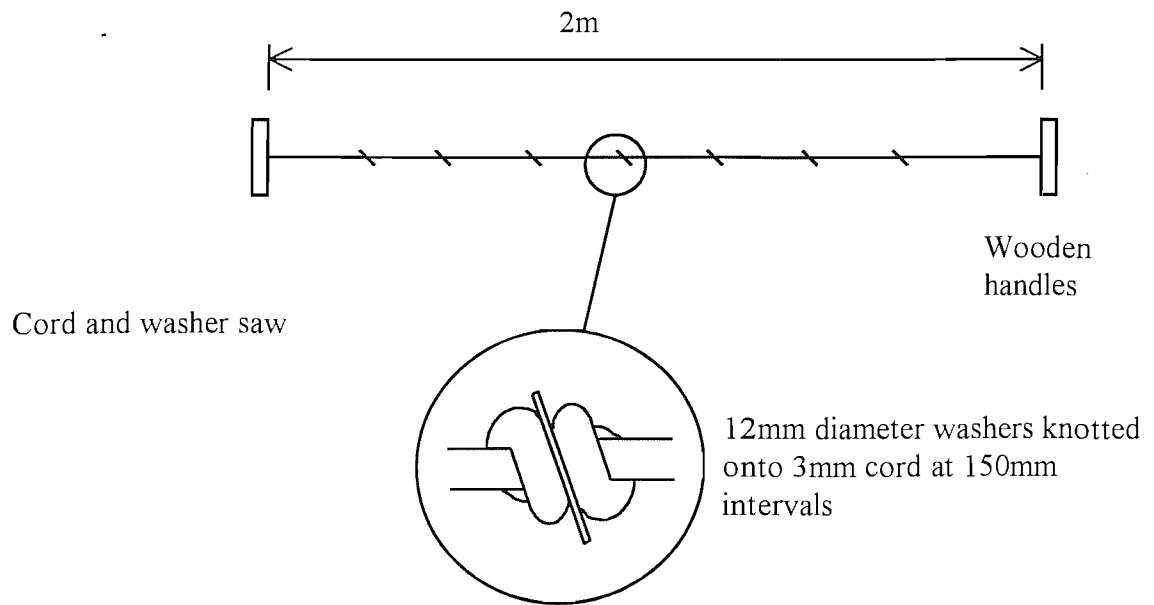
2.1.1 Introduction

Extracting intact blocks of A2 from the Park Pit was problematic. Barton and Palmer (1990) had developed a collapsible-sided box that allowed a brittle sample to be easily contained and a small confining pressure applied. These were used and found to be adequate for a material with very little cohesion. Problems however were also encountered in cutting the material out from its insitu position. Although a 5mm layer could be easily shaved off A2, it resisted impact to a remarkable degree due to its high density and stiffness; grains will only move if they have somewhere to move to. A scraping technique was used to remove a layer of sand with each pass; the chisel end of a geological hammer being the usual tool utilised for this (see Barton and Palmer 1990). Scraping was time consuming and physically tiring, only small amounts of block sampled material could be removed in one day.

The obvious method to speed up this process was to use some form of saw. Problems were encountered if a standard saw, with either hardened steel teeth or surface set diamond, was used:

1. The sand dilated when it was disturbed. This bound onto the blade preventing it moving. The problem was made worse by the sand being damp and therefore not flowing out of the saw groove.
2. A saw that required a frame or was not rigid could not make cuts into a blank face.
3. Detaching the block by making the final base cut was very awkward and often resulted in loss of the sample.

To overcome these problems two saws were developed (figure 2.1); the first a modification of the traditional wood saw design, the second based on a wire saw design. The criteria for the two saws are as follows.



Wide set scraper saw

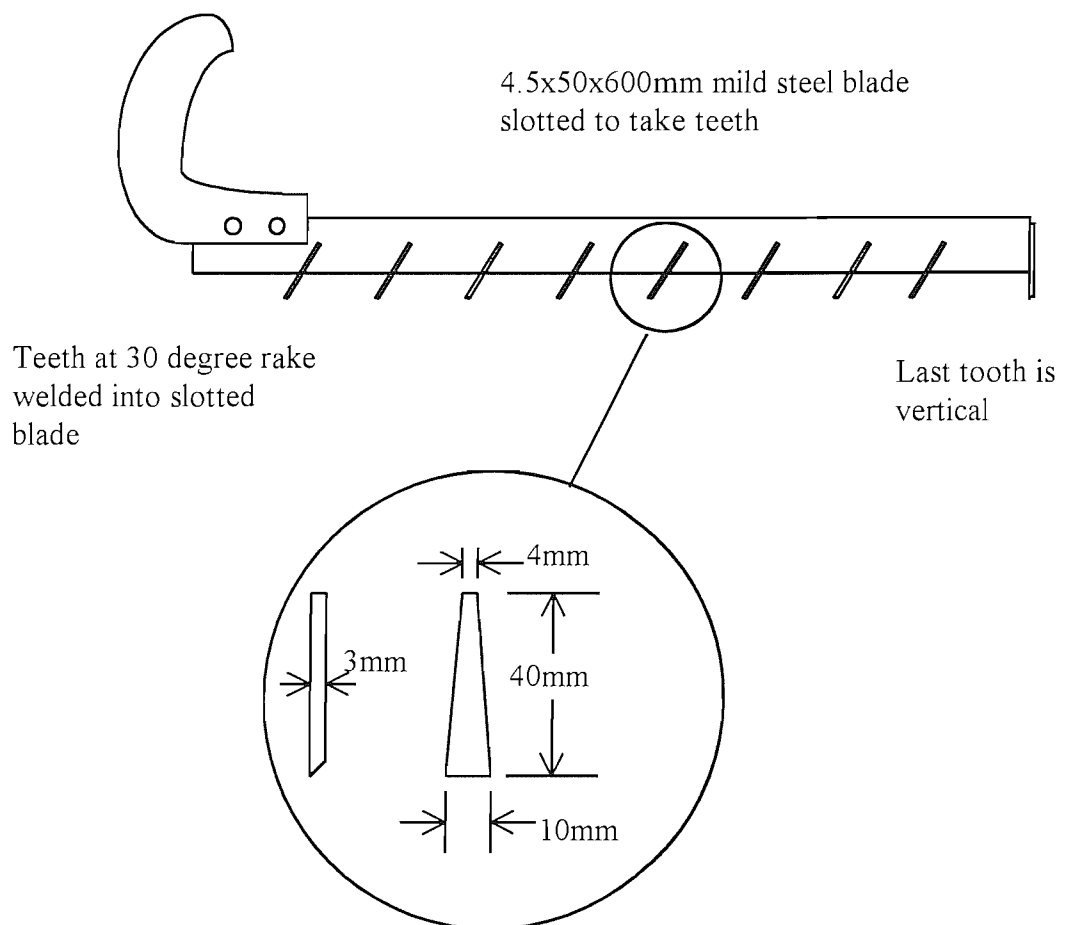


Figure 2.1 The two saws developed for extracting intact samples of a highly dilatant locked sand with very little cohesion.

2.1.2 Wide-set scraper saw.

1. The saw cut must be much wider than the saw blade to prevent binding, this was achieved by giving the teeth a wide “set” of 10mm compared to the blade thickness of 4mm.
2. From observations when using the chisel on a geological hammer; saw teeth should be chisel-like with a rake of 30 degrees.
3. The teeth should be widely spaced to prevent clogging.
4. To allow the saw to cut into a blank face it must be rigid and have a right angle “dog” tooth at its extremity to remove material from the end of the cut. Teeth must also face backwards to remove material from a blind cut.

2.1.3 Cord and washer saw

1. This saw must be flexible enough to be passed around the back of the block to cut the block from its base.
2. As for the above saw the teeth should be widely spaced and considerably wider than the connection between them.

2.1.4 Extractive method

Figure 2.2 shows the two saws in use. The method was as follows:

1. The face was cleared of debris and weathered material using a spade
2. The scraper saw was used to make vertical cuts into the face (figure 2.2a). Unwanted material could be snapped off at this stage by using a lever (e.g. strong spade or bar) inserted into the cut.
3. The bottom of a block was detached by cutting with the washer saw (figure 2.2b). As this cut was made the block was supported with packed sand to prevent collapse.
4. If the block did not have enough strength to be picked up it could be slid onto a flat surface and from there to the sample box of Barton and Palmer (1993).

Using these methods and equipment 25 blocks of intact sand (dimensions 200x200x300mm) were extracted by two people in 3 hours.



Figure 2.2a The wide set scraper saw in use



Figure 2.2b The washer saw in use.

2.2 Hard shell

2.2.1 Introduction

Moving intact blocks of A2, even when air dry ($w = 0.12$ to 0.03%), posed problems. Often blocks of $150 \times 150 \times 200$ mm would collapse almost explosively into a granular aggregate. Unlike sands with some degree of bonding A2 did not become more stable as it was reduced in size to produce a test sized sample; it became less stable with diminishing size.

2.2.2 Hairspray

This problem was overcome by the use of hairspray to create a hard enclosing shell around the sample. Hairspray has the following advantages:

1. It is quick setting, only a small amount of heat is required to harden it within 20 seconds.
2. Non-toxic.
3. Inexpensive.
4. Easily available

The main ingredient of hairspray is octylacrylamide/acrylates/butylaminoethyl methacrylate copolymer. A 1-2 mm thick hard shell is produced that renders the sand proof against damage during handling. No other surface layer cementing media were tried due to the success of the use of hairspray. The assumption was made that the bonding agents did not migrate further into the material than the superficial hardened layer. No comparison was made between different hairsprays; all those used were found to be adequate. The method was not used in the field and it is considered that very dry conditions would be required for this to be successful.

The enclosing shell allowed small intact samples to be made. Details are given for 60×60 mm shear box samples and 38×76 mm triaxial samples in the relevant sections.

2.3 Pluviated sample preparation

2.3.1 Introduction

The results of tests carried out on an intact sand will show a component of strength due to the structure but will also show a component of strength due to the shape and friction properties of the disaggregated sand grains. Intact tests must therefore be compared to those carried out on the disaggregated material. The densities of intact A2 and A3 cannot be reproduced from their recompacted disaggregated grains, and any comparison has to be between intact sand and a sand at a lower density. It is obvious that the density used should be as high as it is possible to achieve without grain crushing occurring.

2.3.2 Why this investigation was instigated

The filling of shearboxes with granular materials to maximum density utilised a slow pour method that was highly unsatisfactory. The apparatus consisted of a funnel to act as a hopper and bung to regulate flow rate (figure 2.3a). This apparatus gave rise to two problems:

1. To achieve reliable results pouring had to take place very slowly, times of 40 minutes being usual for a 100mm square shearbox.
2. The apparatus could not be left unattended; the orifice produced by the bung against the side of the funnel was a narrow slit and this blocked very easily, requiring the funnel to be tapped to restart the flow.

In order to overcome these problems the fundamentals of slow pouring were explored and a simple and highly efficient apparatus for the production of high density sand samples developed.

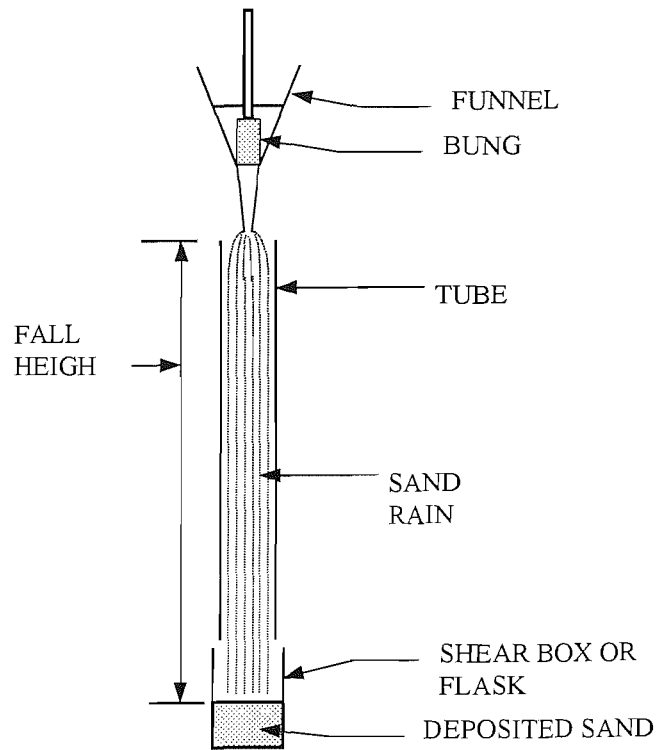


Figure 2.3a The original pouring apparatus

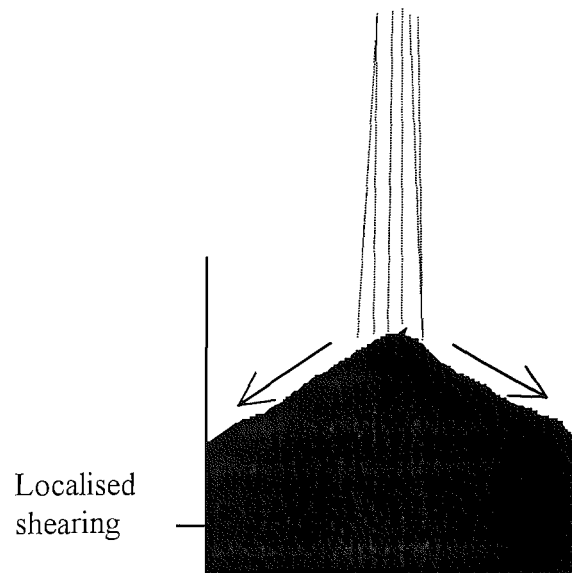


Figure 2.3b Slow pouring with a concentrated central stream

2.3.3 Past studies

Both a slow pouring method to achieve high density and a fast pour method to achieve low density in sand samples was developed by Kolbuszewski (1948). Granular materials in general often display complex and contra-intuitive behaviour. Various ‘normal’ methods of compaction such as vibration and tamping may produce the opposite result to that intended.

Kolbuszewski (1948) suggested that the density depends upon the height of fall of the sand and the rate at which pouring takes place. Pouring at a slow rate from a large height results in high and uniform densities and for any given height of drop; the density increases with time of pouring to some limiting value. Other, mechanical, methods however such as tamping or vibrating to achieve high densities result in grain crushing (Barton and Palmer 1990) and anisotropy within the sand mass. This anisotropy was called ‘inherent anisotropy’ by Arthur and Menzies (1972) differentiating it from the ‘induced anisotropy’ due to the applied stresses. For the above reasons various pouring methods have been used preferentially when forming uniform beds of sand for model foundation tests (Butterfield and Andrawes, 1970; Walker and Whitaker, 1967).

2.3.4 Observations of slow pouring

The apparatus of figure 2.3a produces variable densities for the same height of fall and rate of pour unless pouring is carried out slowly and carefully. It is suggested that this is due to flow taking different forms; either a concentrated stream or a spray. A large concentrated stream produces a depositional cone, this then collapses or, if the cone is at a smaller angle, a creeping surface develops, both of these result in areas of lower density (figure 2.3b). Smaller areas of concentrated flow may develop which do not produce cones and are thus difficult to observe but they also result in low density areas. This low density is caused by the areas involved being subjected to the equivalent of

quick pour where grains come to rest after sliding or rolling over subjacent grains. The spray form however results in a uniform rain and a high density. Kolbuszewski's (1948) apparatus used a cone with many orifices to produce uniform rain, it is possible that the apparatus was not very efficient at this as he found a relationship between fall height and density, which has not been confirmed by other authors. Head (1980) suggests that over 450mm fall, little change occurs to the density, which is reasonable as fine and medium sand will reach its terminal velocity before this length of fall. A uniform rain can be achieved by pouring from a great height therefore allowing time for any concentrated areas to break up. It is suggested that this is what was happening with Kolbuszewski's apparatus and it was the production of a uniform rain rather than a higher sand velocity that increased the density.

Pouring very slowly also removes the risk of any concentrated flow areas developing due to the sand spraying out of the nozzle (or if pouring extremely slowly individual grains exit the nozzle with different directions and velocities) rather than taking the form of a stream. It is suggested that the stream, formed when pouring faster than a certain rate, does not break up (unless a very large fall height is used) due to the sand dragging a column of air along with it and therefore remaining stable.

The production of an evenly distributed rain over the whole of the receiving container surface with the sand at or above terminal velocity is here referred to as pluviation.

2.3.5 Fundamentals of deposition during pluviation

Careful observation of the depositional surface during pluviation shows that a 'boiling' or energetic layer develops consisting of grains undergoing many elastic collisions (figures 2.4a and 2.4b). This layer shows grains moving rapidly with any displacement primarily in the horizontal plane and grains disappearing from view and reappearing again. It is 2 to 4 grains thick and in the photograph (fig. 2.4a) is visible as a paler

layer than the darker stationary sand below. Above this grains move with a large vertical component (several 10's of millimetres), these are grains that have bounced up from the surface or are grains that have being ejected from the surface by falling grains (see Bagnold 1941). These layers are only formed when a dispersed rain of grains is falling with sufficient energy. They are always present when high densities are being achieved at reasonably quick rates of pour and it is suggested that they are a requirement for achieving high densities quickly.

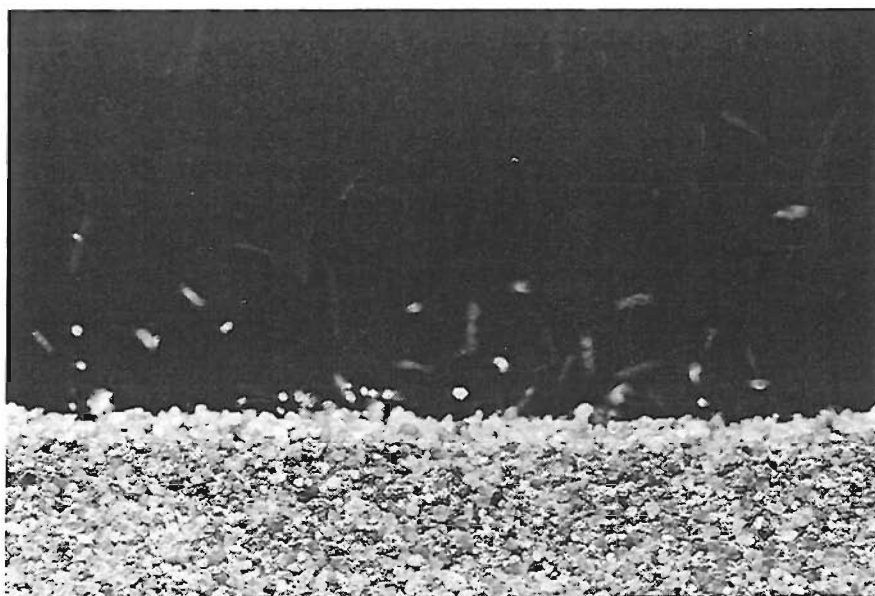


Figure 2.4a Photograph of deposition during slow pouring with the development of an energetic layer

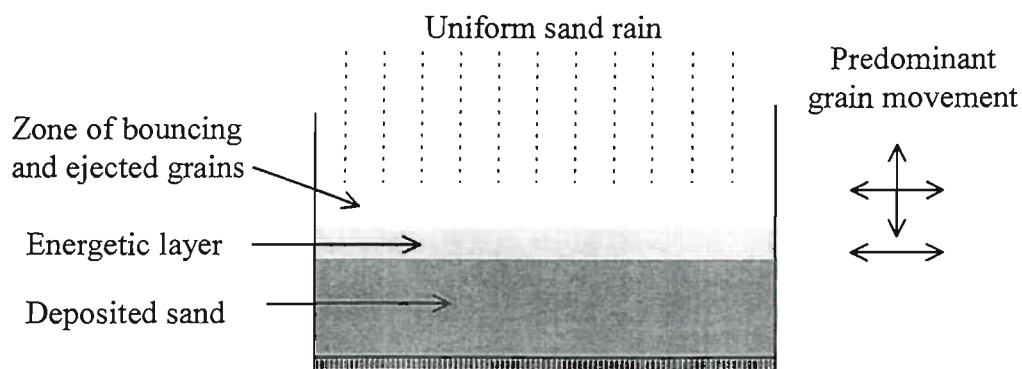


Figure 2.4b Deposition during slow pouring with the development of an energetic layer

The mechanism proposed here is that the energetic layer compacts the almost stationary layer below it by repeated individual impacts. Only when a grain has become almost stationary can it be wedged in a location until it is closely packed. These grains in the topmost 'stationary' layer undergo no translation but are rotated, vibrated and 'hammered' into a closely packed state by the energetic layer above. It is suggested that the similar size of the energetic grains to the near stationary ones allows this to occur; impacting larger particles would cause shearing i.e. displacement of the stationary grains relative to their neighbours and cause a lowering of density.

When pluviation occurs at *too slow* a rate for an energetic layer to develop the above model would predict a reduction in density. The near stationary layer will still undergo compaction by the falling grains and indeed the amount of energy available for this must always be the same for a certain height of fall, but the mechanism would not be as efficient. Individual grains will impact on the stationary surface grains and minimal horizontal displacements would be produced. When the rate of pluviation *is increased* until an energetic layer develops, falling grains impact with grains that are already in motion. The energy of these grains is then given to the energetic layer. It is the presence of layers of declining energy uniformly covering the whole surface that results in high density. Ultimately, at very slow rates of pour, a limiting density value slightly smaller than the one created by the energetic layer is predicted. Once the rate of pour is slow enough to eliminate interaction between grains set in motion by impacting grains any further reduction in pouring rate will have no effect.

The above varies from the traditional understanding in that energy is used to increase the packing density of particles no longer undergoing any relative displacement rather than being used to bury a falling particle in a high density location. This is shown by the presence of the moving layers; particles come to rest over a period of time after repeated interactions with other grains.

A similar process has been postulated by sedimentologists to explain the high relative densities in accretion deposits such as sand dunes (For example: Denekamp and Tsur-lavie, 1981). The newly formed layers of sand are bombarded by descending sand particles that are being transported by a mechanism known as saltation where grains move in short jumps. These repeated impacts result in a dense sand mass.

2.3.6 Modifications to the slow pour apparatus

IN the light of the above ideas, modifications to the slow pour apparatus were made. Details are shown in figure 2.5. The important changes were;

- The introduction of several spreader meshes to separate the stream of sand and prevent any concentrated flow. The spacing of the meshes must be great enough to allow the falling grains to strike each mesh with enough energy to be deflected considerable horizontal distances before falling through the underlying mesh. Note that the first three meshes are closely spaced due to the energy available from the fall from the hopper orifice and also to prevent an individual wire in the top mesh deflecting the bulk of the stream to one side. The presence of several meshes within a short distance corrects this. A uniform rain is formed by the meshes and results in a very level surface of deposition. The uniform rain enables an energetic layer to form over the whole depositional surface at high rates of pour.
- A circular orifice of 3 to 4mm minimum size depending on the sand used - when lower rates of pour are required part of the flow is diverted by a flow divider before the spreader meshes and the excess is recycled to the top hopper. Dividing the flow enabled rates of deposition as low as 0.25mm/min to be achieved, this filling a half litre, 84mm high flask in 8 hours.

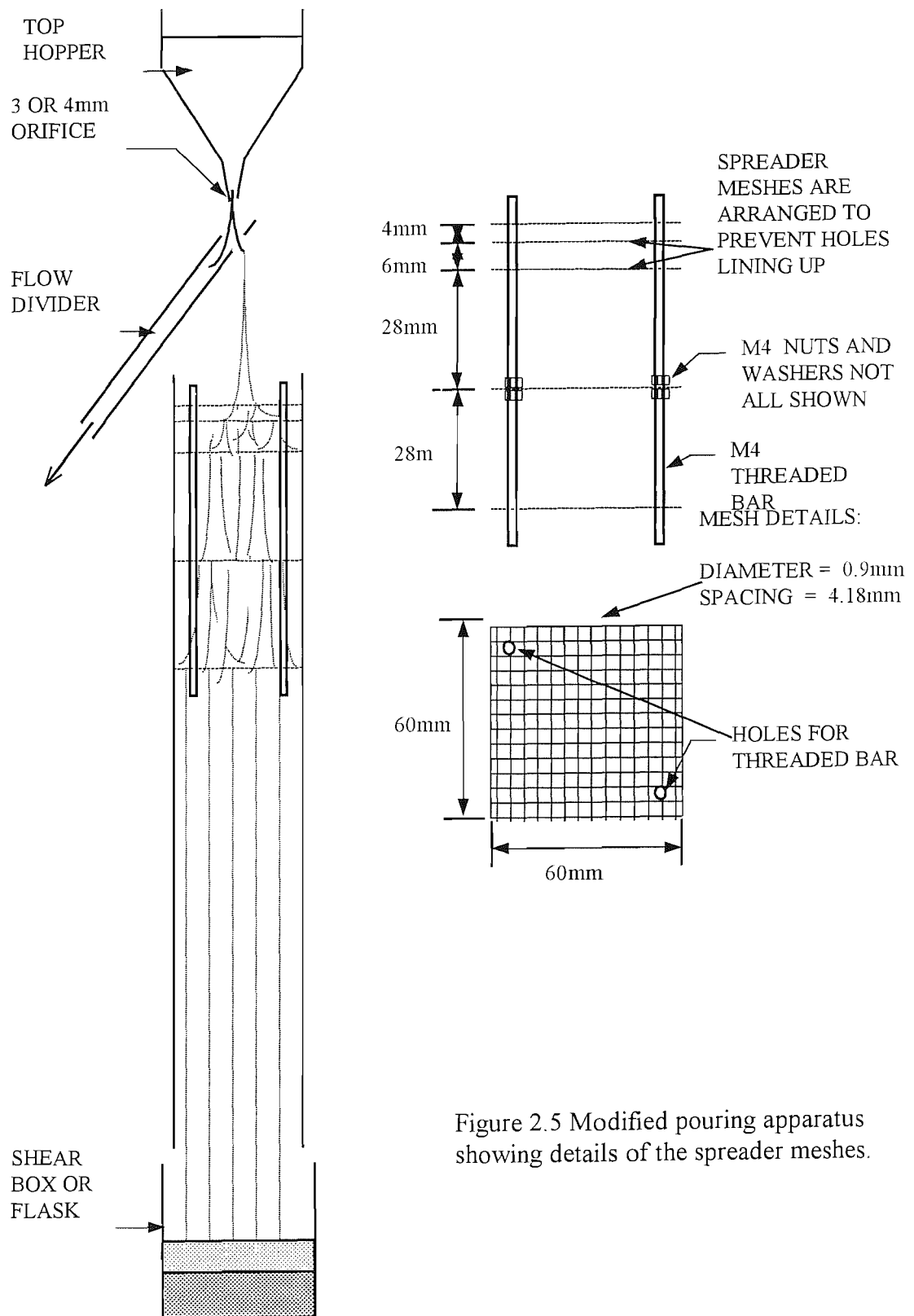


Figure 2.5 Modified pouring apparatus showing details of the spreader meshes.

2.3.7 The experimental method

The apparatus was then used to produce pouring rates varying between 0.1 and 240 minutes to fill the flask. Slower rates can be achieved by the apparatus but time considerations prevented this area being explored. The height of fall was kept constant at 560mm between the bottom of the hopper and the base of the flask. This entails some change in fall height during flask filling but was not considered important as it is small compared to the total fall. The density of the poured sand was found by weighing a flask of known volume after levelling the surface, this method was found to be surprisingly accurate and weights for the same pour times were repeatable to within 2 grams out of a total sand weight of 800grams. Reigate silver sand and Leighton Buzzard sand were used as examples of angular and rounded sands. These were prepared simply by sieving through a 1.18mm sieve to remove any particles that might clog the orifice. Grain size distribution curves for these sands are given in figure 2.6.

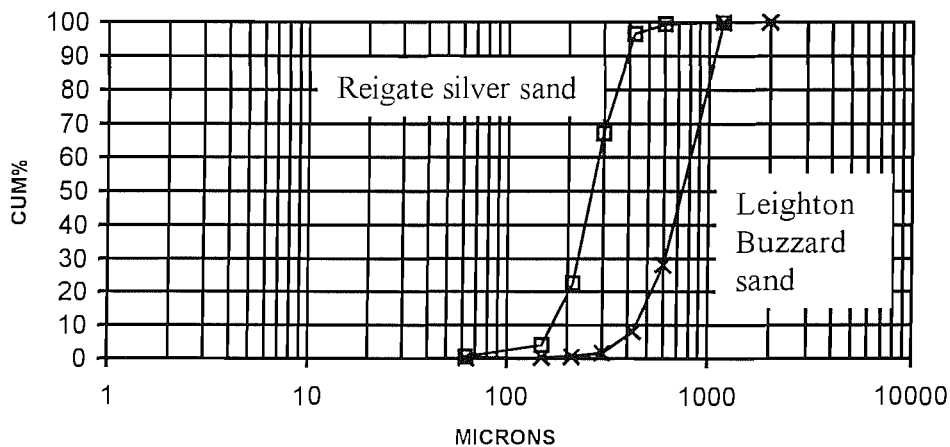


Figure 2.6 Grain size distribution for Reigate silver sand and Leighton Buzzard sand

Leighton Buzzard Sand was also used to compare pouring, using the apparatus of figure 2.3a giving a central stream, to pluviation using the apparatus of figure 2.5.

2.3.8 Results

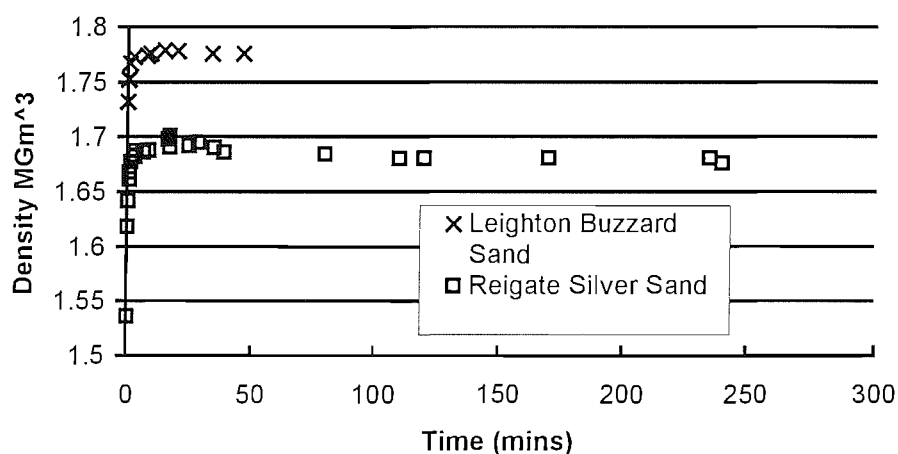


Figure 2.7 Density vs time of pour plot

Figure 2.7 shows the effect of variations in pouring rate on the density obtained for Reigate silver sand and Leighton Buzzard sand respectively (see Cresswell and Barton, 1999, for more extensive results). As predicted by the energetic layer model a slight peak in density is apparent especially in the Reigate silver sand. This is followed by the density remaining steady with further decreases in pour rate. Continued, repeated pouring using Reigate silver sand, with all other parameters remaining the same, was found to produce increases in density. This was possibly due to the sand being altered by the abrasive action of pouring (see Walker and Whitaker, 1967), literally ‘having its corners knocked off’. This does not affect the conclusion that the maximum density is obtained when an energetic layer is present. In fact in the case of both sands, near maximum density was reached with relatively quick pours of 3min to fill the flask which is equivalent to a rate of deposition of 27mm/min. Maximum density occurred at 25mins (equivalent to 3.2mm/min) for Reigate silver sand and

15mins (equivalent to 5.3mm/min) for Leighton Buzzard sand. The maximum density for Reigate silver sand using the modified apparatus was 1.701Mg/m³. This is still below 1.771Mg/m³ achieved using BS1377. However BS1377 involves the use of powerful vibrating machinery that produces obvious grain crushing.

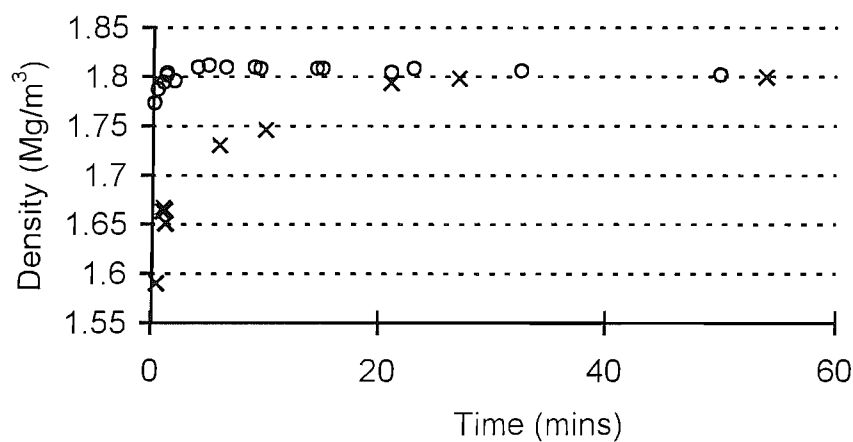


Figure 2.8 Comparison of pluviation and pouring for Leighton Buzzard sand

Figure 2.8 shows the difference between pluviation and pouring on the densities obtained for Leighton Buzzard Sand. Note how the plots come together at very long pour times; pouring very slowly (60 mins to fill the flask) gives the same density as quick pluviation (2mins to fill the flask). Pouring however does not quite achieve the maximum density of pluviation.

2.3.9 Conclusions and discussion

The modified apparatus proved to be completely satisfactory in producing uniform high density small sand samples quickly and with high repeatability. The limited preliminary study of how density varies with the rate of pour has confirmed the presence of a peak in the density versus time of pour graph and also that it is possible to achieve high densities relatively quickly. The energetic layer interpretation of slow pluviation has

been verified by observation and by its ability to predict the novel result of the peak in the density versus time of pour graph. Further work (Cresswell and Barton 1999)) has utilised this apparatus; it has performed satisfactorily and has also confirmed the presence of a peak density.

2.3.10 Consequences for uniform sand bed preparation

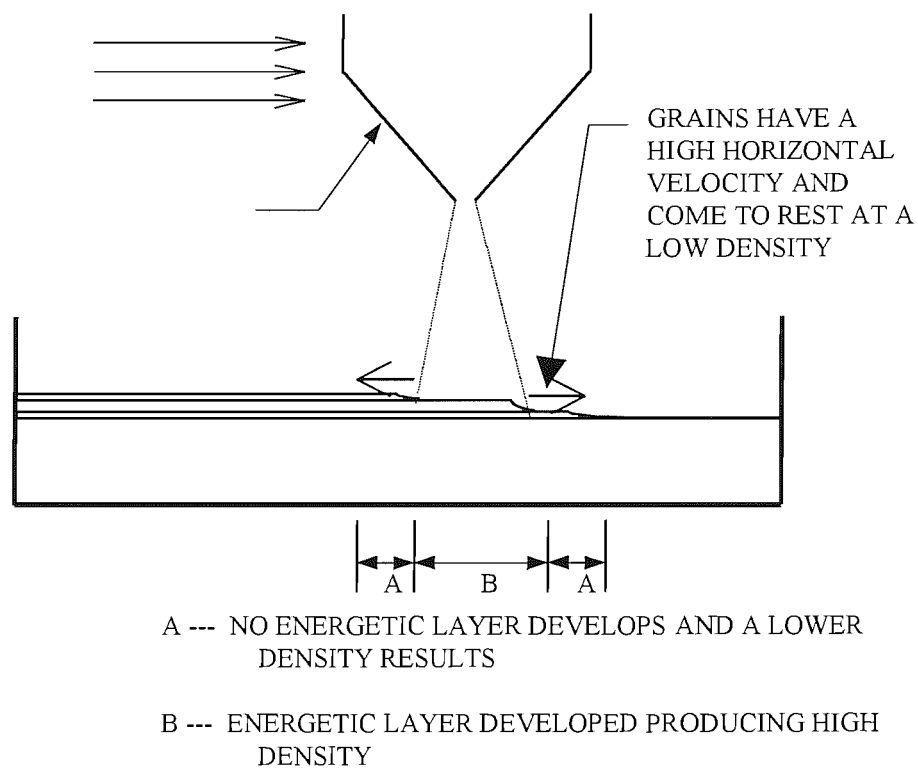


Figure 2.9 Explanation of the layering produced by the moving curtain method.

Laboratory scale soil experiments require the formation of uniform sand beds. These are usually formed in two ways; either a rain over the whole bed area or a falling curtain that traverses the bed. Very long fill times are reported with both methods and the moving sand curtain has an inherent defect in that it produces distinct layers that can be detected by X-ray techniques (Butterfield and Andrawes, 1970). Figure 2.9 shows a suggested mechanism for production of the reported anisotropy inherent in the falling

curtain method, (another possible source of anisotropy is the development of grain size heterogeneity due to the winnowing effect of the falling curtain). Directly under the curtain an energetic layer will be formed, in front and behind the curtain, the layer peters out with commensurate changes to the density produced. As the curtain traverses back and forth over the bed a layered structure develops. Although the energetic layer will pass over the grains that have come to rest after having a high horizontal velocity, it may not be able to condition them to the same high density as that produced under the centre of the curtain. The problem is exacerbated by the low density layer being the combined thickness of the grains ejected behind the last pass and the grains ejected in front of the current one.

The above results show that a pouring apparatus designed to produce an energetic layer covering the whole of the bed surface will be able to prepare isotropic beds to near maximum density at rates up to 25mm/min. It is suggested that the fluid like behaviour of the energetic layer will ensure that the whole of the bed is homogeneous and isotropic; it is also suggested that to a small extent a well developed layer is able to flow into any corners and other areas where the rain is not present.

2.3.11 Development of insitu density

Some reported insitu densities are very high, with relative density values of over 130% (Barton and Palmer, 1989). The mechanism given above may be helpful in explaining this phenomenon as being in part contemporaneous with deposition. The energetic layer produced by the apparatus above can only impart so much conditioning to the stationary top layer before more stationary grains are deposited. However in nature saltating grains, for example, can condition the top surface for an unlimited period resulting in very high densities.

2.4 Impregnation methods

2.4.1 Introduction

Impregnation with colour dyed resins before thin sectioning to investigate porosity and microfracturing is a standard petrographic technique. Epo-tec 301, a two part cold setting epoxy resin (supplied by Promotech, Cirencester, Glos., GL7 1YS) was used for both the intact and the sheared samples. Details of the methods employed are given in Palmer and Barton (1986) and the references quoted there.

Intact samples were vacuum impregnated using a Logitech vacuum impregnation unit. This allows a vacuum to be applied to the resin before it is poured onto the sample as well as applying a vacuum to the sample itself. This is a convenient method of impregnation requiring less care than the drip method. The application of a vacuum whilst applying the resin is not necessary with A2 and A3, as capillary forces are sufficient to draw the resin into the sample if an escape route is provided for the pore air, and the drip method is sufficient.

2.4.2 Direct shear sample impregnation

Impregnation was used to produce thin sections showing the shear zone and other structures developed during shearing. The methods used for the intact samples were not suitable for impregnation of the sheared samples; any movement of the shear box would disturb the shear zone so the use of a vacuum chamber was prohibited. The sample was therefore impregnated whilst the sample and the shear box were still in the shear box apparatus.

When using this non-vacuum method of impregnation it was important to provide a route for any air to escape. If this was not done, air was trapped, capillary forces were overcome by air pressure within a shrinking “bubble” and a pocket of non-impregnated sample resulted. The resin was therefore applied in the centre of the sample in a shallow reservoir or dribbled onto the centre line of the sample; both of these allowed air to escape.

The method employed a small diameter reservoir of resin placed on the surface of the sample (figure 2.10). The head in this reservoir was kept below 5mm so that capillary forces could draw the resin in to the sample without any saturated flow taking place that would allow resin to escape from the sample. Any resin escaping from the sample would adhere to the shearbox itself resulting in great difficulty in extracting the impregnated sample from the box and long clean up times. When applied carefully the resin did not penetrate the pluviated edge to any appreciable extent. This was considered due to the pluviated edge having a greater void ratio than the intact material, producing a higher matrix potential. During unsaturated conditions, given that other potentials remain constant, liquids will not flow from an area of low matrix potential to one of high matrix potential.

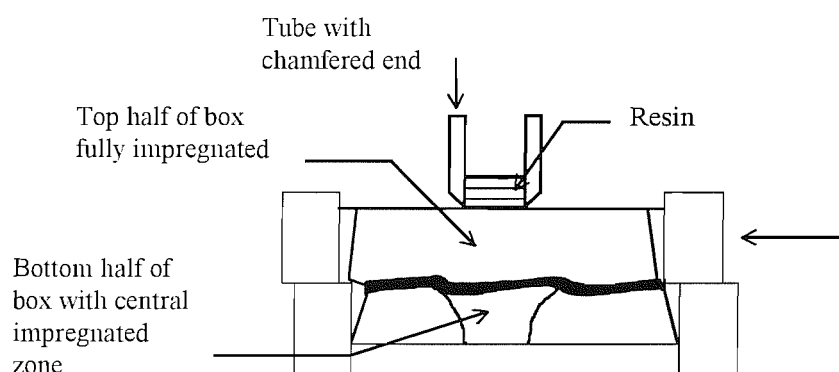


Figure 2.10 Impregnation of shearbox sample using reservoir

This however did cause problems in trying to get the resin into the shear zone and below it into the intact material in the bottom half of the box. The shear zone, compared with the intact material, was either of higher void ratio in the case of low and medium pressure tests or of lower void ratio in the case of high pressure tests where grain crushing had occurred. Both of these created an interface involving the resin having to move from a lower void ratio (low matrix potential) to a higher void ratio (high matrix potential) if it was to progress into the lower half of the sample.

Oda (1998) reported difficulties in impregnating the shear zone: he used an injection method but it is possible that capillary forces were the dominant mechanism by which the resin progressed through the sample.

2.4.3 Method of impregnating direct shear samples

1. The jack was stopped at the point required.
2. The vertical load and the shear load were removed simultaneously whilst trying to keep the sample from further dilating or contracting. This was made difficult by the elastic energy stored in the apparatus.
3. The lid and top platen were removed.
4. A 25mm diameter metal tube with a chamfered end was placed in the centre of the sample and gently rotated to seat it 1mm into the surface (figure 2.10).
5. 23g of resin was poured into the tube over a period of 20 minutes; never allowing the head of resin to reach more than 5mm.
6. The resin was left overnight to set.
7. The shearbox was removed from the apparatus and the bottom half gently split from the top. The bottom half of the sample was left adhering to the top half by a large central bridge of resin that had penetrated the shear zone. The whole sample was usually attached to the top half of the box by several small bridges of resin that had crossed the pluviated layer .
8. The top half of the box, containing the sample, was inverted and resin applied to the bottom of the sample, starting at the centre, to impregnate any areas remaining.
9. If the resin had bridged the pluviated edge in several places, removing the sample from the top half of the shear box was facilitated by heating the box to 80°C using a hot air gun.
10. Thin sections, through the centre of the sample, running parallel to the direction of shear, were produced in the usual manner.

2.4.4 Results and recommendations

The thin sections of the sheared samples are shown in the direct shear section. They provide visual evidence of grain crushing, shear zone thickness, and the orientation of secondary shears/tension cracks. Several problems of interpretation arose due to incomplete impregnation of the tension cracks: these are discussed in the direct shear section. This method also requires the loads to be removed and therefore the possibility that the shear zone has been disturbed arises. Information on the shear zone thickness and morphology must be reliable to the extent that the shear zone is observed as surrounded by intact material and only small scale adjustments could have occurred on removal of the loads.

An obvious recommendation is the impregnation of the sample with the loads still in place. This is explored in detail for the triaxial apparatus in the section on recommendations for further work and is envisaged to require the use of an interim cementing agent.

CHAPTER 3: THE TESTED MATERIAL - REIGATE SILVER SAND, AND QUARRY STABILITY

3.1 Reigate Silver Sand

3.1.1 Stratigraphical position

The Reigate Silver Sand lies within the Folkstone Beds which is the uppermost formation of the Lower Greensand. Stratigraphically it is located at the top of the Lower Cretaceous system in the Lower Albian stage. The stages of the Cretaceous are named mainly from France, however the local lithological terms fit into these fairly well (Rayner 1981). In the Wealden outcrops of south east England the Lower Greensand spans the Aptian and the Lower Albian with the Folkstone Beds representing the Lower Albian, see table 3.1.

Stratigraphical stages	Lithological divisions of the Lower Greensand at the Weald and neighbouring areas
Lower Albian	Folkestone Beds
Upper Aptian	Sandgate Beds
	Hythe Beds
Lower Aptian	Atherfield Clay




Table 3.1 Stratigraphical position of the Folkstone Beds

The stratigraphical palaeontology of the Lower Greensand has been covered in detail by Casey (1961). The Lower Greensand in Britain consists of up to 250m of near shore sediments. These have been deposited in a variety of shallow marine

environments and detailed zoning of the stages has been possible due to the fossil rich nature of most of the beds.

3.1.2 The Silver Sand - A2 and A3 - location and characteristics

Geotechnical investigations into the Lower Greensand, especially the Folkstone Beds (Richards 1992, Richards and Barton, 1999), have identified certain sands that stand as steep cliffs and vertical quarry faces. These vertical faces remain stable during periods of rainfall and do not fail by slump or topple mechanisms but erode as individual grains. Direct shearbox tests produce ϕ' angles of up to 65° with low cohesion intercepts; hand samples can be disaggregated easily by finger pressure. These dense sands can be classed as locked and cemented sands using the classification system of Barton et. al. (1993).

Two particular locations (20m apart) from the A.R.C. Park Pit Quarry, Buckland, Reigate, (TQ 225507), here designated A2 and A3, were chosen for this study because they contain beds of the well known Reigate Silver Sand (RSS) which was considered to be the best material to use in the investigation of strength due to an interlocked fabric. They contained less kaolinite than the Reigate Silver Sand investigated by Richards (1992) and fulfilled the following criteria:

1. Zero matrix and cement for A2, trace cement for A3
2. ϕ' of 65 degrees at low normal loads
3. Apparently isotropic and homogeneous
4. Block sampling is possible with care

These criteria implied that the strength of the material was coming predominantly from the interlocked fabric and not from any bonding between grains. This was emphasised by estimated tensile strengths of less than 5kPa and such small amounts of cohesion that hand specimens could be quickly eroded by gentle brushing. The uniformity of the material chosen would be of obvious benefit, the only problem being the difficulties of intact block sampling and sample preparation. A2 has no

visible cement in thin section, A3 has trace amounts of iron minerals at grain contacts and these are thought to be responsible for its greater cohesion. It was found possible to form right 100mm diameter cylinders of A3 for uniaxial testing.

3.1.3 A2 and A3 - description and index tests

Visually A2 is silver in colour whereas A3 is pale gold. The gold colour of A3 is thought to be due to the iron minerals and is distributed in bands of varying intensity from 2mm to 300mm wide. These are discussed later. The more homogeneous areas of A3 were chosen for testing. Grain size distribution is shown in figure 3.1. A2 and A3 are well sorted with a mean grain size of 0.25mm. A3 shows a slightly greater amount of fines.

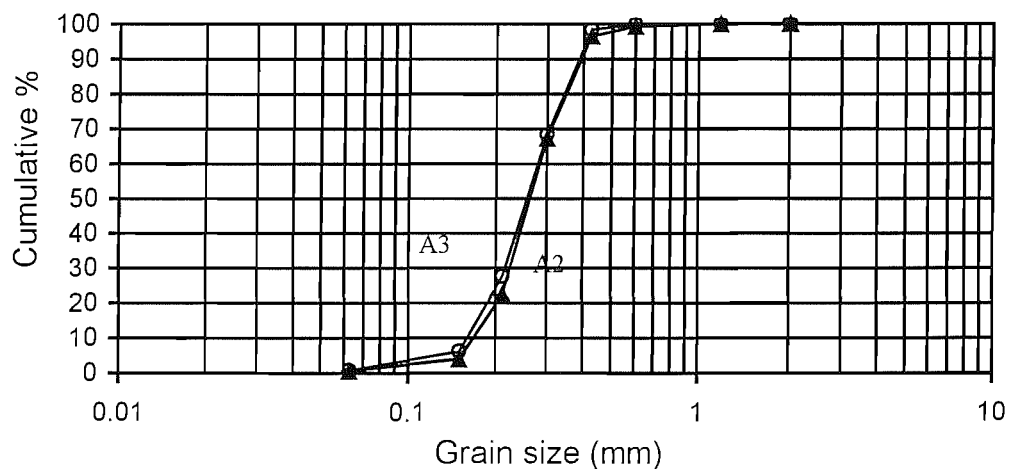


Figure 3.1 Particle size curves for A2 and A3

Dry insitu density was measured by coating a minimum of three intact samples with resin and immersing:

$$A2 \quad \rho_{d \text{ insit}} = 1.862 \pm 0.003 \text{ Mg/m}^3$$

$$A3 \quad \rho_{d \text{ insit}} = 1.796 \pm 0.003 \text{ Mg/m}^3$$

Minimum dry density from the rising tube method of Walter et al (1982):

$$A2 \quad \rho_{d \min} = 1.401 \pm 0.002 \text{ Mg/m}^3$$

$$A3 \quad \rho_{d \min} = 1.394 \pm 0.002 \text{ Mg/m}^3$$

Maximum dry density from a dry pluviation method (see chapter 2):

$$A2 \quad \rho_{d \max} = 1.701 \pm 0.002 \text{ Mg/m}^3$$

$$A3 \quad \rho_{d \max} = 1.667 \pm 0.002 \text{ Mg/m}^3$$

Relative density is the relationship of the dry density (ρ_d) to the limiting dry densities.

Relative density (D_r) of the intact sand was calculated from:-

$$D_r = (\rho_{d \text{ intact}} - \rho_{d \min}) / (\rho_{d \max} - \rho_{d \min}) \times (\rho_{d \max} / \rho_{d \text{ intact}})$$

Giving: A2 $D_r = 140\%$ and A3 $D_r = 136\%$

3.1.4 A2 and A3 - grain mineralogy and morphology

Freshly disaggregated A2 is shown in figures 3.2 and 3.3. Thin sections of A2, figures 3.4 and 3.5 show that grain mineralogy is virtually 100% quartz with only a trace of opaques. The vast majority of grains are monocrystalline with non-undulatory extinction, only 1 to 2% are polycrystalline. Grain fracturing is abundant, with the fracture often originating at or near a contact. Grain morphology varies from high sphericity, rounded grains to angular, highly non-spherical grains with embayments and fractures (figures 3.5 and 3.6). Some of the grains show euhedral morphology even though they are up to 0.25mm in size, others have features (figure 3.7) such as long noses or necks.

Note that the fines consist predominately of euhedral tabular or bladed grains (10 - 100 μ m). The number of fines is exaggerated compared to the number of grains visible in photographs 3.2 and 3.3. Fines are tightly clustered at grain contacts and

are not easily observed on the surface of intact blocks. They are visible on a rare aggregation of several grains as shown in fig.3.8.

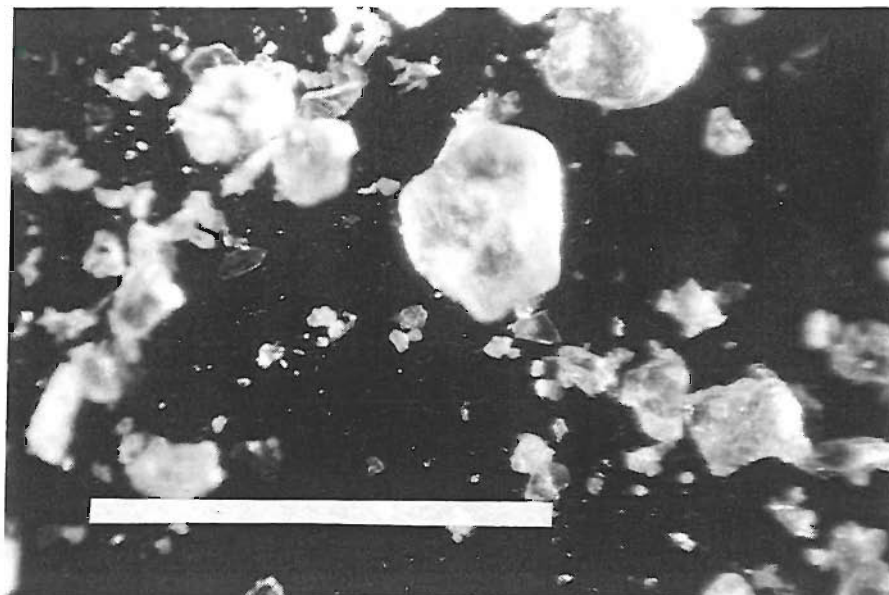


Figure 3.2 Freshly disaggregated A2. Scale bar is 1mm

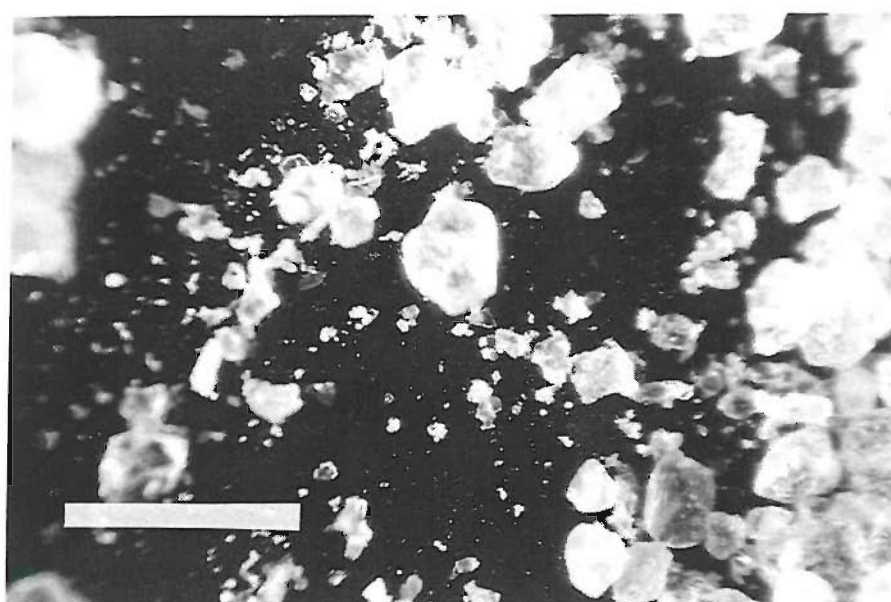


Figure 3.3 Freshly disaggregated A2. Scale bar is 1mm

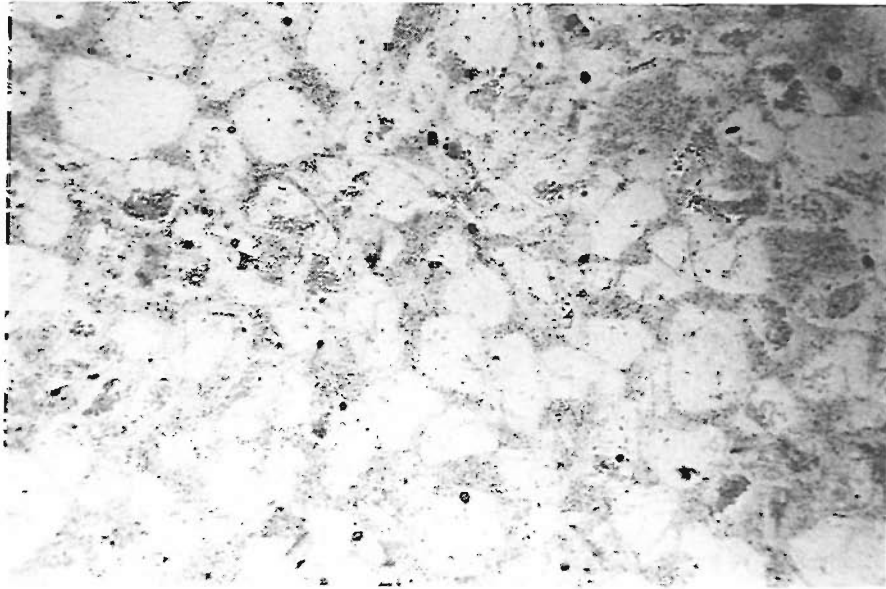


Figure 3.4 Thin section of A2. PPL, field of view 3mm.

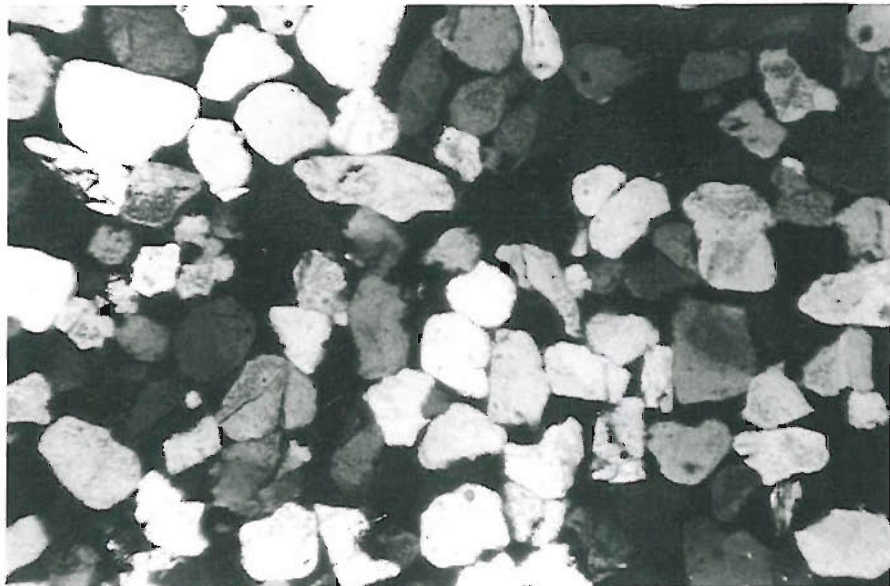


Figure 3.5 Thin section of A2. XP, field of view 3mm.

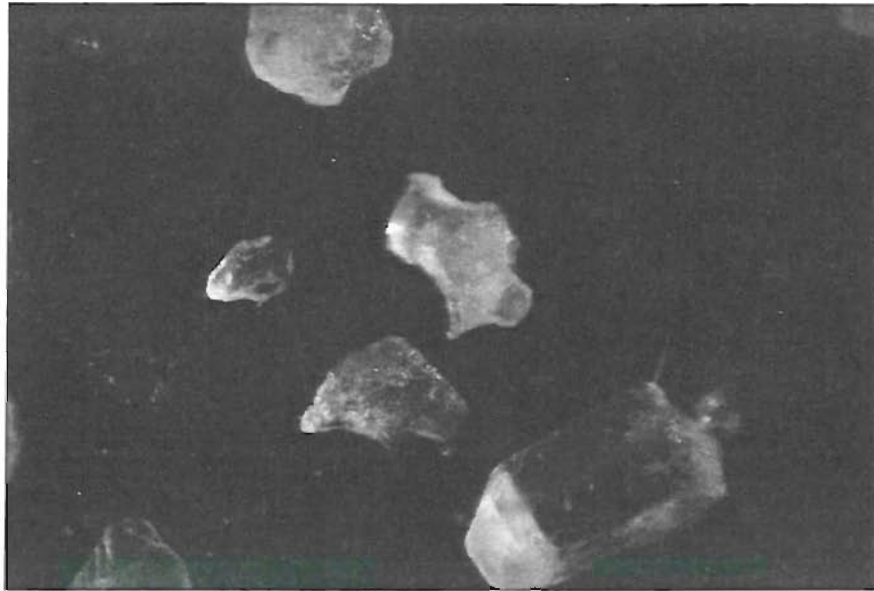


Figure 3.6 Angular, highly non-spherical grains with embayments and fractures, field of view 2mm.

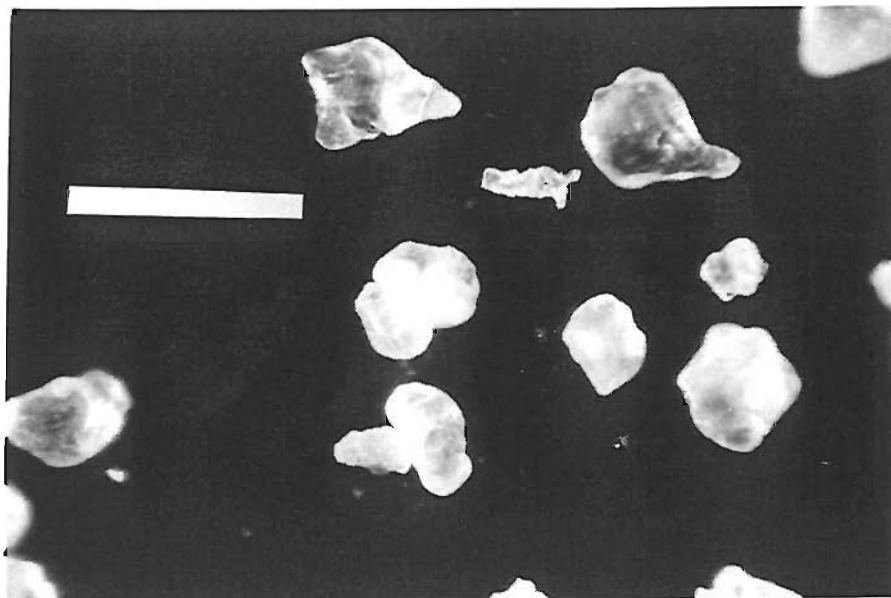


Figure 3.7 Grains with long noses or necks, field of view 3.7mm.

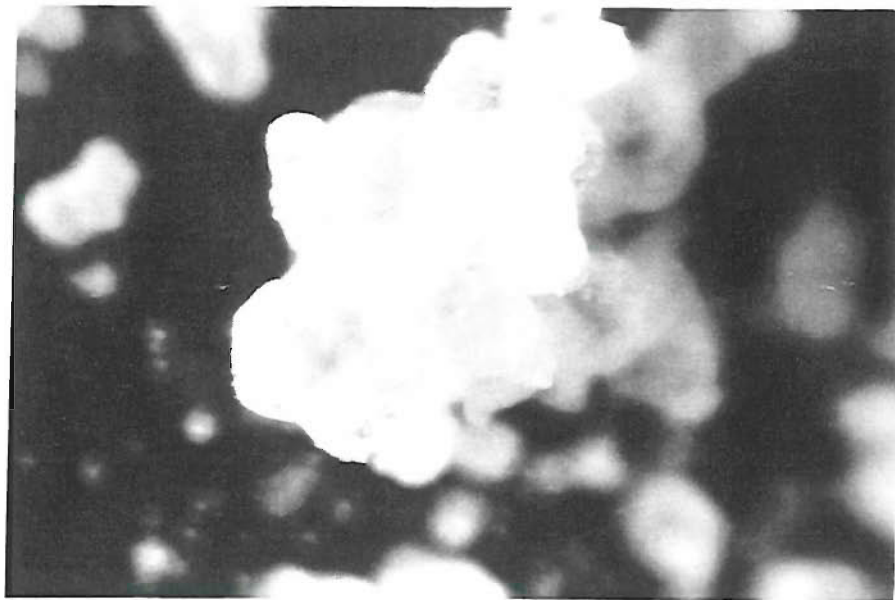


Figure 3.8 A rare aggregation of A2 showing fines clustered at grain contacts, field of view 2mm.

Disaggregated A3 is shown in figs. 3.9 and 3.10, these are similar to those of A2. Thin sections of A3 (figs. 3.11, 3.12 and 3.13) are also similar but occasionally show opaques (iron oxide minerals) and clay minerals at grain contacts. Richards (1992) explored in detail the distribution of these minerals and identified the clay component as being predominantly kaolinitic. These minerals are not present in the sections of A2.

3.1.5 Grain surface texture

Two grain surface textures predominate; glassy on transparent grains and rougher on more opaque grains. Some grains show an almost brain like surface; these are possibly due to radiolaria skeletons mimicking terrigenous grains (Tucker 1991). Electron micrographs of Reigate Silver Sand by Richards (Richards 1992) also show the grains as having surfaces that vary widely in texture.

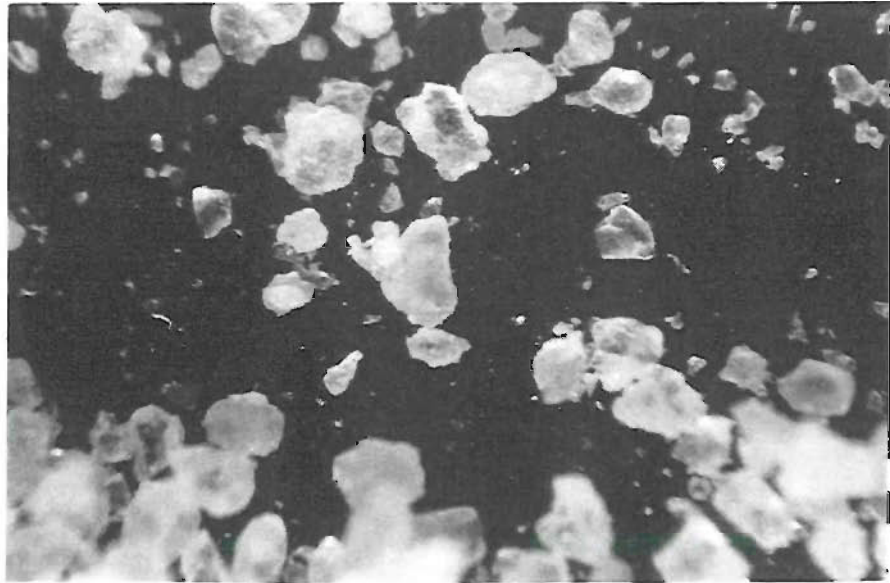


Figure 3.9 Freshly disaggregated A3, field of view 3.7mm.

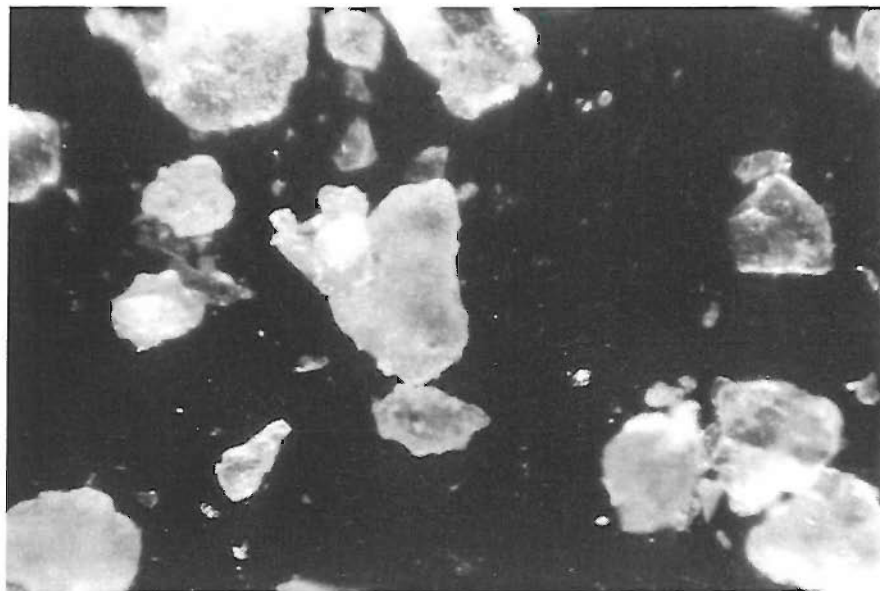


Figure 3.10 Freshly disaggregated A3, field of view 2mm

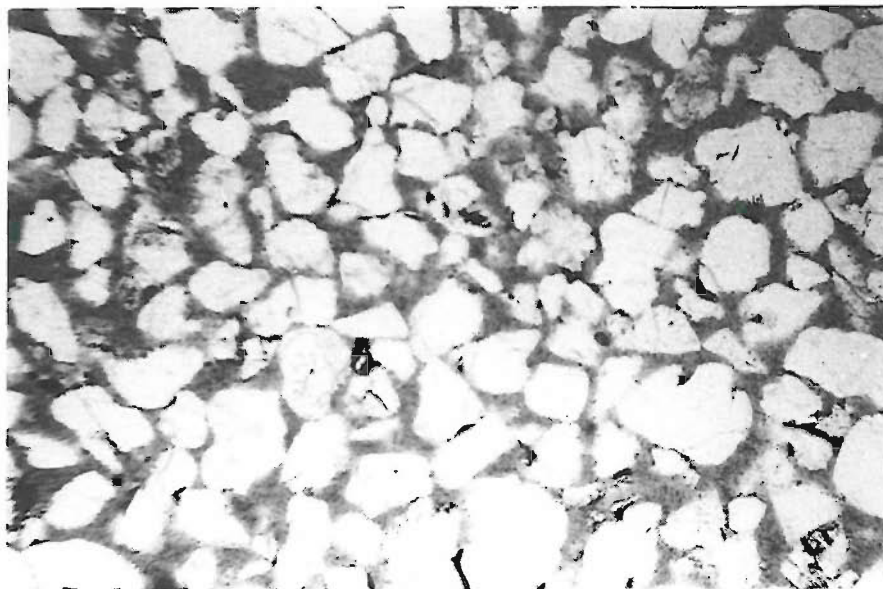


Figure 3.11 Thin section of A3. PPL, field of view 3mm.

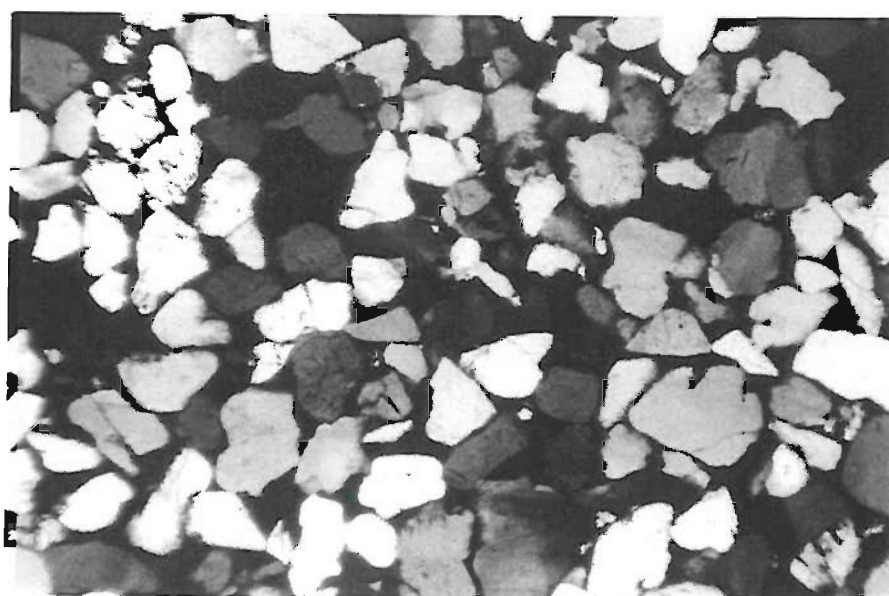


Figure 3.12 Thin section of A3. XP, field of view 3mm.

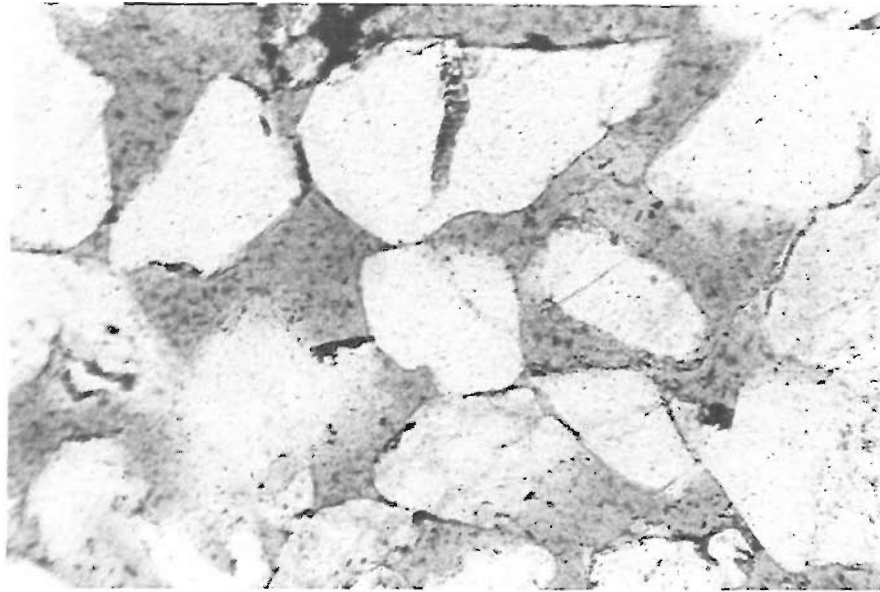
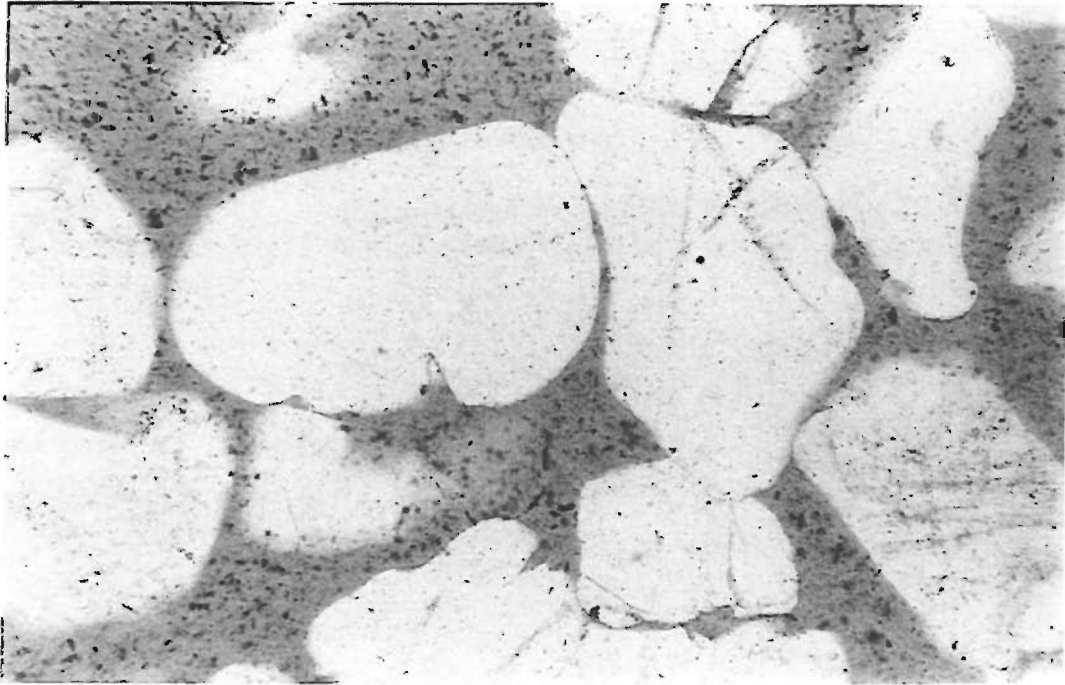


Figure 3.13 Thin section of A3 showing iron oxide and clay minerals at grain contacts. PPL, field of view 1mm.

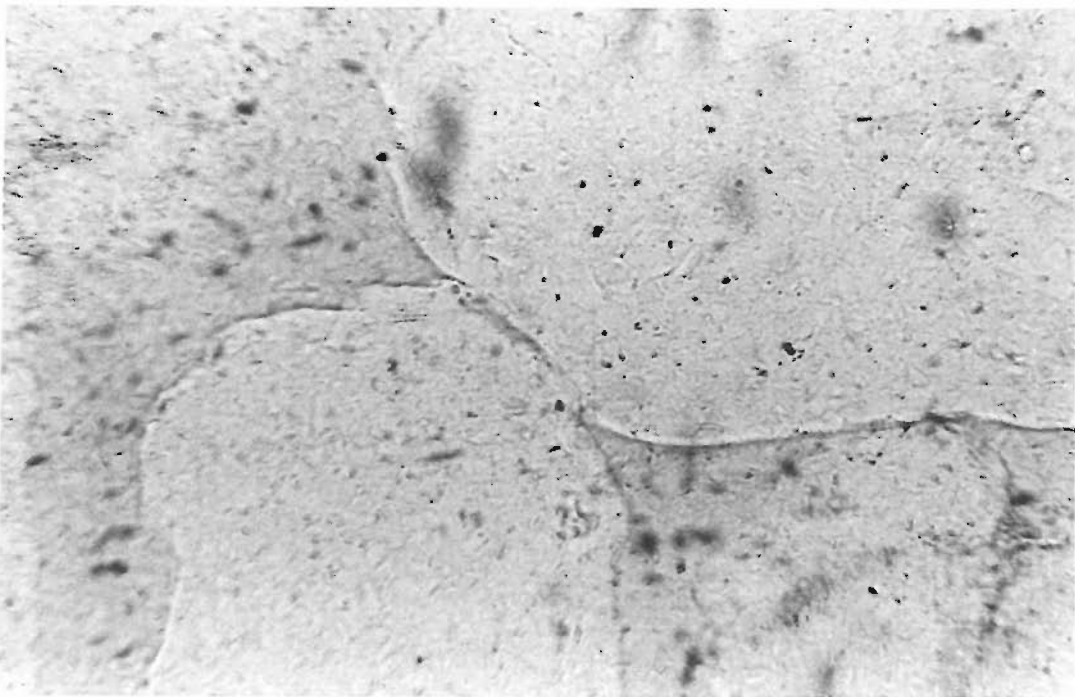
3.1.6 A2 and A3 grain contacts

The grain contacts of A2 and A3 (fig.3.14 and 3.15) are dominated by straight and concavo-convex contacts, resulting in a very low tangential index of 26%. Figure 3.15 shows an amount of interpenetration has occurred, and at these magnifications micro - suturing is just visible.



G1

Figure 3.14 Thin section showing grain contacts dominated by long/straight and concavo-convex contacts, field of view 1mm.



G1

Figure 3.15 Interpenetration and micro-suturing at grain contacts, field of view 0.5mm.

3.1.7 Spicules

The most striking feature of A2 is the presence of thread like forms within the intact material (figure 3.16). These are approximately 10-30 μ m in diameter and vary from 0.2mm to 0.7mm in length, with some showing a tapered form. The quantity of these fibres has been estimated by dissaggregating an intact block of known mass. Over 30 were found out of a sample of 350g. These are most likely to be sponge spicules or in some cases possibly radiolaria spines. Mats of spicules or individual spicules are found in rocks extending back to the Cambrian (and possibly further) and ancient spicules can usually be related to modern families. The spicules in A2 show similarity to those of *Leucandra* and *Chaetetes* members of the class Demospongea subphylum Gelatinosa which have monotaxon (single ray) spicules (Clarkson 1986). No multiple ray spicules were found in A2.

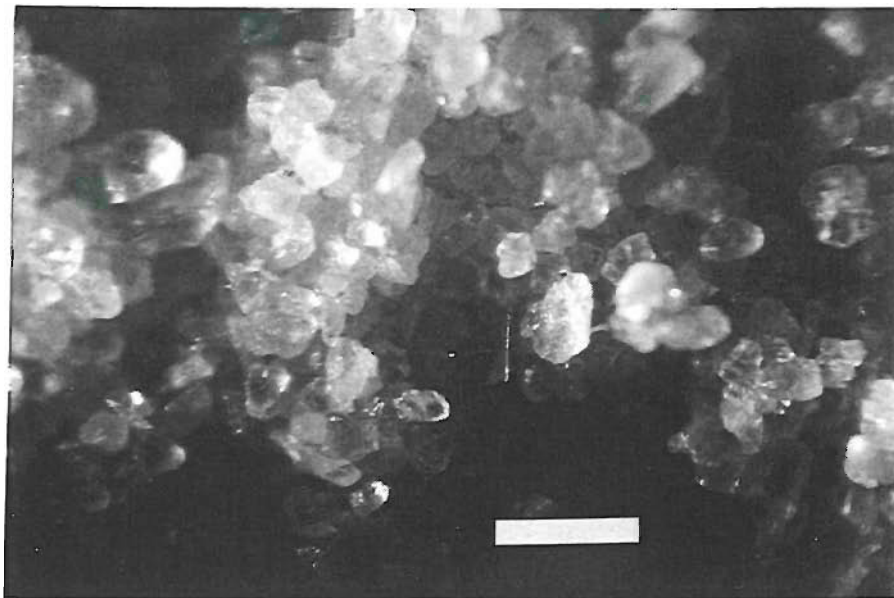


Figure 3.16 A thread-like form, possibly a sponge spicule, in A2, field of view 6mm.

Sponge spicules and siliceous skeletons in general consist of metastable, amorphous opaline silica. They have a higher solubility than quartz and are easily mobilised. Because of this and the increasing solubility of opal-A with depth they are considered to be an important source of authigenic quartz (Tucker 1991).

3.1.8 Fabric - discussion and conclusions

The grain morphologies observed in A2 and A3 show features that are presumably not detrital. High grain angularity could possibly be due to the grain provenance; if derived directly from igneous rocks and quickly buried then non-spherical, and angular quartz grains with crystalline nodes, embayments, and fractures could be preserved (Mazzullo and Magenheimer 1986). This also fits well with the grains being mono-crystalline with unit extinction but is an unlikely scenario for the Folkstone Sands which were deposited in a shelf environment after considerable transport and sorting.

Grains with very high angularity and large embayments and fines with perfect euhedral form are features that must be authigenic. The presence of interpenetration and microsuturing is also indicative of authigenic alteration of grain morphology. It is suggested that the mechanism for this is not large amounts of pressure solution and recrystallisation. No overgrowths are visible on the grains and no passive or bonding cement has been deposited, indicating that the morphological change has probably occurred in the solid state. This is an accepted mechanism; see Taylor (1950) and Stephenson et al (1992). It is possible that the more bizarrely shaped grains are the result of distortion of siliceous skeletons by a process of solid diffusion. The euhedral fines, unless they are detrital, which is considered unlikely, must be due to recrystallisation. Fines are clustered at grain contacts and these are possibly responsible for producing some of the very small cohesion measured in A2. The iron minerals at the grain contacts of A3 are an obvious source of its greater cohesion. No evidence has been put forward in the literature that small scale interlock (micro suturing) is occurring in aged sands, this has however been observed in A2 and A3 and must contribute to their high strength and small but measurable cohesion.

3.2 Wetting of Reigate Silver Sand

3.2.1 Introduction

When the quarry slopes of Reigate Silver Sand are wetted during heavy rainfall they do not fail. For over half their height they are 40° steeper than the ϕ'_{ult} values and loss of peak strength would cause failure (see Park Pit Stability section): therefore the intact fabric must be unaffected by field wetting. This is difficult to reconcile with the observation that hand samples of A2 and A3 disaggregated into a slurry in seconds when immersed in water, presumably by the action of slaking forces. Several experiments were carried out both with and without a vacuum and at different normal loads to investigate how A2 and A3 retained their fabric during wetting.

3.2.2 Methods and results - with vacuum

Four cylindrical samples (38mm diameter x 29mm high) were given a small (≤ 0.1 kPa) confining pressure by enclosing them in a finger bandage. Two were left open at the top surface and two were given a vertical confining stress of 4.38 kPa from a 600g mass. The samples were then placed in a vacuum chamber and a vacuum pump applied. De-aired water was added until the samples were covered. The vacuum was then removed and the samples oven dried. The samples were then manipulated with a probe and observed under x400 magnification to ascertain if and where the fabric had been disturbed.

On commencing to pour the de-aired water around the samples a dark wet patch was seen on the top surfaces of the samples without a vertical confining pressure within 3 seconds. After oven drying the samples with no vertical confining pressure had 14mm (equal to 0.28 kPa) of disturbed sand at the top, under this was intact material. The samples with 4.38 kPa vertical confining stress showed no fabric disturbance. These were then tested for Unconfined Compressive Strength and gave results of over 200 kPa. Results are summarised in table 3.2.

3.2.3 Method and results - no vacuum

The method was the same as above except the wetting was carried out without a vacuum. Only samples with 4.38kPa vertical confining stress were tested; these remained intact.

Condition	σ_v kPa	Result
No vacuum	0	Not tested but earlier observations showed that instant disaggregation would result
No vacuum	4.38	Remained intact
With vacuum	0	Top 14mm disturbed
With vacuum	4.38	Remained intact

Table 3.2 Summary of wetting results.

3.2.4 Observations, discussion and conclusions

Both A2 and A3 behaved in a similar fashion. Water was undoubtedly drawn rapidly into the pore spaces of RSS and it was the slaking forces produced by this that disrupted the fabric. RSS needs only a small confining pressure to prevent fabric disturbance on wetting. Therefore at a small depth the quarry sides will retain an intact fabric during wetting and drying cycles.

The above mechanism alone cannot produce a weather resistant quarry face, each wetting and drying cycle would disaggregate the topmost layer by slaking forces, resulting in steady but persistent lowering of the quarry slope to an angle approaching the ultimate friction angle. This is not observed. A full discussion of the mechanism that produces a weather and erosion resistant surface is given in the Park Pit stability section.

The above results showed that the preparation of wet intact samples is possible. A small confining pressure is essential for this, the application of a vacuum may not be necessary but was considered prudent when carrying out triaxial tests.

3.3 Park Pit - dark crust and banding

3.3.1 Dark crust

The Park Pit quarry face at the location of A3 displayed a dark grey persistent crust 3 to 5 grains thick (figure 2.2). The crust contained pick marks of the mechanical shovel used in the excavation of the face and was assumed to have formed after the face had been excavated approximately one year previously. Figures 3.17, 3.18, 3.19, and 3.20 show thin sections of the dark crust.

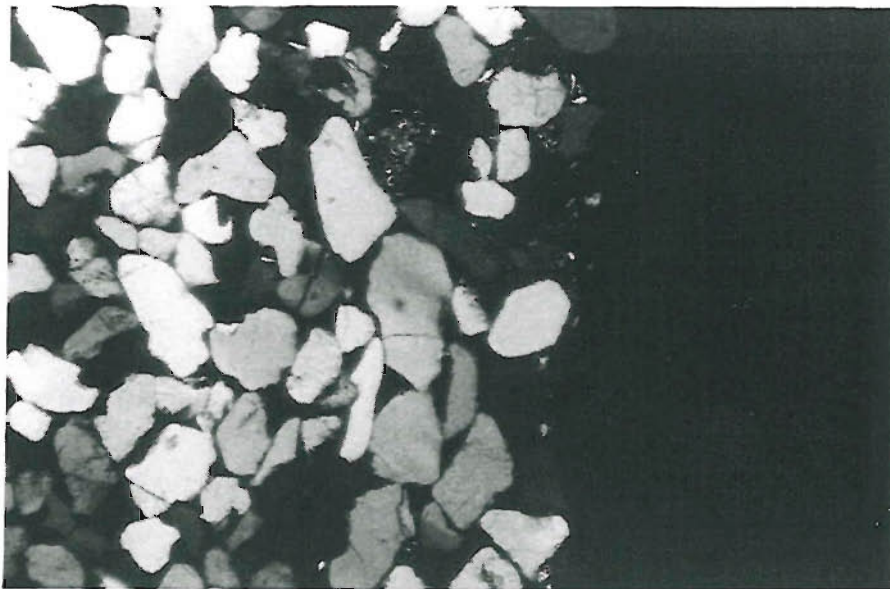


Figure 3.17 Thin section showing the dark crust. XP, field of view 3mm.

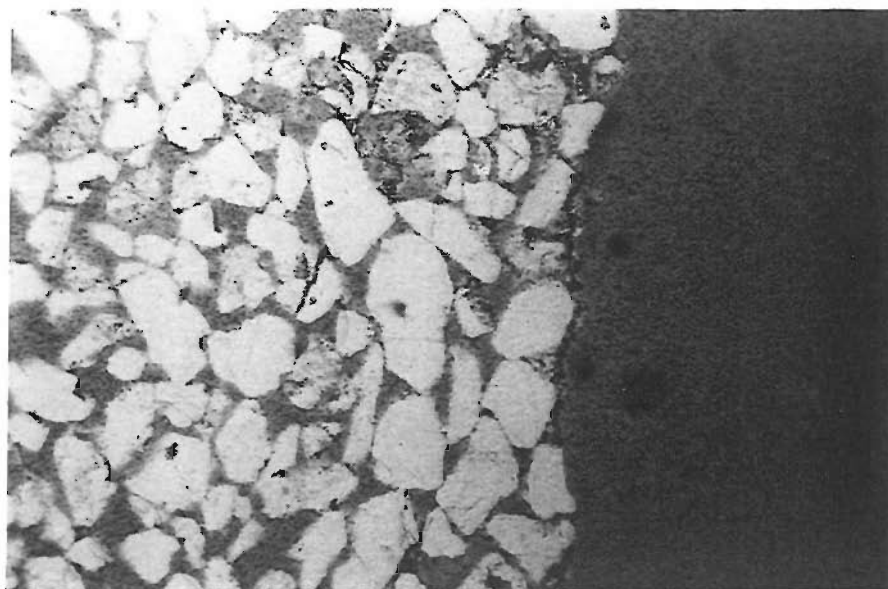


Figure 3.18 Thin section showing the dark crust. PPL, field of view 3mm.

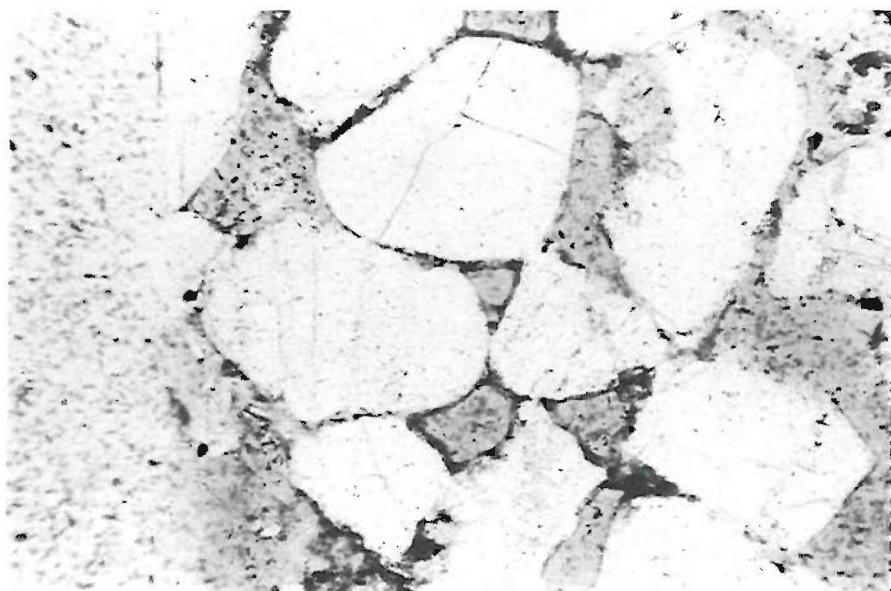


Figure 3.19 Thin section of the dark crust; the quarry face is to the left. PPL, field of view 1mm.

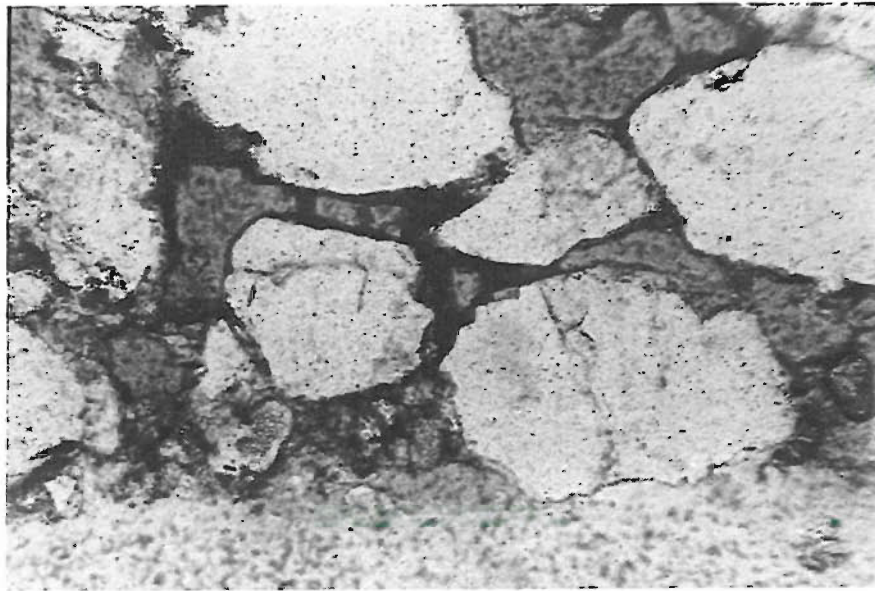


Figure 3.20 Thin section of a heavily cemented area of the dark crust; the quarry face is at the bottom of the photograph. PPL, field of view 1mm.

The iron minerals show up as opaque in both PPL and XP, and are clustered at the grain contacts, presumably where the pore water remained during evaporation. Also visible within the crust are silt sized euhedral quartz grains these are concentrated at the outermost edge of the crust (figure 3.17). It is possible that these have formed by the same mechanism as the iron mineral component of the crust or have been incorporated within it during its formation; the quartz arriving as airborne quarry dust. The A2 location showed no crust. This, however, was visited within days of being exposed. Though only 20m away from A3, and at the same height, the A2 location was covered up by the berm of a new haul road when A3 was visited 10 months later. It is possible that the dark crust would have been seen on A2 if it had still been exposed.

3.3.2 Banding

The A3 location showed a coloured banding from pale gold to the same white as the A2 samples. The bands varied in intensity and were from 2 to 300mm wide (these are just visible in figure 2.2). They were assumed to be due to concentrations of iron minerals.

3.3.3 Mechanism of formation

It is proposed that the formation of both the dark crust and the banding is due to iron minerals precipitating out of a solution, or a colloidal form, when the hydrological conditions changed during the construction of the quarry. During wetter periods, or possibly during the initial excavation, unsaturated flow takes the iron minerals to the surface of the face where the water evaporates leaving the concentrated iron minerals to precipitate and form the crust. The banding is formed either:

- during dryer periods when hydraulic gradient is such that the iron minerals precipitate earlier within the sand mass, or
- by minerals that precipitate earlier than those that form the crust.

The influence of the crust on the stability of the quarry is discussed in next section.

3.4 Park pit slope stability

3.4.1 Mohr - Coulomb analysis

Figure 3.21 shows a typical section of the Park Pit reproduced from Barton and Cresswell (1998). A Mohr - Coulomb analysis (ϕ' between 59° and 65° , c' between 27kPa and 40kPa i.e. intact sand) showed that both the overall slope and the steeper mid section, even when fully saturated, lie within a factor of safety of 2 (figure 3.22 reproduced from Barton and Cresswell, 1998). This conclusion assumes that there are no significant discontinuities affecting the overall strength and that the

interlocked fabric of the sand remains intact during periods of rainfall. As discussed in the wetting section only a small overburden is required to achieve this even for the areas such as A2 which have zero iron mineral cement. Thus the bulk of the sand will remain intact.

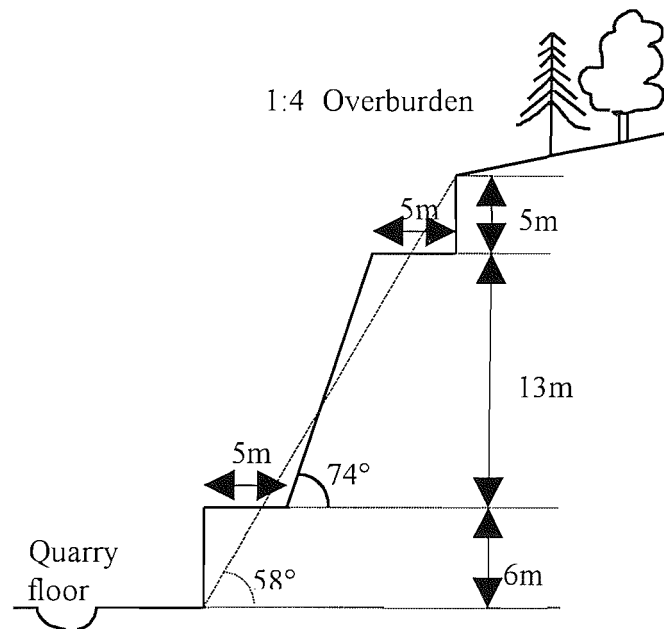


Figure 3.21 Typical section of the Park Pit Reigate. Reproduced from Barton and Cresswell (1998).

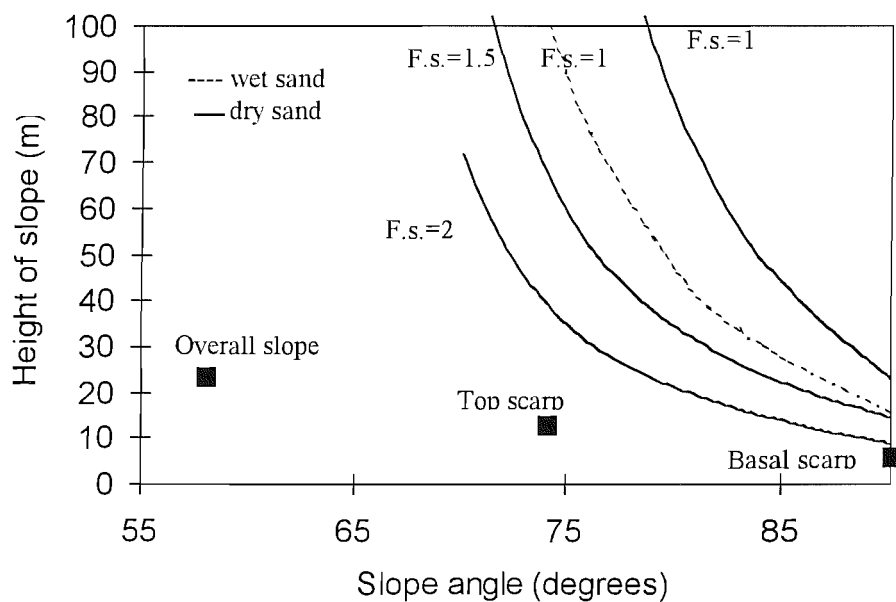


Figure 3.22 Mohr - Coulomb analysis of the slopes at Park Pit Reigate. Reproduced from Barton and Cresswell (1998).

3.4.2 The surface layer

The surface layer is obviously without any confining stress and must be protected by some other mechanism. It is suggested that it is the presence of the iron mineral crust that prevents the very outermost layer from being disaggregated and preserves the quarry face from repeated encroachment during each wetting and drying cycle.

The resistance of the crust to weathering will be dependent on the angle of the quarry face. This has been the experience of the quarry workers and management; the Park Pit manager suggests that a steep face is more stable and resistant to weathering than a shallower one (J. Sedman pers. comm.). The reason given was that water can penetrate if the angle is shallow whereas a steep slope is exposed to less rainfall and sheds water without it penetrating. It is possible that the crust may not even form if the slope angle is less than some critical value.

CHAPTER 4: INTRODUCTION TO TESTING AND DIRECT SHEAR TESTS

4.1 Introduction to testing

4.1.2 Difficulties

A2 and A3 are obviously intermediate arenaceous materials between a soil and a rock. The standard soil or rock testing procedures give rise to two difficulties if they are used for these materials: forming the intact sample to the required morphology and tolerances might not be possible, and the mode of failure may be different to that required for the usual interpretation of the test result. The testing program evolved and was carried out as sampling techniques improved and apparatus became available. With hindsight better testing programmes, methods and apparatus could be proposed and these are given in the recommendations for further work section.

4.1.2 The program of testing

The direct shear apparatus was used extensively in this study because it uses a sample morphology that was initially thought to be the only one possible for an intact material with very little cohesion. It is a widely used laboratory test for measuring the friction angles of granular soils (where pore pressure measurements are usually not usually required). When used on granular soils no shear plane is developed and the peak strength has to be interpreted with care (see Jewell and Wroth 1987).

The development of a hard shell sample preparation technique allowed triaxial testing of intact A3. Different testing methods give different modes of failure; it was considered that the greater the number of testing methods the more fully the behaviour of these materials would be understood. Triaxial tests also allowed accurate measurement of volume changes occurring during shearing. The tests were carried out wet but fully drained as were the few direct shear tests that were carried

out wet. The term wet is used rather than saturated. Saturated implies that an acceptable B value was achieved, which was not required due to all the tests being fully drained.

Whereas direct shear is generally used to test the strength of rock discontinuities, uniaxial testing is used to obtain the unconfined compressive strength, and the elastic constants, of intact rock. With soils, such as overconsolidated clays, accurate sample preparation for uniaxial and triaxial testing does not pose a problem; the soil is forgiving in that it can deform to the test boundaries. 'Hard' rocks also create no great problem; they can easily be ground to within any required tolerance. A2 and A3 however cannot be accurately ground, their dimensions are reduced by a process of grain plucking, and they are not able to deform to fit the test boundaries due to their brittleness. This difficulty combined with the problem of sample disintegration meant that uniaxial testing was the most difficult to carry out. It was considered necessary as the other tests had not produced any precise data on the stiffness of A2 or A3.

4.1.3 The “squeeze” test

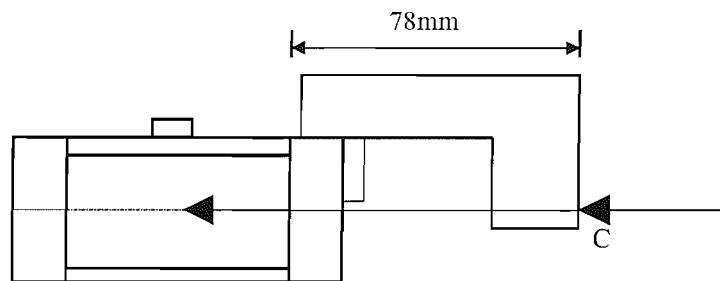
As a block of A2 gets smaller during sample preparation it becomes more difficult to handle without it breaking up into individual grains. A minimum number of grains is required to produce sufficient interlock cohesion to allow a piece of A2 to be handled. Eventually if the reduction in size is continued past that of a test piece it reaches a size where any further handling results in instantaneous failure with total separation of particles.

Very few geologically aged sands have only fabric, the majority have a combination of bonded and fabric structure. From the above observation a quick test was developed to differentiate between geologically aged sands with the two types of structure and geologically aged sands with fabric structure alone. A small (15 x 20 x 20mm) piece of the intact sample is squeezed between the forefinger and thumb nail. Sand with no grain bonding will fail to individual grains. Sand with bonding will break into pieces consisting of grains still bonded together.

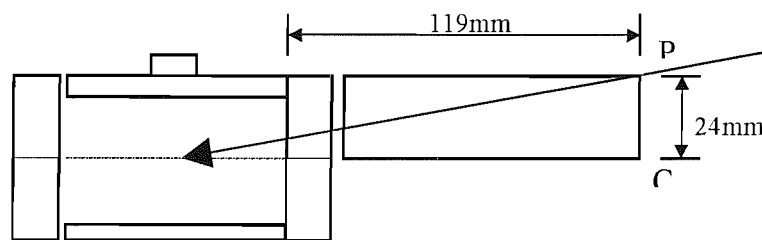
4.2 Apparatus and methods

4.2.1 Apparatus

Two shearbox apparatuses were used; firstly a Wykeham Farrance WF25400 fitted with a 10:1 loading lever able to produce a vertical stress of 1.25MPa on a 60x60mm shearbox, secondly a Wykeham Farrance WF2550, usually used for testing 300x300mm samples but fitted with inserts and a 60x60mm shearbox giving over 10MPa vertical stress from a hydraulic ram. Differences between these two machines in terms of how the shear load was applied are shown in figure 4.1, and how these may have influenced the results in practice is covered in the discussion section.



A) Tests with normal loads of 1250kPa and below used the standard shearbox apparatus. Shear force is applied to the top half of the box at the centre line. Any rotation is about point C.



B) Tests with normal loads equal to 1250kPa and above used a modified large shearbox. To apply the shear load a simple push block pressed against the box, this allowed the applied load to move from anywhere between point C and point P. Arrow shows the maximum displacement of the shear force from the horizontal.

Figure 4.1. Comparison of the two apparatuses used for direct shear testing.

Both apparatuses were fitted with load cells to measure mobilised shear strength, although in preliminary tests a proving ring was used. This however was found to cause problems due to the energy stored in the ring and the highly brittle nature of the material (see discussion). The large shearbox also had a load cell to measure vertical load. Both shearboxes were equipped with LVDTs to measure vertical movement. Relative displacement of the shearbox halves was calculated from the jack speed. A correction was made for any compliance of the proving ring or load cell.

A glass sided shearbox was used to investigate how the failure plane developed. This was used at normal loads less than 200kPa.

4.2.2 Method

A sample height of 34mm was used, which was greater than the usual 20mm to compensate for the thickness of, and any interference by, the hairspray layer on the bottom of the intact samples. The shear tests on A2 were carried out dry, this was not only convenient but essentially similar to the insitu state of the sand. Previous work by Richards (1992) showed little strength loss between wet and dry samples when shearing a very similar material. Preliminary U.C.S. tests on A2 showed strength loss of up to 50% on wetting but this was considered to be due primarily to fabric disturbance in the unconfined state (see wetting section). Testing dry also enabled the shear zone to be investigated by observation after the test. When the load is removed after testing wet the sample retains none of the stress induced structures; samples of A2 and A3 disaggregate when wetted unless confined.

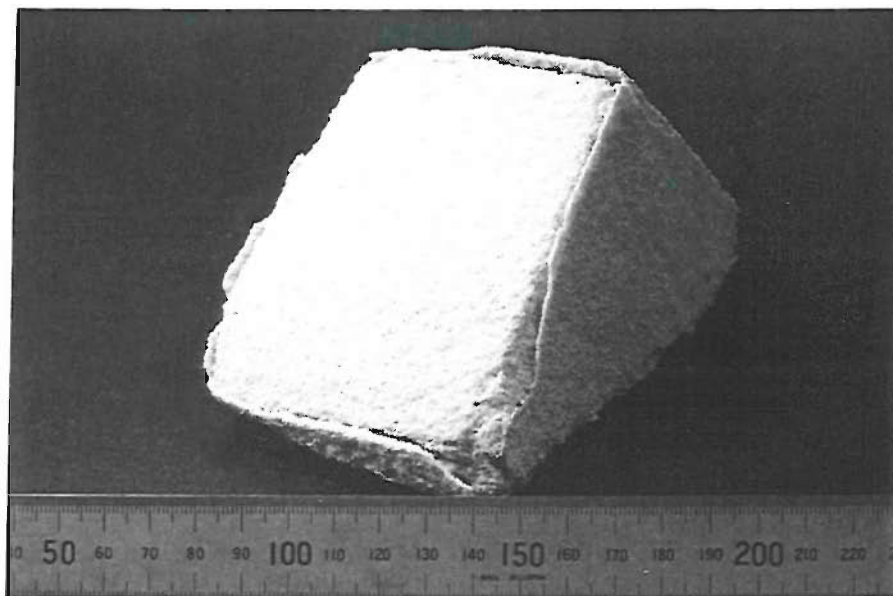
4.2.3 Intact sample preparation.

1. The whole block was hairsprayed in two stages, firstly the exposed top surface followed by the underside after the top had set and the block turned over.
2. The block was cut to a smaller size using a surface set tungsten carbide hacksaw blade. After each cut the new surface was sprayed to maintain a continuous shell.
3. The final cut was chosen to be the boundary at the bottom platen. This was ground smooth on a glass plate before spraying (fig. 4.2).
4. Double sided sticky tape was placed onto a smooth bottom platen
5. The base of the block was placed on the platen and pressed gently until stuck.
6. Further material was trimmed off by sawing to leave only 10-20mm excess overhanging the platen.
7. The block was filed down to the dimensions of the platen using a 13mm paint brush and 80 grade abrasive cloth stuck to a right-angled wooden block. It was found necessary to keep the sample as rounded as possible to prevent corners becoming detached. A gentle all round finger pressure was also found to be helpful in keeping the sample intact (fig. 4.3).
8. It was found that 3mm clearance was needed between the top of the sample and the shearbox sides (see below).
9. The top surface was levelled using height spacers to lift the wooden block to the correct height.
10. A pedestal was placed into the shearbox and the bottom platen complete with sample placed upon it. The shearbox was then lifted up around the sample. Any grains dislodged at this stage would jam the bottom platen and stop it rising.
11. The clearance gaps were filled using pluviation and gentle tapping of the box.

The use of a pluviated edge to fit the sample into the shearbox required 3mm of clearance at the top of the sample, any less than this and arching prevented the grains from penetrating to the bottom of the gap resulting in a void. This was

displayed as a “bench” at the beginning of a stress vs. strain graph. The use of a pluviated edge will have affected the test results, due to the area of intact material being reduced, resulting in a small underestimation of the samples shear strength. Other methods of fixing the sample into the shear box were explored, especially those from rock testing procedures (see Hoek and Bray,1981), but none of them were considered suitable for this material.

A slightly different method was required when using the glass sided shearbox where intact material must abut the glass wall. Clearance was only given on three sides with the side abutting the glass wall made as flat and perpendicular as possible. Inserting the sample was facilitated by the glass sided box having sides that could be removed.



E11

Figure 4.2 A2 sample with hard shell

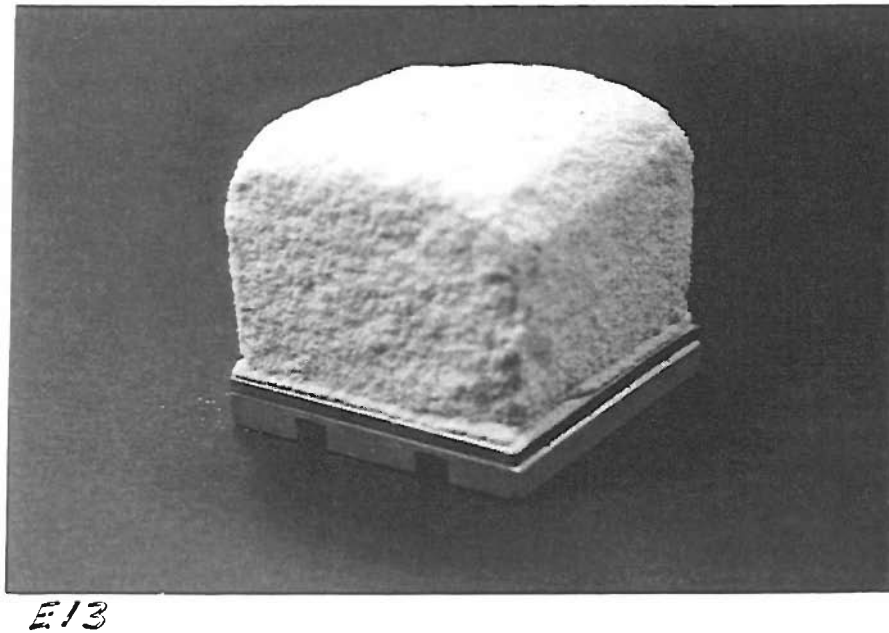


Figure 4.3 A2 sample stuck to the shearbox bottom platen, note the rounded top corners and the hard layer adjacent to the platen.

4.2.4 Pluviated sample preparation

Pluviation was used to produce the reconstituted samples; details are given in the pluviation section. For the majority of the tests the highest possible density was attained. A series of tests at 750kPa normal load were carried out at densities between the maximum achievable by pluviation and the minimum achievable by a fast pour method.

4.3 Results of Shearing A2

4.3.1 Introduction

In total shear tests were carried out on 56 pluviated and 32 intact samples of A2. Intact samples from other areas of the Park Pit Quarry were used in preliminary tests and gave similar shear strengths and modes of failure. Of the A2 samples, 24 pluviated and 6 intact samples were tested on the large shearbox apparatus. The large numbers of pluviated tests were carried out to develop testing skills and also to act as a calibration by comparison against published results. The shear strain and the volumetric strain were calculated, for both pluviated and intact tests, using a nominal value of 34mm: which was the height of the sample at the start of the test (and not the shear zone thickness).

4.3.2 Pluviated samples

Figures 4.4 and 4.5 show pluviated dense and pluviated loose samples behaving in the expected stress-strain manner with dilation and contraction respectively. Figure 4.6 shows the variation of mobilised shear strength (both τ_{ult} and τ_{peak}) with density at a normal load of 750kPa. Note the large gap between the highest density obtainable by pluviation and the density of the intact material.

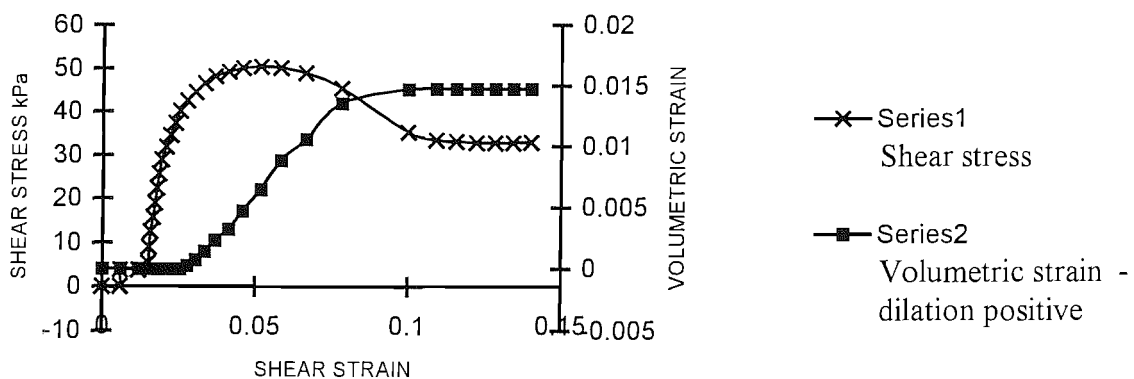


Figure 4.4 A2 at 50kPa vertical stress. Pluviated dense (1.67Mg/m^3)

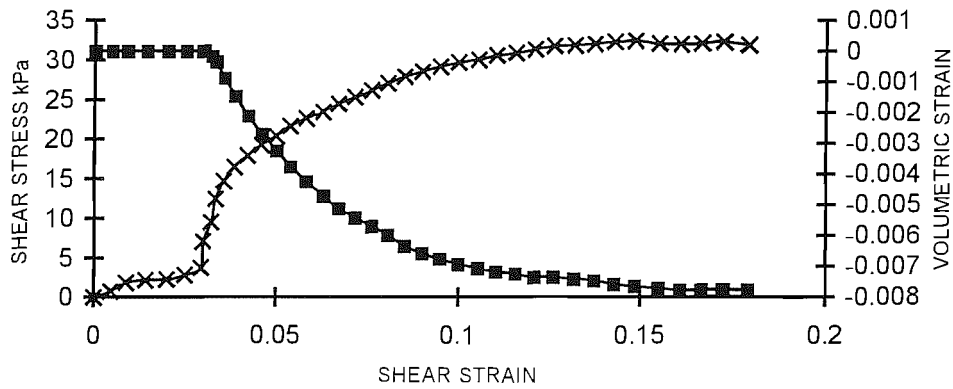


Figure 4.5 A2 at 50 kPa vertical stress. Poured loose (1.43 Mg/m^3)

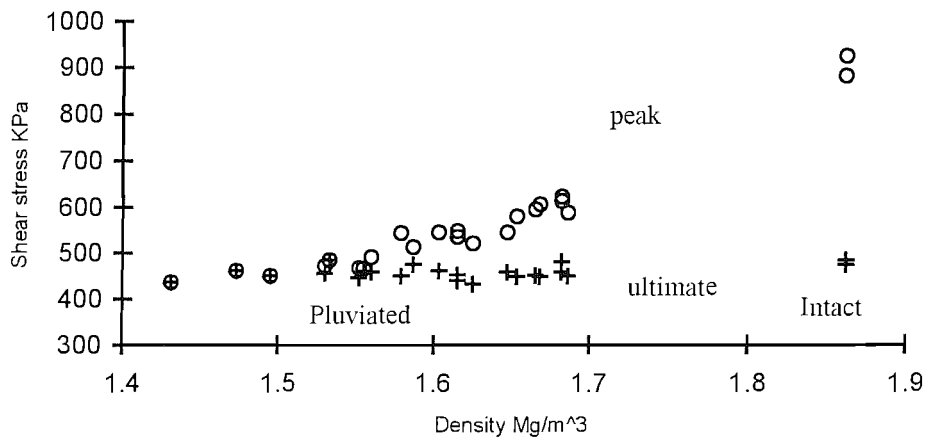


Figure 4.6 A2 at 750 kPa normal stress. Strength values of intact material compared to those of sand pluviated to densities between minimum and maximum .

Graphs of mobilised shear strength against normal load are given in figures 4.7 and 4.8. For these tests the samples were pluviated to a maximum density, this varied between 1.685 and 1.693 Mg/m^3 . The peak strength of the pluviated dense samples gave a ϕ' angle of 37° with R^2 of 0.9986 up to a normal load of 1250 kPa . Above this the peak is suppressed until at a normal load of 11 MPa only a slight peak is observed. The ultimate strength has a ϕ' angle of 30° with $R^2 = 0.9983$.

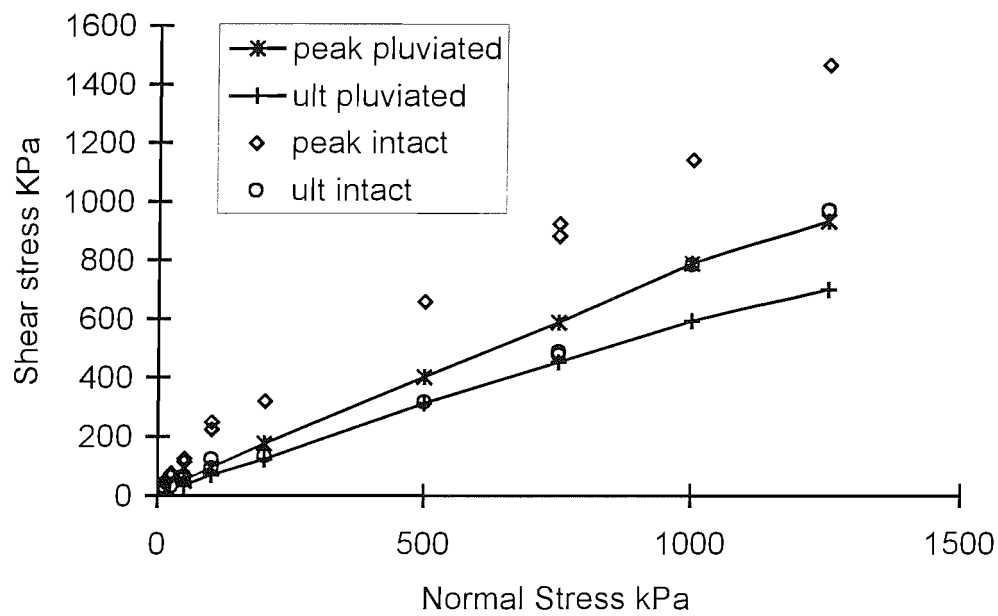


Figure 4.7 Strength envelope for pluviated and intact samples at normal loads below 1250kPa. The data points for the pluviated samples are averages.

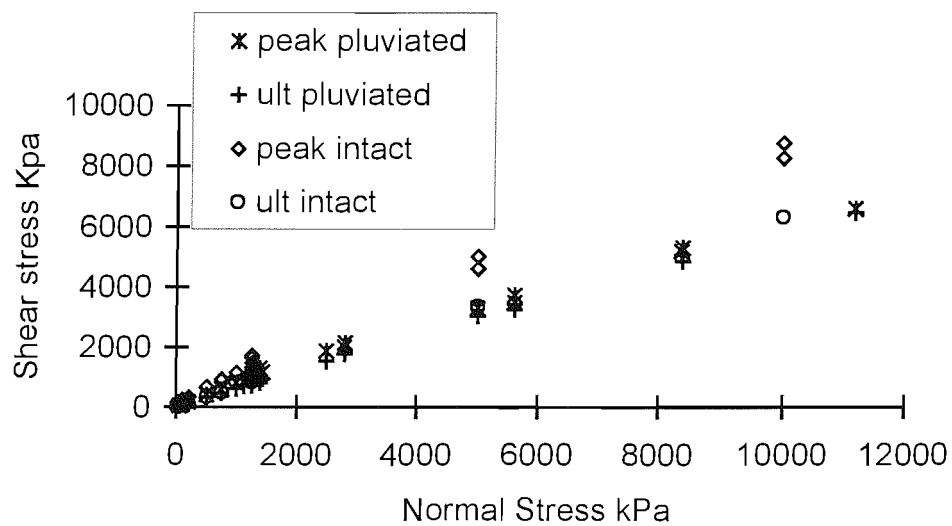


Figure 4.8 Strength envelope for pluviated and intact samples at normal loads up to 11MPa

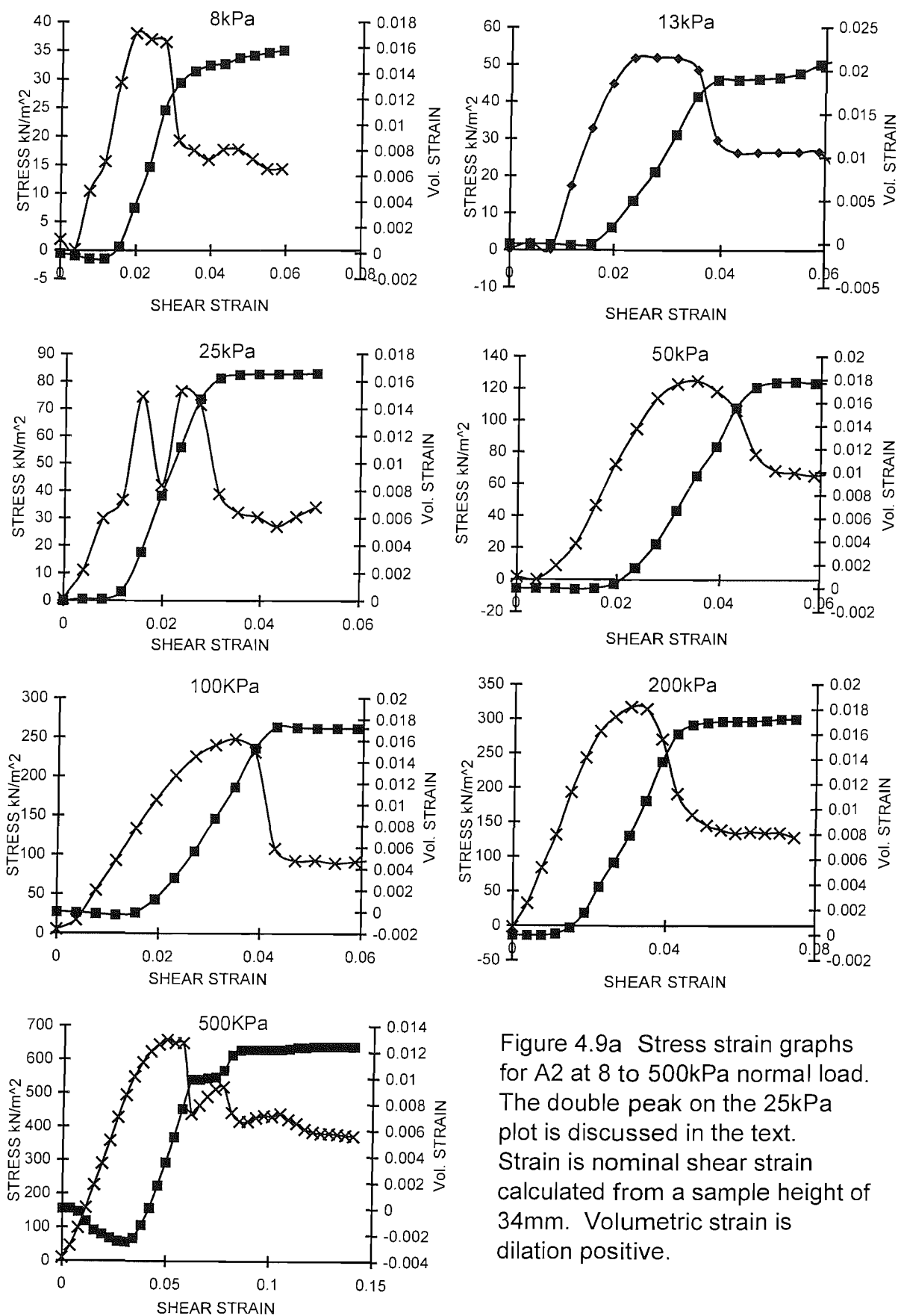


Figure 4.9a Stress strain graphs for A2 at 8 to 500kPa normal load. The double peak on the 25kPa plot is discussed in the text. Strain is nominal shear strain calculated from a sample height of 34mm. Volumetric strain is dilation positive.

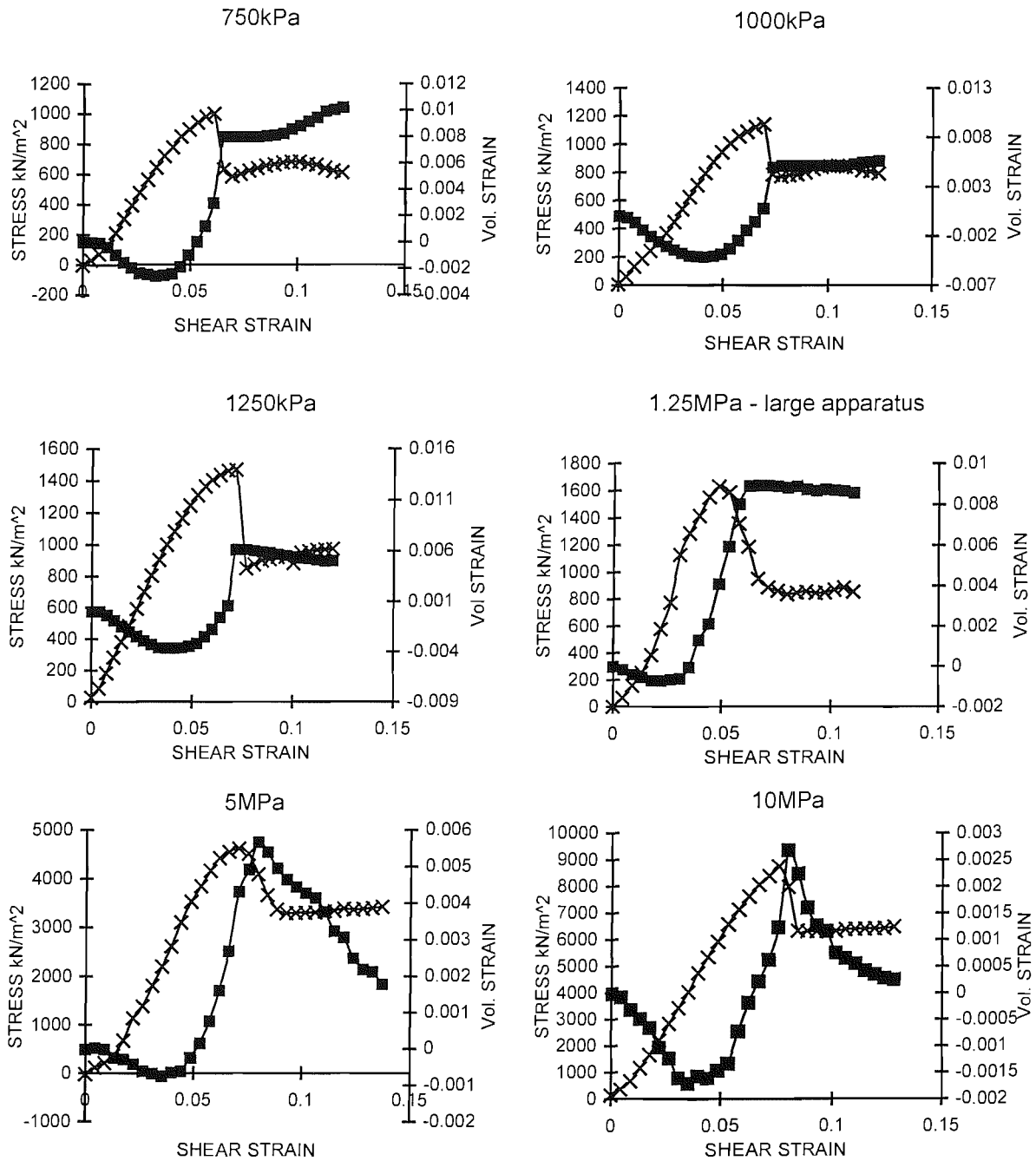


Figure 4.9b Stress strain graphs for A2 at 750kPa to 10MPa normal load. Strain is nominal shear strain calculated from a sample height of 34mm

4.3.3 Intact samples

Figure 4.9a and b shows typical stress strain graphs of tests on intact samples. Intact samples did not always settle down to a steady state after the decline of the peak. Undulation in the post peak strength occurred in over half of the intact sample tests (figure 4.9 8kPa, 500kPa and 750kPa) this took many forms; from a simple whale back to complex diminishing undulations. Another remarkable feature of tests between 750kPa and 5MPa was the instantaneous loss of strength from maximum to ultimate. This never occurred at the lower normal loads used but occurred in over 80% of tests over 750kPa and in all of the tests over 750kPa using the small shearbox apparatus. The peak was not suppressed even at 10MPa; tests at this normal load produced peak strengths of 39% and 31% above the ultimate strengths.

The intact samples produced large variations in ϕ' peak angles and intercept values depending upon the normal load. Three highly linear areas can be discerned: below 100kPa $\phi'_p = 65^\circ$, $c = 16\text{kPa}$, $R^2 = 0.989$; between 100kPa and 1250kPa $\phi'_p = 47^\circ$, $c = 103\text{kPa}$, $R^2 = 0.996$; and above 1250kPa $\phi'_p = 38^\circ$, $c = 736\text{kPa}$, $R^2 = 0.995$.

The ultimate strength of intact samples varied in a complex manner with normal load. Again three distinct areas can be discerned: below 100kPa $\phi_{ult} = 50^\circ$, between 100kPa and 750kPa $\phi_{ult} = 33^\circ$, with intercepts of zero in each case, and above 750kPa strength increases rapidly to $\phi_{ult} = 38^\circ$ followed by a gentle concave down curve until $\phi_{ult} = 32^\circ$ at a normal loads towards 10MPa.

4.3.4 Proving ring/loadcell results

Several preliminary tests on A2 and other samples from the Park Pit Quarry were carried out with the shear force measured by a proving ring. When pluviated samples were tested no difference was found between results from tests using a proving ring and results from tests using a load cell. The intact blocks however

failed explosively as the energy stored in the ring was released after the peak strength of the sample had been reached.

Both the peak and ultimate strengths of the intact samples were apparently larger when a proving ring was used. When tested in the range 200 to 500kPa the ϕ'_{ult} was increased by an average of 5°. Observation of the shear surface showed that the explosive nature of the failure had produced large amounts of grain crushing.

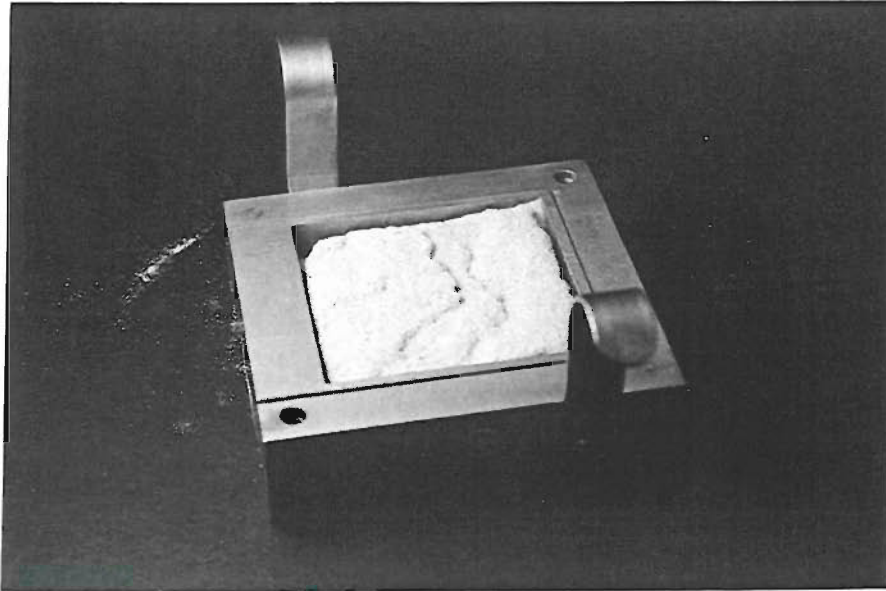
During tests on intact samples using a proving ring the dial gauge was seen occasionally to swing rapidly with a deflection equal to 0.03mm, afterward returning to the original reading. Tests using a load cell with a continuous graphical readout on a pc monitor showed spikes where the measured force dropped to zero. These spikes were only observed at the lower normal loads. The data capture was at 10sec intervals so these were usually missed; one is shown on the 25kPa plot of figure 4.9a giving rise to an apparent double peak in the stress strain plot.

4.3.5 Shear surface morphology

Intact blocks of A2 did not disintegrate during shearing but sheared along a distinct band leaving intact material above and below. After splitting the shearbox the extremely fragile upper half of the sample was removed. Any disaggregated material was then carefully tipped off the lower half of the sample and the shear surface observed.

The most interesting feature of the lower shear surface was the presence of 3 - 5mm steps angled at 23° to 25° with the steep surface facing against the shear direction. At normal loads of less than 100kPa they were always present. Figure 4.10 shows these steps on intact A2 sheared at a normal load of 100kPa and figure 4.11 shows a generalised diagram of their morphology. Figure 4.12 shows the steps at 750kPa. At loads of less than 50kPa the steps became erratic in scale, varying from 7mm to 1mm in height often with a highly curved plan view. The shear surface also tipped toward one side of the box to a depth of up to 6mm on some of

these very low normal load tests. Shearing intact A2 at normal loads above 100kPa produced a flatter shear surface often with only a single step.



E21

Figure 4.10 shear surface of intact A2 sheared at 100kPa. The steps are opposing the shear direction.

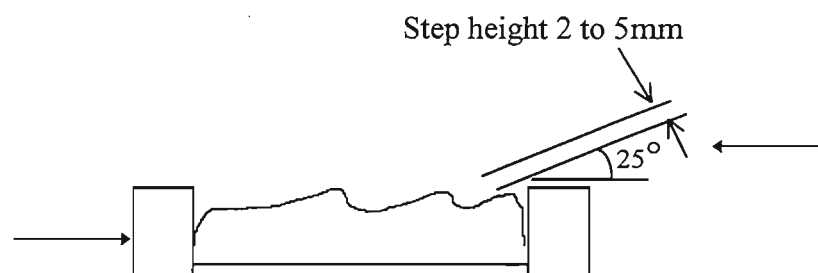


Figure 4.11 Generalised morphology of the steps produced on the intact samples of A2 at low normal load. Note the sharpness of the corners. Arrows show the shear direction

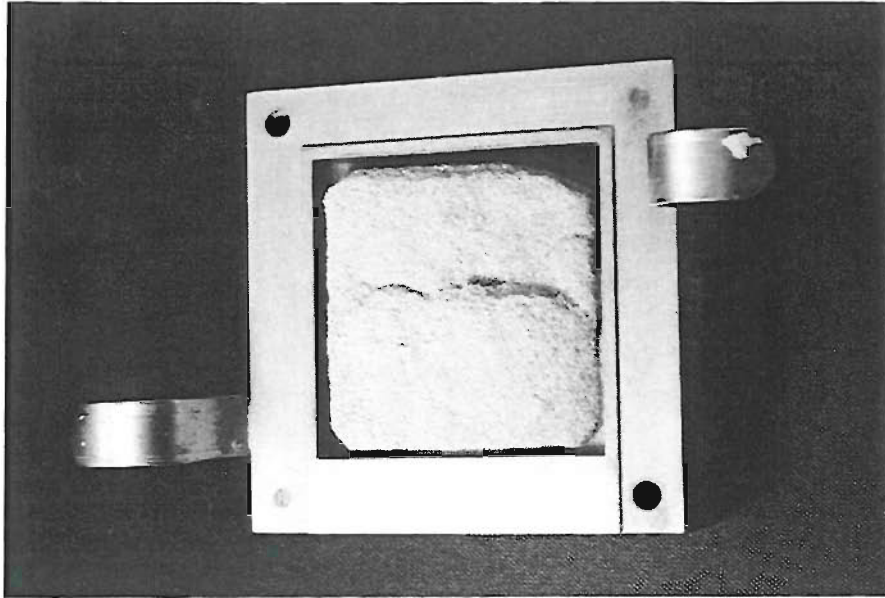


Figure 4.12. The shear surface of intact A2 sheared at a normal stress of 750kPa. The step is opposing the shear direction.

Shear surface undulation continued to be observed at higher pressures until at 10MPa and above plumose structures developed as shown in figure 4.13. These had a slight (1 - 3mm) convex up surface.

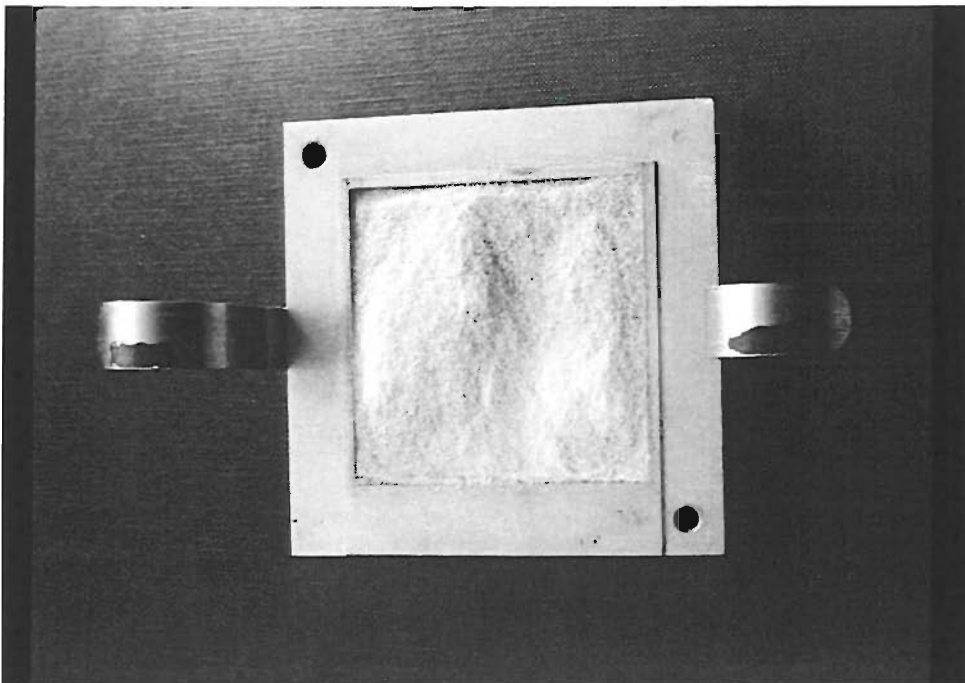


Figure 4.13 The shear surface of intact A2 sheared at a normal stress of 10MPa. The top half of the sample moved across this from top to bottom.

4.3.6 The shear zone and shear induced structures of intact blocks

Two tests were carried out using a glass sided shearbox with normal loads of 50 & 100kPa. These allowed the development of the shear zone and the steps to be observed.

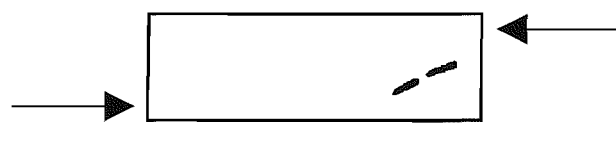
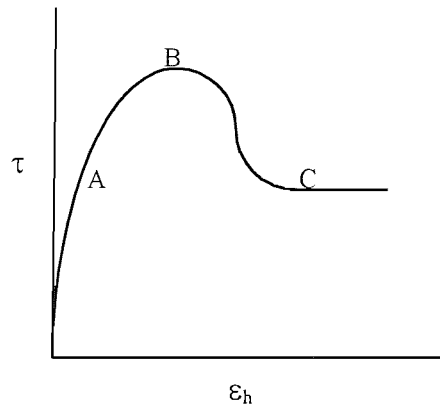
Thin sections were made of five intact sample tests by impregnating the sheared samples with a blue dyed resin (see impregnation section - 2.4). Four of these sections were of tests at a normal load of 100kPa, stopped at different points of the test, and one section was of a test at 10MPa taken to a steady ϕ'_{ult} .

The thin sections gave rise to interpretation problems due to the resin not impregnating areas that had a high void ratio. The shear zones (at a normal load of 100kPa) were impregnated but other areas were not impregnated. These areas contained disaggregated sand that was able to fall out when the sheared block was cut up for thin sectioning. In the thin sections these show up as macro-voids impregnated with a clear resin that was introduced during the thin section making process. The shear zone however shows up as darker line due to it consisting of a greater proportion of pore space containing blue dyed resin. Any macro-void showing in the thin sections has therefore to be interpreted as either an area with a void ratio less than the critical state of the sand at 100kPa or it could possibly be a true macro-void. The glass sided shearbox observations strongly support the interpretation that the macro-voids seen in thin section were true macro-voids due to the opening of cracks, though the thin section process has overemphasised their width.

Figure 4.14 displays the results of the thin sections on the 100kPa tests showing the development of the high void ratio areas and shear zone. Figure 4.15 shows the thin section of the 100kPa test that was taken to position C; the end of the test when a

steady state had been reached. It shows the shear zone and front high void ratio area. It is apparent that:

- no grain crushing occurred at these pressures
- the shear zone was 2 to 4 grains thick



Thin section of a test stopped at A. No evidence of a shear plane. Small macro void at front.



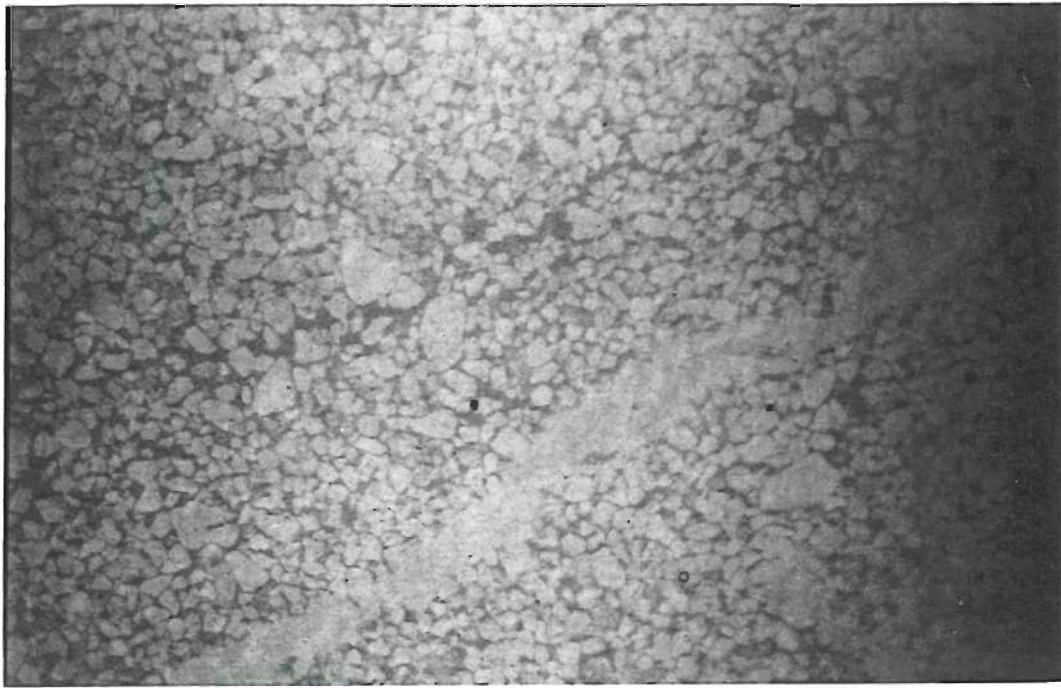
Thin section of a test stopped at B. No evidence of a shear plane. Large macro void at front.



Thin section of a test stopped at C. Evidence of a shear plane (dotted line). Detail is given in figure 4.15b.

Arrows show direction of shear

Figure 4.14. Thin section investigation results showing the development of shear zone during a 100kPa normal load test.



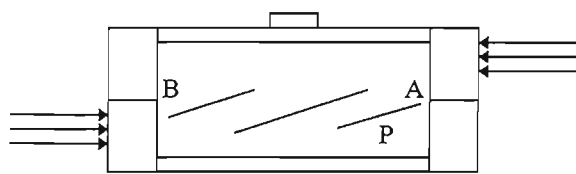
K17

Figure 4.15 Photomicrograph showing the shear zone and high void ratio area. Field of view 13mm

Figure 4.16 summarises the information (from the impregnation and glass sided shearbox tests) on how the areas of high void ratio and the shear zone developed. The areas of high void ratio are interpreted as tension cracks (see discussion) these started at A, before the peak at a shear load similar to that of the ultimate load, and developed toward B as the test progressed, the crack at A was more open than the rest and remained visibly open after the test.

Above 750kPa a white powdery appearance was apparent on the shear surface of the lower intact material. Figure 4.17 is a photomicrograph of the surface of A2 after shearing at 1MPa. Note the abundance of fines compared to the surface of unsheared material (fig 4.18).

Figure 4.19 shows the convex up shear zone of a test carried out at 10MPa normal load. Obvious grain crushing has occurred (figs 4.20, 4.21) at the front of the zone. The rear of the shear zone is represented by a macro-void (fig 4.22) with less grain crushing evident.

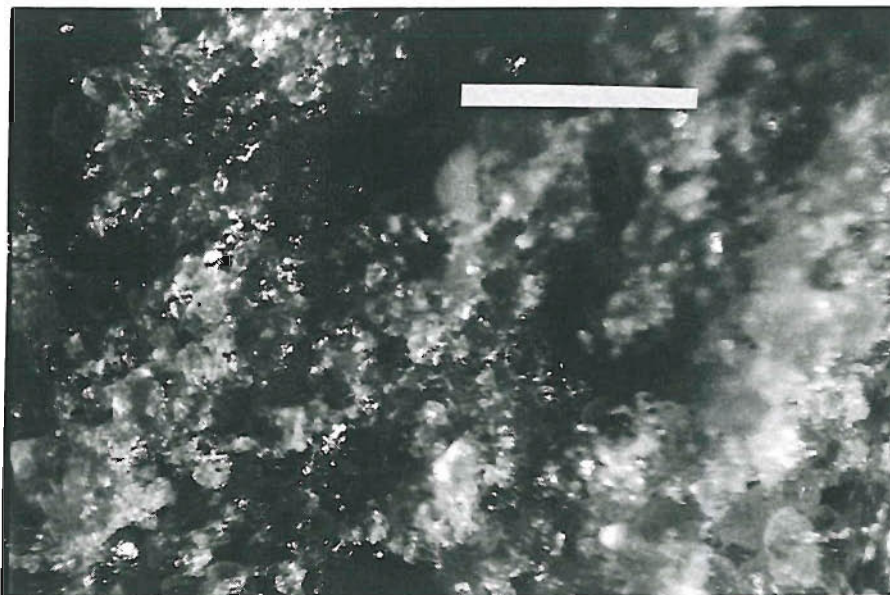


A) Cracks develop at $\theta = 90 - \phi'$ (23° to 25°) only the crack at P widens enough to become obvious and easily visible.



B) Shear plane develops following the cracks to produce a toothed shear plane. Note that the shear plane is very narrow and that the sawtooth ramps are in the opposite direction to those found in soil mechanics models of dilation during shearing.

Figure 4.16. Development of the low pressure shear plane.



E33

Figure 4.17 The surface of A2 after shearing at 1MPa. Note the abundance of fines compared to the surface of unsheared material (fig 4.18).

Scale bar 1mm.

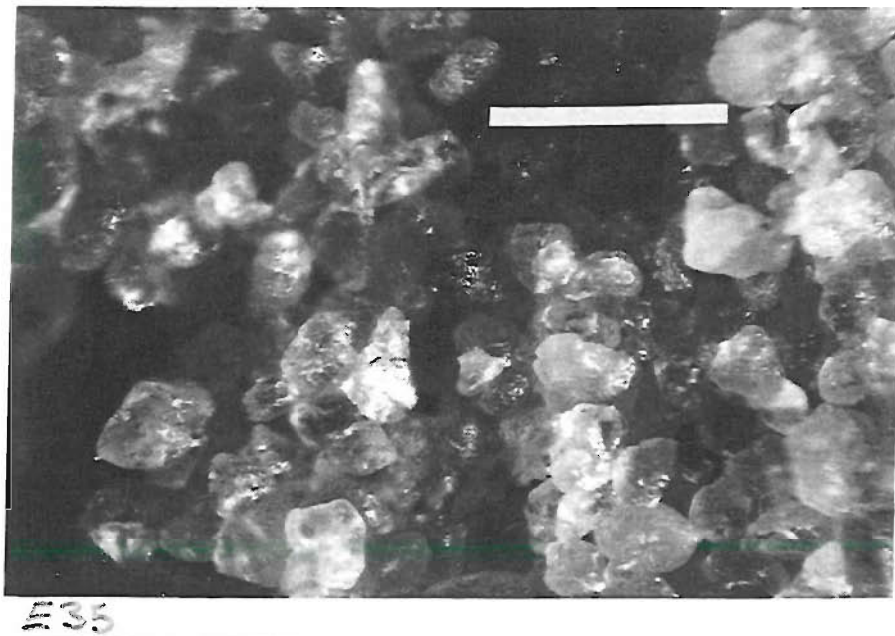


Figure 4.18 The surface of unsheared A2. Scale bar 1mm.

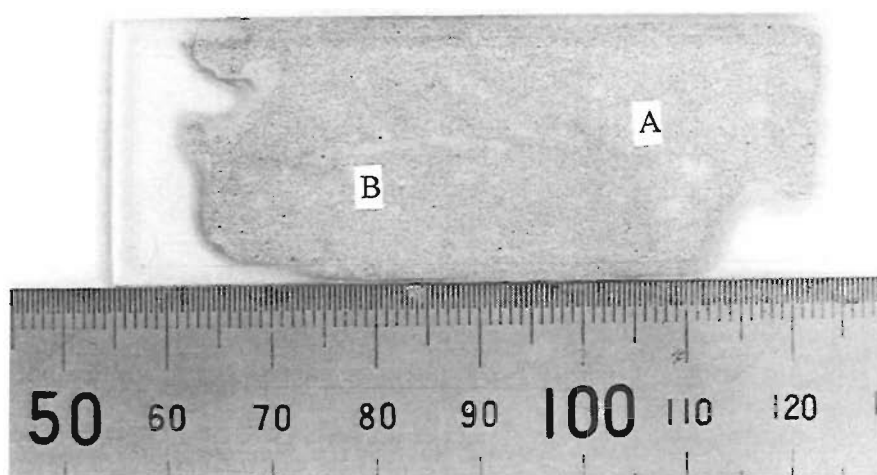


Figure 4.19 Thin section of a test carried out at 10 MPa normal stress. Note the convex up shear zone.

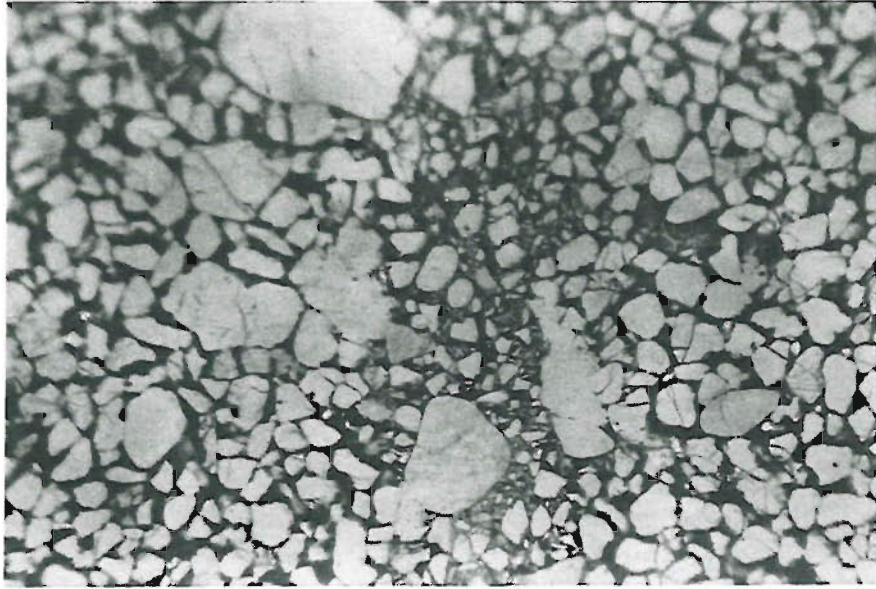


Figure 4.20 Detail at location A of figure 4.19. Obvious grain crushing. Field of view 6mm.

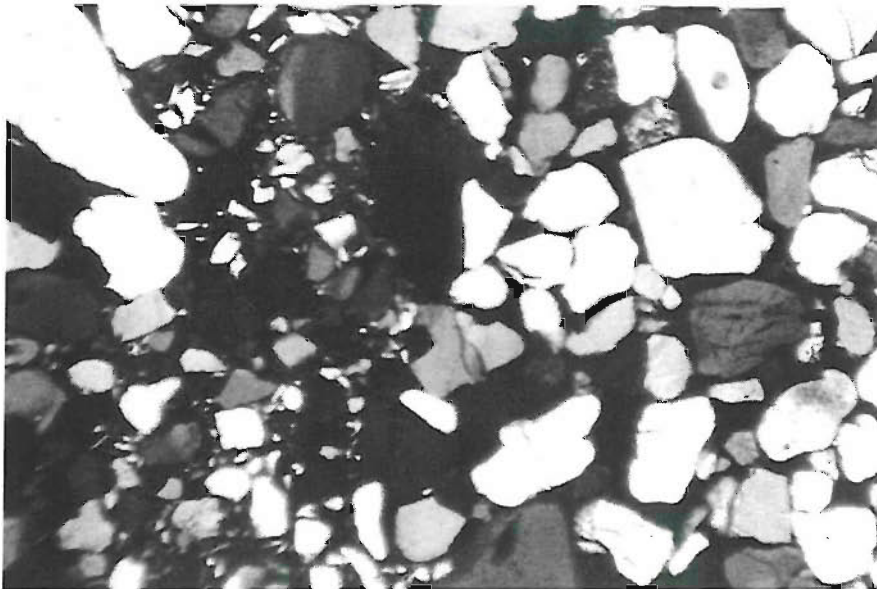


Figure 4.21 Detail at location A of figure 4.19. Obvious grain crushing. Field of view 3mm, XP.

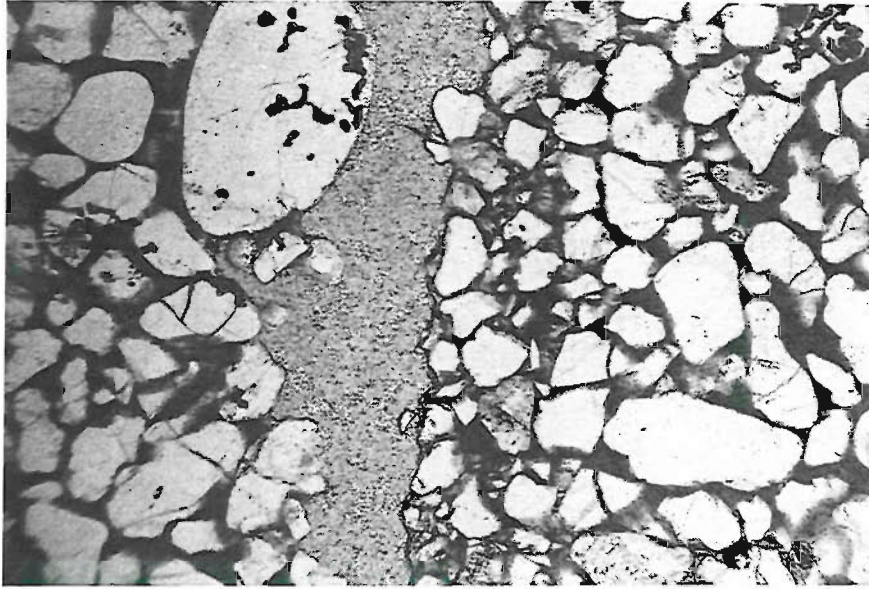


Figure 4.22 Detail at location B of figure 4.19. The shear zone is represented by a macrovoid with less evident grain crushing. Field of view 2.6mm.

4.3.7 Dilation during shearing

Table 4.1 lists the total dilation that occurred during shearing. Below 50kPa the intact material shows great variability in the dilation produced during shear. From 100kPa to 5MPa both the intact and the pluviated samples show a similar decline in dilation, over 5MPa however the pluviated samples show no dilation whilst the intact material continues to dilate even at the maximum normal load tested (10MPa). Accompanying the sudden strength loss in some intact tests above 750kPa (figure 4.9) was a sudden jump in volumetric strain. This feature occurred less frequently at normal loads over 1250kPa.

No analysis of dilation rates (with respect to horizontal displacement) was attempted; the measurement of ϵ_h was calculated from the jack speed and was not considered reliable enough to allow comparison of dilation rates with published

results. The peak dilation rate for the intact samples appears to be 2 to 3 times higher than that for the pluviated samples.

Normal stress kPa	ϵ_v intact	ϵ_v pluviated
8, 13 and 25	highly variable between 0.016 and 0.030	no results
50	0.018	0.015
100	0.018	0.017
200	0.017	0.016
500	0.012 (0.014)	0.010 (0.012)
750	0.010 (0.012)	0.009 (0.011)
1000	0.006 (0.010)	0.008 (0.010)
1250	0.006 (0.009)	0.007 (0.011)
2801	no test	0.006 (0.008)
5000	0.006 (0.007)	no test
5615	no test	0.0015 (0.004)
8346	no test	0.0000 (0.001)
10000	0.0025 (0.0035)	no test

Table 4.1 Dilation totals. The first column of figures represent averages of the total dilation measured as strain from the start of shear. The figures in brackets represent averages of the total dilation measured from the low point after any compression occurring during shear at the beginning of the test. Above 50kPa the spread of results was no greater than 10%.

4.4 Observations and Discussion

4.4.1 Friction angles of arenaceous materials

Reported friction angles (Hoek and Bray, 1981) for flat unweathered sandstone surfaces are 25° to 35° and for intact sandstone 35° to 45° . Uniformly graded sand varies between 28° to 34° for ϕ'_{ult} , and 32° to 40° for ϕ'_{peak} (Barton and Choubey, 1977). The high figures for ϕ'_{peak} are explained in the literature as being due to the dilation component of strength. Bolton (1986) summarises ϕ'_{crit} values measured by different workers for 17 different sands placing them between 30° and 37° . The higher values are for sands with a high feldspar content.

The published friction angles for flat unweathered sandstone surfaces show a large variation. The problem lies with the flatness of the surface; granite can be ground to a certain flatness that will be maintained during shearing, whereas sandstone will pluck resulting in a surface with much greater roughness

The peak friction angles of intact A2 are greatly in excess of those reported above, they are however in keeping with those measured for other locked sands (Dusseault and Morgenstern, 1979; Barton, 1986; Richards, 1992; Richards and Barton, 1999). Dusseault and Morgenstern, (1979) considered that the high friction angles were due to large dilation rates. The ultimate friction angles of intact A2, and the friction angles of the pluviated A2, are within the range given above for quartz sands except for the lower normal load peak results which are above 45° .

4.4.2 Shear zone width and testing methods

The shape of the shear zone in dense sands when using the direct shear box has been recorded by many authors (see references in Jewell and Wroth, 1987). It forms a lens shape with considerable thickness in the middle of the box, tapering to a narrow band at each end (figure 4.23a). This is different from the ultimate shear zone produced by the triaxial test which is commonly shown as a 1 to 2mm wide linear

band. Roscoe (1970) proposed that the width of shear bands in triaxial tests is about 10 times the average grain diameter, other authors confirm this to be roughly correct although 16 times the grain diameter has also been given (Muhlhaus and Vardoulakis 1987). Further work by Ord et al (1991), using a poorly cemented sandstone in a biaxial apparatus, produced the approximation of 1-2mm, this was 4-8 times the D_{50} .

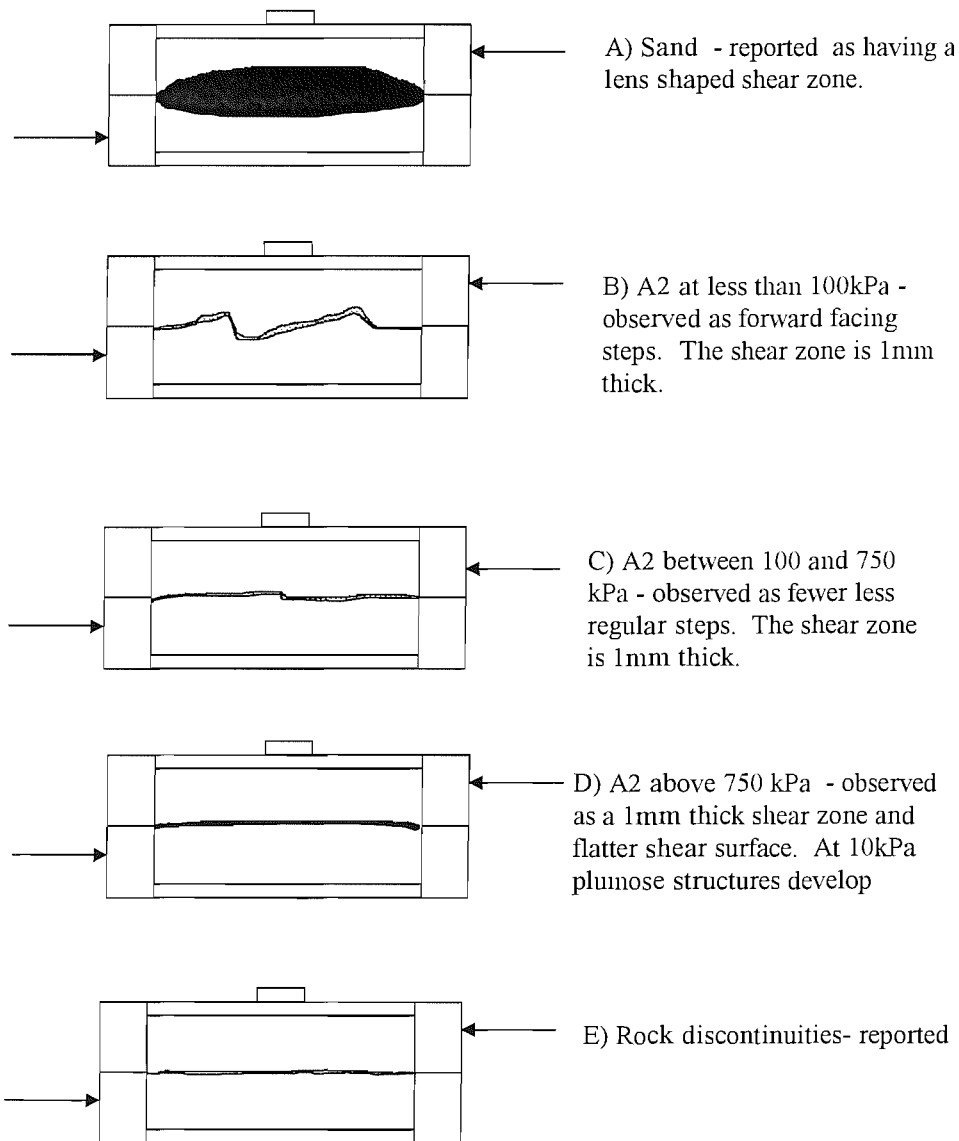


Figure 4.23 Comparison of the shear zones in sand, A2 and rock

Figures 4.15 and 4.20 show the shear zones of A2 sheared at 100kPa and 10MPa respectively, in both cases the shear zone is approximately 1mm wide, this is 4 times the D_{50} of A2. There are two notable observations:

- the normal stress range did not influence the thickness of the shear band
- the shear band is narrow compared to those previously reported for tests on both sands and weak sandstones.

A major difference between direct shear tests and triaxial or biaxial tests is the maximum displacement measured along the shear plane. Direct shear tests using a 60x60mm sample often stop only after 4 to 6mm of movement along the shear plane, triaxial tests usually stop before this amount of movement. The difference in the amount of local strain produced by the different testing methods will have an influence upon the degree of grain crushing and the position of any threshold values where changes in grain crushing behaviour occur.

4.4.3 Pluviated sample strength envelope

Vesic and Clough (1968) suggested that the deformation mechanism of sands varies with the pressure range. Below 100kPa no grain crushing occurs, grains are free to move relative to each other, and significant dilation occurs. Crushing becomes intense between 1MPa and 10MPa until at 10MPa a “breakdown stress” is reached. They defined breakdown stress as that stress at which all effects due to initial void ratio are removed. Above this stress the sand behaves “essentially as a linearly deformable solid”.

Pluviated A2 still shows a small peak at 10MPa, its “breakdown stress” has not been reached and there is no evidence of grain crushing (although the latter was only investigated by sieving). This resistance to the large pressures may be due to its high quartz content or the differences in testing using direct shear rather than triaxial apparatus.

Other authors also report that the peak friction angle for dense sand is dependent upon the confining pressure. Although Vardoulakis and Drescher (1985) detected an appreciable range of confining pressures ($50\text{kPa} \leq \sigma_c \leq 300\text{kPa}$) for a medium grained sand over which the pressure had no effect upon the peak friction angle, they found that below the lower boundary of this range the friction angle increased rapidly with declining confining pressure. This was interpreted as being due to interlocking of microscopic asperities at grain contacts. Above the upper boundary they suggest that grain crushing dominates, grain size changes during shear, and the peak friction angle drops.

4.4.4 Intact sample strength envelope

The tests on intact A2 at 10MPa normal stress showed that the total dilation and the dilation rate, measured at the boundaries, was an order of magnitude lower than that at 100kPa. At 10MPa however the peak strength was still 35% higher than the ultimate strength. The peak strength of the intact A2 was not suppressed at these high normal loads. It is proposed that the fabric structure imparts behaviour almost opposite to that reported for cemented, but poorly interlocked, sands where high normal loads produce frictional behaviour identical to that of the uncemented sand (Clough et al, 1981; Coop and Atkinson, 1993). At high normal loads there is widely reported convergence between the failure envelopes of cemented sands and similar but uncemented sand. This behaviour does not occur in sands with fabric structure; at high pressures they have characteristics that cannot be attributed to friction and dilation alone.

Although many authors suggest grain crushing as a mechanism that produces a lowering of ϕ'_{peak} it will also result in an increase in ϕ'_{ult} . Grain crushing produces more fines, changing the material's grain size distribution and producing a higher friction angle. This is referred to by Barnes & Dusseault (1982) as “clastic hardening”. A2 undergoes this transition at 750kPa, where an increase in ϕ'_{ult} is

discernable, and it is suggested that other quartzose sands may show this transition at different pressures depending upon the grain fabric and fracturing.

The large amount of grain crushing observed above 750kPa in the intact samples was not observed in the pluviated samples. This is thought to be due to the shape of the shear zone. Figure 4.23c shows the narrowness of the shear zone in the intact material at these medium pressures. The shear zone in pluviated material (figure 4.23a), however, is reported to be large in the centre of the box. In the narrow shear zone of the intact material (figure 4.23b,c,d,) grains will undergo more relative movement (local shear strain) and be less able to manoeuvre away from positions of very high stress. It is obvious that a single state of stress does not occur in these materials. Grain crushing may have been enhanced by the development of large local stresses at positions on the stepped failure surface and, with higher pressures, at the front of the convex up plumose structures.

Testing intact A2 using a proving ring to measure the shear force led to clastic hardening at lower normal loads. If the loss of strength of the sample occurs at a higher rate, with respect to displacement, than the reduction in the force provided by the ring then the sample will be broken explosively.

More difficult to explain is the increase in intact ϕ'_{peak} when a proving ring was used. Although this was not as pronounced as the increase in ϕ'_{ult} and showed some variability it was consistently higher. The good agreement between the load cell and the proving ring results for the pluviated samples and the care taken during calibration of the proving ring and loadcell exclude any calibration problem. The most obvious change that a proving ring causes is a change in strain rate. As the ring deforms then the strain rate is reduced.

Several tests were carried out to ascertain if the materials were rate sensitive but these were inconclusive. A proving ring also provides a certain amount of “softness” to the shear force. When using a proving ring the dial gauge was sometimes seen to swing rapidly with a deflection equivalent to a maximum linear

displacement of 0.030mm. This was followed by a return to the original reading. When a load cell was used spikes were produced showing the load dropping down to near zero. What this represents is not clear but if it is a time dependent rearrangement of the sample's structure (involving temporary elastic displacements of the apparatus) then substituting a load measuring device that has a compliance two orders of magnitude smaller will undoubtedly have an effect.

4.4.5 The intact peak strength envelope

Although the peak strength envelope for intact A2 shows three distinct areas (figures 4.7, 4.8) the change or step at 1.25MPa is possibly due to differences in the machines used for testing above and below this normal load combined with an overall concave down shear strength profile produced by a gradual change in the failure mechanism. Figure 4.1 shows the differences between the low normal load apparatus and the high normal load apparatus. The shear force remained horizontal in the low load apparatus whilst the shear force on the high normal load apparatus was able to move from the horizontal to a maximum angle α , where;

$$\tan\alpha = 24/149$$

$$\alpha = 11.4^\circ$$

assuming that the line of action is through the centre of the shear box. Figure 4.24 shows that only τ_{peak} is substantially different between the two machines, this could be due to a certain amount of dilation being required to displace the line of thrust and the ultimate strength conditions were without dilation. The difference is easily accounted for by a movement of the line of thrust of 11.4° .

Instantaneous failure and dilation was observed mainly in the tests carried out using the low normal load apparatus. There are two obvious explanations:

- The low normal load apparatus is less stiff than the high normal load apparatus. The energy required for this mode of failure came from the elastic energy stored in the apparatus.

- The two machines used have different mechanisms for applying the normal load; the low normal load apparatus used a hanger and weights with or without a lever arm. For instantaneous failure and dilation to occur the mass of the loading system has to be accelerated. The tests at 200kPa and above used a hanger combined with a lever system utilising less mass but more movement required for a similar dilation, this is considered to give similar behaviour to that of the hanger alone. The high normal load apparatus used a hydraulic ram to produce the normal load. This requires fluid to be moved through the hydraulic system during displacements of the shear box lid, and may have suppressed instantaneous dilation and caused the observed increase in strength.

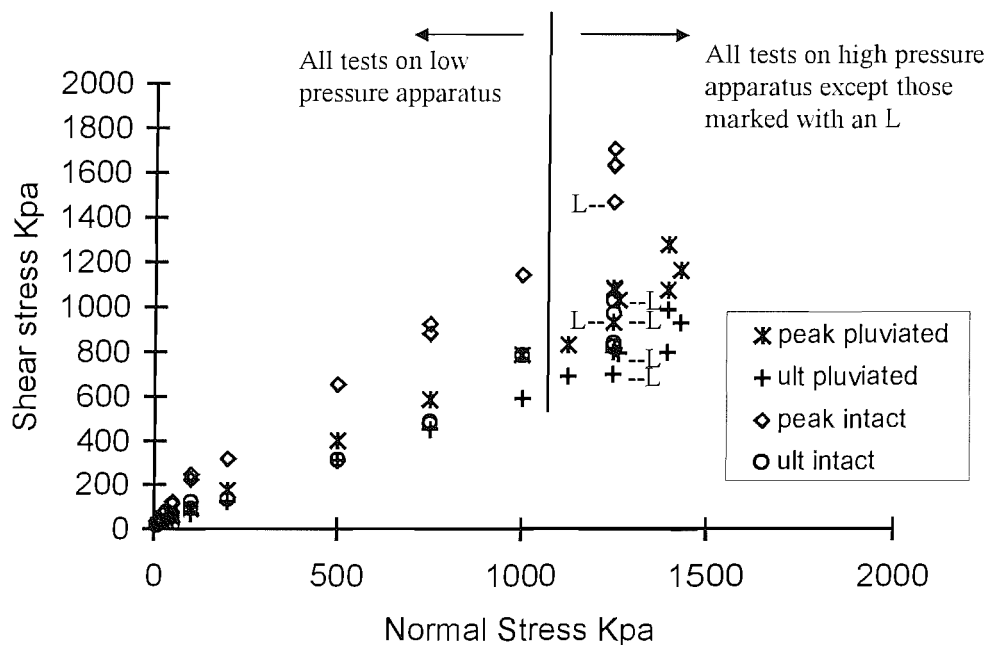


Figure 4.24 Detail of high and low normal load apparatus results at overlap.

The abrupt change at 100kPa in the peak strength envelope requires explanation. It is also at this load that there is a change observed in the shear plane after testing (see figure 4.24) and in how the shear zone develops. Highly curved failure envelopes have been observed for rock discontinuities for many years: these are discussed in the next section.

4.4.6 Rock joint models

Although concave down graphs (of τ vs. σ'_v) are produced by many geomaterials, and highly curved envelopes have been reported for rock joints, abrupt changes in ϕ' have only been reported in rock discontinuity models.

The work of Patton (1966) using plaster of Paris with sand and clay fillers to produce toothed samples gave the conclusions:

1. Irregular failure surfaces produce curved failure envelopes.
2. Slope changes are due to changes in the mode of failure.
3. Changes in the mode of failure are related to the properties of the failure surface asperities.

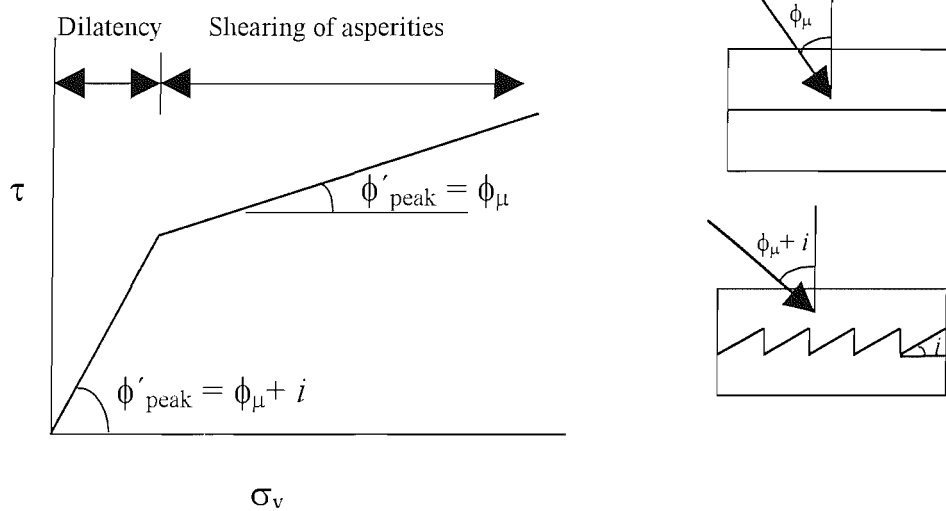


Figure 4.25. Patton's rock joint model giving an abrupt change of slope in the failure envelope

He noted an abrupt change in slope (figure 4.25) and suggested that this was due to a change in the mode of failure at that stress. At higher stresses asperities are sheared through before rotation and dilation can occur. Irregular rock surfaces usually produce a continuous curved failure envelope and no abrupt change is seen.

Patton (1966) suggested that no abrupt change occurs because “real failure envelopes for rocks do not reflect a simple change in the mode of failure but changes in the intensities of different modes of failure occurring simultaneously”. For A2 to show an abrupt change in its failure envelope at 100kPa an equally abrupt change in failure mode must be occurring.

Further work (see Hoek & Bray 1981) showed that $\phi' + i$, where i = dilatency angle (figure 4.24), can give very high friction angles (66° to 80°). Given that $\phi'_\mu = 30^\circ$ then the effective roughness angle varied between 36° and 50° . These large angles were considered to have been due to steep sided secondary projections controlling the shearing process at very low normal loads. As the normal load is increased the small steep projections are sheared off and the larger first order projections ($i = 10$ to 15°) take over as the controlling factor. It is possible that with A2 these secondary projections exist as grain surface morphology and the primary projections are the grains themselves causing shear surface roughness. A shear plane of infinitesimal thickness must be postulated for this model to work. With A2 at low normal loads there is a high ϕ' due to dilation which removes any secondary projection interlock and the strength it produces.

4.4.7 Failure modes of closely jointed rock masses

Determining the shear strength of closely jointed rock masses has produced a large body of work (see refs. in Hoek and Bray 1981, Hoek 1983). Of especial interest are the model studies carried out by Ladanyi and Archambault (1972, quoted with diagrams in Hoek and Bray 1981) using compressed concrete blocks. The model consisted of 1800 prismatic blocks measuring 12mm x 12mm x 63mm regularly packed into a biaxial loading frame (the scale of this experiment is as near to A2 as it is to jointed rock masses). Three distinct modes of failure occurred depending upon the orientation of the joints and the primary stress. The list below is in order of declining normal stress at failure:

1. Shearing was along a well defined plane inclined to the edges of the blocks and passing through blocks.
2. A narrow failure zone formed in which block rotation had occurred in addition to the sliding and block failure observed at high pressures.
3. A kink band formed, consisting of rotated and separated columns, 3 to 5 blocks wide.

Hoek (1983) commented that “intuitive reasoning suggests that the degree of interlocking of the model blocks is of a major significance in the behaviour of the model since this will control the freedom of the blocks to rotate”.

These three failure modes show a great similarity to the three modes displayed by A2 during direct shear. What is especially interesting is the formation of rotated and separated columns. It is unfortunate that these three modes were produced by different angles between the primary stress and the discontinuities and not directly by different stress levels, so a comparison cannot be easily made to the A2 results.

Ladanyi and Archambault (1972) proposed equations to predict the shear strength of closely jointed rock masses. These were refined by Hoek and Bray (1981). This mechanistic approach included considerations of block movement but required geometrical and material property parameters that are difficult to define. To overcome this a more empirical failure criterion was adopted. However, the equations do produce a bilinear failure envelope and merit further investigation as to their applicability to a locked sand.

In an attempt to produce the ideal model material of a jointed rock mass, Rosengren & Jaeger (1968) heated a coarse grained marble to 600°C. This destroyed any bonding cement and left an assemblage of extremely interlocked but independent grains, with a porosity of 4%. The mechanical properties of this “granulated marble” were found to be very different to those of soils. Small amounts of confining pressure produced large increases in the strength of the material resulting in the initial slope of the Mohr-Coulomb envelope being approximately 65°. Even if

one of the principal stresses was tensile a perpendicular compressive stress greatly increased the materials strength. This work was repeated by Gerogiannopoulos (1979, quoted in Hoek and Bray, 1981) and a bilinear failure envelope, initially at 65° is discernible.

4.4.8 Intercept - cohesion in A2

The shear test results for intact A2 produced an intercept of 16kPa. Extrapolating this at $\phi_{\text{peak}} = 65^\circ$ using the equation:

$$\sigma_T = (2c \cos \phi)/(1 + \sin \phi) \quad 4.1$$

gives an apparent value of tensile strength of 7kPa; this is a tensile strength that would support a column 350mm long of A2 and, although not tested, this was considered too large from experience of handling block samples. Testing the uniaxial tensile strength of rock is problematic and results when carefully measured are lower than predicted by the equation above (Hoek & Bray 1981). This tensile strength would represent that of the completely intact material free of any discontinuities but in practice samples often contain incipient joints or bedding planes along which the tensile strength is negligible. A tensile cut-off is therefore applied at a selected value of tensile stress, in practice this is often given the value of zero. A material with an interlocked fabric could have no uniaxial tensile strength and yet display a large direct shear strength at low normal loads; this is explored in the modelling section.

Cohesion in A2 could come from the following sources:

1. Adhesive bonds due to cold welding involving covalent or ionic bonds at grain contacts.
2. Mineral cement (clay, quartz or other minerals) in very small amounts (invisible using a optical microscope) at grain contacts.
3. Fines clustered at grain contacts.
4. The observed interlocked fabric.

Cold welding does not agree with the total disaggregation observed when handling block samples. If cold welding had occurred aggregations would be expected to be present after blocks had been broken up; since the cohesion would be due to adhesion between grains. Mineral cement could be expected to have the same influence as cold welding in this respect. Fines, by adhering to adjacent grains could directly cause cohesion or they could increase any interlock cohesion. Fines do not remain on the surface of grains after disaggregation so the former must be discounted. The most likely cause of cohesion in A2 is therefore interlock assisted by the presence of fines at grain contacts.

However the remarkable feature of A2 is the relative lack of cohesion not the presence of cohesion, given the extreme age of the material and degree of solid state diffusion and/or solution/deposition of silica that must have occurred to produce the euhedral fines and the interpenetrating and microsutured fabric.

4.4.9 Post peak undulations

There is doubt about what use to make of post peak information in rock like materials. It is widely considered that post peak behaviour represents the interaction of the test geometry and the shape of any localisation features. A2 produced highly defined localisation features and post peak undulations and these are thought to shed light on the failure mechanism. The secondary peaks could be due to the stepped failure surface or the new material produced by the formation of the shear zone dilating to a critical state.

4.4.10 Mode of failure of A2

Figure 4.23 compares the different failure modes for sand, locked sand at different normal stresses and rock. 'Hard' rock discontinuities generally fail along a plane that becomes polished with shear movement. However, some weakly cemented sandstones pluck, i.e. they release grains into the shear zone, whilst others form a shear band. This band is thought to be formed by grain movement followed by grain fracturing before peak stress is reached (Ord et al 1991).

The usual mechanism proposed for the shear failure of granular materials, at low normal loads, is the rotation of grains (Dobereiner and deFreitas, 1986); A2 is dense and angular and this mechanism would be prevented until the material dilates. Rotation could only take place in the shear zone; the rest of the sample remains intact.

No evidence has been collected to show whether A2 failed initially as a plane of infinitesimal thickness or a 1mm layer of disaggregated grains. Observations of the cracks and the stepped shear surface of low normal stress tests suggest that little material is bled into the shear zone from the surface of the steps, although little material is needed as the shear zone at full strain is only 1mm thick. It is difficult to explain how shearing can continue against the backward facing steps especially as these remain sharply defined throughout the test. The presence of these steps has an effect upon ϕ'_{ult} . Below 100kPa ϕ'_{ult} is 50° i.e. 19° higher than the ϕ'_{ult} for pluviated samples. Between $\sigma_v = 100\text{kPa}$ and $\sigma_v = 750\text{kPa}$, i.e. above the region where steps are formed and below the region of grain crushing, ϕ'_{ult} intact is only 1 to 2 degrees higher than the ϕ_{ult} for the pluviated samples.

4.4.11 Mode of failure - high pressure tests

The high pressure tests on A2 produced plumose structures with a convex up surface. Grain crushing occurred at the front of these structures (figure 4.20, position A in figure 4.19) but the rear (figure 4.22, position B in figure 4.19) shows

a macrovoid in thin section with little grain crushing. This macrovoid observed in thin section could have been either an area of sand at a void ratio less than the critical state void ratio at 100kPa or a true macrovoid. The lack of evidence for grain crushing at position B points to the conclusion that either:

- The sand failed before crushing began and therefore grain breakage is not the mechanism that allows failure to occur at high loads but is a consequence of continued strain after a shear plane has developed, or
- The load was preferentially borne by material toward the front of the box and grain crushing only occurred at this location, or
- Crushing did take place at location B to the same extent as at location A but the resulting fines were lost during the thin sectioning process - this is doubtful as the resin is more, not less, likely to enter fine grained areas.

At 10MPa, shear surface undulation was replaced by plumose structures. These have a convex up profile, which raises the question of how dilation is suppressed if the top has to ride over this domed surface. This is answered by the observation that the box lid rotates during shearing and the top half of the sample can rotate; the direct shearbox test is non-symmetrical. Plumose structures are related to crack propagation in brittle failure (refs in Einstein et al 1970).

4.4.12 Mode of failure - medium pressure tests

Instantaneous failure and dilation was a feature of the intact tests between 750 and 1250kPa and to a lesser extent above this. The instantaneous dilation was not due to rotating columns (as occurred in the low pressure tests - see below) but the top half of the sample riding over an uneven shear surface. This mode of failure is not recorded for poorly interlocked cemented sands, which become more sand-like, with predominately frictional and ductile behaviour, at higher loads. The interlocked fabric of locked sands produces a different mode of failure at these pressures which can be thought of as 'locking up'. The columns are sheared through before they can develop and produce the dilation observed at low normal loads. The instantaneous failure was possibly suppressed by the hydraulic normal load mechanism of the high

normal stress apparatus and possibly enhanced by the energy stored in the less stiff low normal stress apparatus.

4.4.13 Mode of failure - low pressure tests

Stepped failure surfaces, where regularly spaced steps point in the wrong direction, i.e. the steep side is opposed to the direction of sliding, have been observed by other workers. Einstein et al (1970) used a highly brittle model material; a gypsum plaster and found steps were formed up to 7MPa confining pressure in triaxial tests. They considered the steps to be part of secondary conjugate shear planes along which displacement occurs after the primary failure surface has been created. Mandl et al (1977) also report regularly spaced steps, opposing the direction of shear, whilst using a large ring shear apparatus to test a 'packed sugar'.

4.4.14 Crack formation

The cracks that determine the shape of the steps in the low pressure tests resemble Reidel shears or fractures. Details of en echelon structures in a micro tectonic environment are given by Hancock (1985). Applying the term Reidel shears implies that the cracks are caused by shear movement secondary to the primary shear direction. In the case of A2 the cracks form with a deviation of 23° to 25° to the primary shear direction when testing at less than 100kPa normal load. Differential compression of the sample base must occur to allow enough shear movement to produce the cracks. Observations using the glass sided shearbox and of the thin section of the shear zone show that as primary shearing continues these cracks open. There is no evidence to show that any shearing takes place along these cracks; any large movement, relative to the grain size, would have to displace grains and no evidence of grain movement is seen in the thin sections. Only the first crack remains open at the end of the test, this is seen in the thin sections as an area of high void ratio. One suggestion is that the cracks begin as shears and then widen as tension features. The alternative is that the cracks are simply tension features. A2 has very little tensile strength and shear failure is not needed to break the material. The

equivalent in micro tectonic terms would be the extension gashes which are observed in well folded non-metamorphosed sediments and are filled with authigenic quartz or carbonate.

4.4.15 Columns

Referring to figure 4.16, whatever the mechanism is that produces the cracks, the result is a series of slender columns, or more correctly walls, leant over in the direction of, and supporting, the primary stress. Oda and Kazama (1998) report that voids are formed periodically in the shear band of a dense sand in a biaxial apparatus. They suggest that “a shear band is nothing but a final structural form produced by buckling of well developed columns”. The scale of the columns reported by Oda and Kazama (1998) is only the width of the shear band whereas those observed in A2 are up to 5mm thick. This difference in scale could be due to the presence of grain fabric, with more long and concavo-convex micro sutured grain contacts, allowing larger columns to form.

Several questions are produced from observation of the columns formed in A2;

1. Is the dilation measured at the test boundaries affected by the movement of the columns?
2. What dictates the column spacing?
3. What dictates the column orientation?
4. If the load is supported by columns at the peak stress, is it supported by columns earlier in the test; when exactly are the columns formed?
5. What is occurring when these columns are sheared through toward the end of the test?

Answers to these questions are attempted below.

4.4.16 Dilation at low normal loads

The measured total dilation (table 4.1) is very similar for both the intact and the pluviated material over the range of normal loads used. The shear zone of the intact

material is known to be only 1 mm wide whilst the shear zone of the pluviated material is widely reported to be many times thicker than this. What would be expected, if both zones are at a critical void ratio for that normal stress, is that the pluviated tests would show much more dilation measured at the test boundary. This however did not occur. It is possible that the extra dilation in the intact samples was due to the columns rotating, although only the first crack (point p in figure 4.16) remains slightly open at the end of the test.

Given the thickness of the shear zone (1mm), the density of the intact material (1.861Mg/m³), the particle density (2.665Mg/m³) and an estimation of the critical void ratio (0.77) the amount of dilation can be calculated. The maximum dilation that can be produced by a 1 mm shear zone is 0.24mm, but this cannot account for 0.62mm dilation produced in all of the low pressure intact tests. The extra dilation produced during the intact material tests must be due to movement outside the shear zone or else parts of the shear zone must be much looser than the critical state. The thin section, glass sided shearbox and shear surface evidence, of tests at pressures under 100kPa, shows that the first crack (at P in figure 4.16) does open during the test and remains open in the thin section (figure 4.15). All the columns could therefore be rotated about their base giving a dilation;

$$\Delta y = R \sin(\arccos(\cos\theta - \Delta x/R)) - R \sin\theta \quad 4.2$$

where R is the length of the column. θ is the angle of the column to the horizontal and Δx is the horizontal displacement to τ_{peak} . The column thickness is ignored. Given $\theta = 23^\circ$ and estimating $R = 40$, and $x = 1.5\text{mm}$; then the dilation possible from this mechanism is over 3mm. This would leave the front crack open by 3.5mm. This is not observed but the dilation required by this mechanism is only 0.4mm, and this can easily be accounted for by the observed open crack.

The alternative to the dilation being due to movement of columns within the intact material is that areas existed within the shear zone that were looser than critical

state. The obvious way this could have occurred is that the stepped failure surface allowed voids to form between highly loaded prominent areas.

Evidence of only very small strains being possible before fabric disturbance within the intact material is given in chapter 6. It is suggested that no significant dilation could have occurred in the bulk of the sample; this remained intact at the end of the test and presumably could not have been strained above approximately 0.2%.

4.4.17 Column spacing and scale

The scale of the observed columns is nearly an order of magnitude larger than those reported by Oda and Kazama (1998). It is suggested that the A2 grains have a better “building” morphology due to their long and concavoconvex contacts and microsuturing; this allows larger scale columns to be produced.

Despite the closeness of the boundary compared to the scale of the steps some tests show two or three steps that have a relatively regular spacing. This can be compared with the spacing between shear planes when a model footing is pushed deeply into its supporting medium. Shearing develops when the material can no longer deform elastically and this occurs only after a particular amount of strain has occurred and a specific amount of energy is available.

4.4.18 Column orientation, formation and shearing.

Jewell and Wroth (1987) suggest that the horizontal plane in the direct shear apparatus is not a plane of maximum stress ratio, due to the boundary conditions of the test. The plane of maximum stress ratio is at α to the horizontal where

$$\alpha = (\phi'_{ps} - \psi)/2 \quad 4.3$$

$$\text{or combining with Bolton's (1986) equation } \phi'_{ps} = \phi'_{cv} + 0.8\psi \quad 4.4$$

$$\alpha = \phi'_{cv}/2 - \psi/10 \quad 4.5$$

Equation 4.3 may be helpful in explaining the orientation of the columns. It is doubtful whether equation 4.5 will be relevant to a locked sand in direct shear where, as has been shown above, the concept of a continuum cannot be applied due to localisation.

At some point in the test the shear plane is forced to correspond to the horizontal line of the box, even if the preliminary localisations cause this to be tortuous path. This is a different situation to that of a sand without fabric structure where a weakened and obvious plane running between the two halves of the box may not necessarily form.

If the columns were responsible for the observed dilation then they cannot have been formed at τ_{peak} , but must have formed, before the sample started to dilate, at a shear stress value roughly equivalent to τ_{ult} . The thin section and glass sided shearbox evidence shows that the cracks, and presumably the rotating columns, are present by the time the stress initially reaches a value equivalent to τ_{ult} .

The columns, if they are bounded by tension cracks, will have had no stress passing between them. Toward the end of the test the columns can be thought of as samples undergoing a form of unconfined compressive strength test, with the primary stress direction rotating.



4.5 A3 direct shear tests

4.5.1 Introduction and methods

Testing intact A3 in direct shear allowed a comparison to be made between A2 and A3; these being two sands with identical fabric structure but with zero, and a small but observable quantity of cement, respectively. No pluviated tests were carried out as it was observed that when disaggregated A2 and A3 were morphologically identical and would presumably give the same results, and also that the ϕ'_{ult} values for the A3 and A2 intact tests were identical. Wet tests were carried out to show the influence of water on the strength produced by fabric structure (and not on the strength due to the presence of any cement). To prevent this confusion it would have been better to have carried out these tests on A2 but a shortage of A2 toward the end of the testing program prevented this. The sample preparation and testing methods used for the direct shearing of dry A3 were the same as those used for A2. The quantity of cement in A3 was variable; the A3 samples were chosen not to include the most and the least cemented blocks. Some variation was still present. For the wet tests the water was added by pouring water into the carrier just prior to the test commencing. No wet tests were carried out at less than 100kPa; this confining pressure was considered to be enough to prevent any fabric disturbance without the need to wet the sample in a vacuum. It was assumed that the degree of saturation was sufficiently high for the influence of any tension within the pore water to be negligible. This was a drained test and the degree of saturation when measuring the change in sample volume was not important.

4.5.2 A3 results

In total 26 direct shear tests were carried out on intact A3, 8 of which were wet tests. Dry test results show the A3 failure surfaces similar to those of A2, with the exception of the tests at a normal stress of less than 200kPa which generally show steps at lower angles (10° to 15°). Typical failure surfaces are shown in figure 4.26.

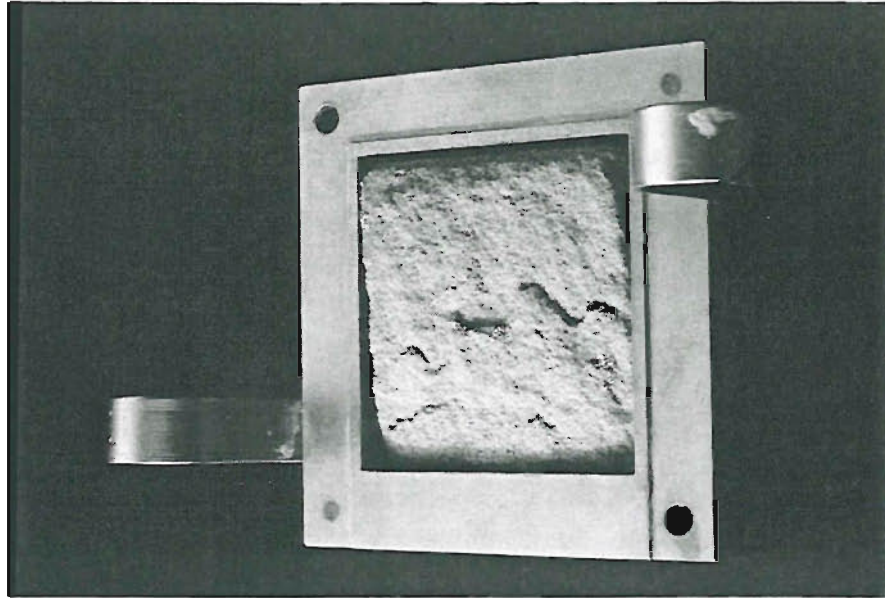


Figure 4.26a A3 shear surface after testing at 25kPa normal stress.

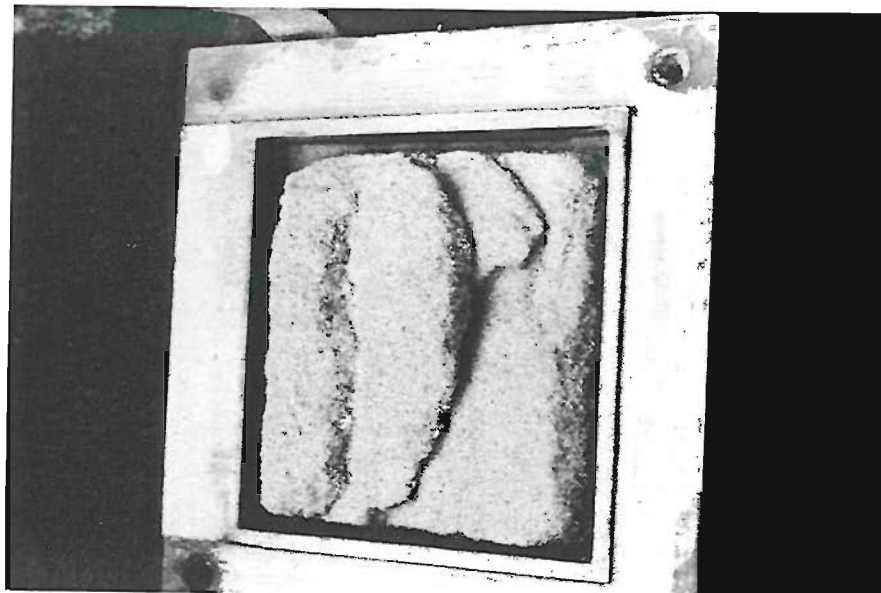


Figure 4.26b A3 shear surface after testing at 100kPa normal stress.

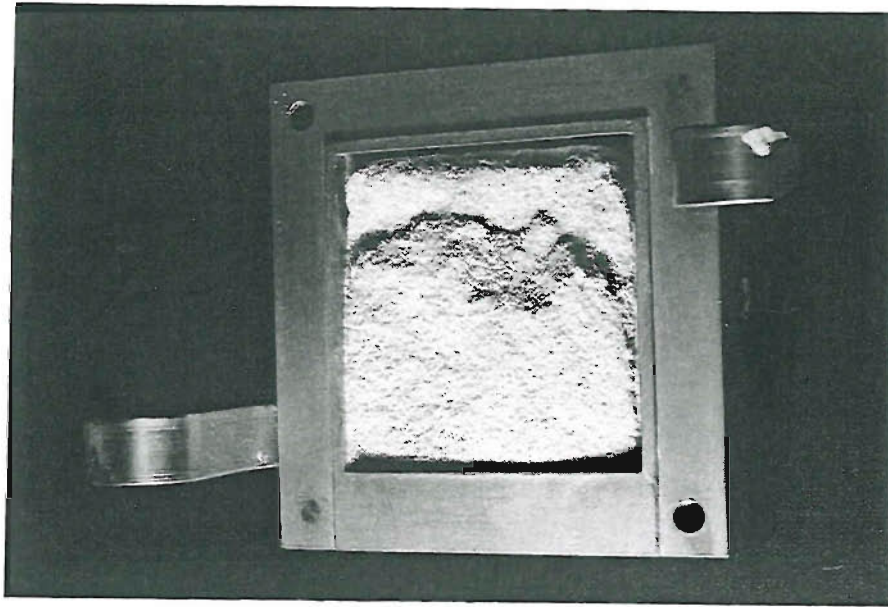


Figure 4.26c A3 shear surface after testing at 750kPa normal stress.

Recorded occasionally with A3 but not with A2 was the mode of failure depicted in figure 4.27 where a wedge of intact material remained at the front edge of the shear box. This occurred in tests up to 500kPa. Generally, in a similar way to A2, the A3 tests showed diminishing step height with increasing normal load.

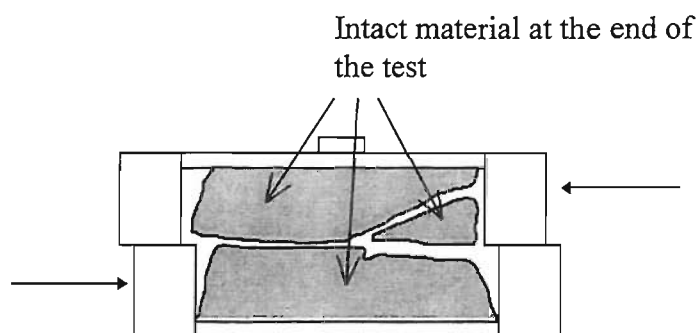


Figure 4.27 Front wedge type of failure seen in A3

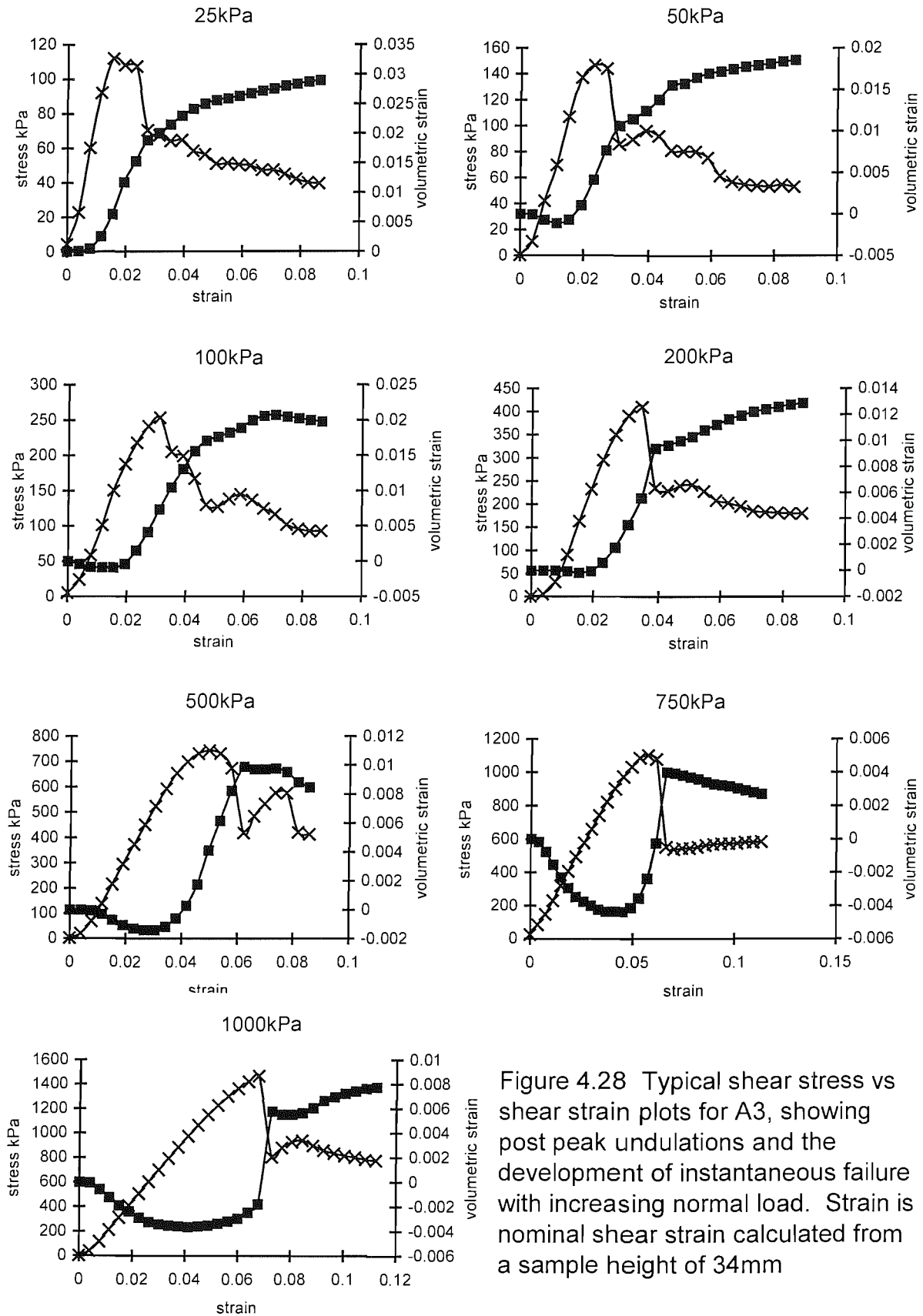


Figure 4.28 Typical shear stress vs shear strain plots for A3, showing post peak undulations and the development of instantaneous failure with increasing normal load. Strain is nominal shear strain calculated from a sample height of 34mm

Stress strain graphs for A3 (figure 4.28) show great similarity to those for A2. Post peak undulations were present in all tests below 750kPa. Their presence gives rise to problems in allocating a value for the ultimate strength. Instantaneous strength loss was observed in the 750 and 1000kPa tests.

Figure 4.29 shows the shear strength vs. normal load plot for A3. Two tests were carried out at each normal load, and these gave close results. Similarly to the A2 results there is a large variation in ϕ'_{peak} and intercept values depending upon the normal load. Two highly linear areas are present: below 100kPa $\phi'_{\text{peak}} = 61^\circ$, $c = 60\text{kPa}$, $R^2 = 0.959$; above 100kPa $\phi'_{\text{peak}} = 52^\circ$, $c = 106\text{kPa}$, $R^2 = 0.977$. Only one test was carried out on A3 at a normal load above 1000kPa. This was at a normal load of 10MPa and gave a τ_{peak} of 8.143MPa and a τ_{ult} of 6.079MPa; both figures are similar to those obtained for A2.

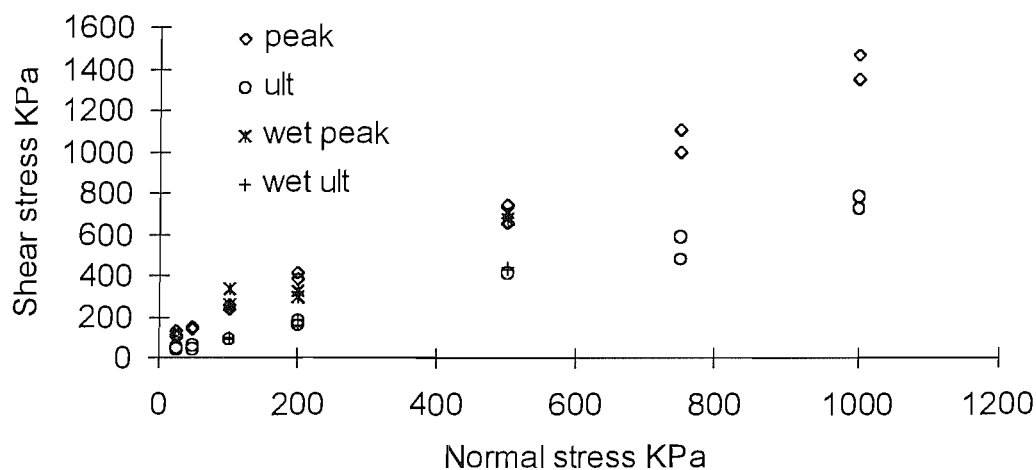


Figure 4.29 Shear strength vs. normal load plot for A3

Some intact material was found after the wet tests, however this disaggregated before it could be observed in enough detail to ascertain the morphology of any shear surface features. Post peak undulations were observed during the wet tests, no tests were carried out at pressures above 500kPa so no information on potential instantaneous failure and dilation was gathered. Figure 4.29 shows the wet tests plotted with the dry tests. Wet tests produced τ_{peak} values slightly varying from those of the dry tests, τ_{ult} , however, was similar in both the wet and dry tests. Of special note is a 100kPa normal load test producing a τ_{peak} value of 330kPa.

4.5.3 A3 tests observations and discussion

It was presumed that A3 would be more variable due to each block containing slightly differing amounts of cement. The results show, however, little variation between A3 tests at the same normal load. A3 was tested after A2 when sample preparation and testing skills had improved, and this was possibly the reason why such repeatable results for A3 were obtained.

Much of the observation and discussion section for A2 is relevant to A3. The failure surfaces of A3 showed steps similar to those of A2 suggesting that the mode of failure was also similar. Some differences were recorded:

- The presence of a front wedge of intact material.
- Sharper steps and steps recorded at a higher normal load than for tests on A2.
- At low normal loads the steps were at lower angles.

The cement in A3 possibly preserved the stress induced structures resulting in the sharper steps. The front wedge formed in A3 showed extreme fragility, a similar structure may have formed in A2 but not have survived the disturbance when the top half of the box was removed. The front wedge would have been fragile due to its size as well as the effect of any strains it had incurred during the test. The smaller step angle recorded at the lower normal loads was possibly due to the influence of the cement.

The top and bottom of the sample remained intact after the wet tests and the assumption that the fabric would not be disturbed by the wetting process was correct. The difference between the τ_{peak} results for the wet and dry tests is probably due to variability in τ_{peak} ; it is unlikely that τ_{peak} is following a different pattern and the small number of tests does not allow firm conclusions to be drawn. The fact that the τ_{ult} values are identical suggests that the mechanism is nothing to do with the wet and dry friction angles of the grains. Unlike the weak sandstones reported in the literature (see references in section 1.2.6), the wet tests show no evidence that the presence of water weakens A3.

4.5.4 A2 and A3 compared

Figures 4.30a and 4.30b show τ_{peak} and τ_{ult} against normal load for both A2 and A3. ϕ'_{peak} and intercept values (extrapolated from data points within the σ'_v range shown) are given in table 4.2.

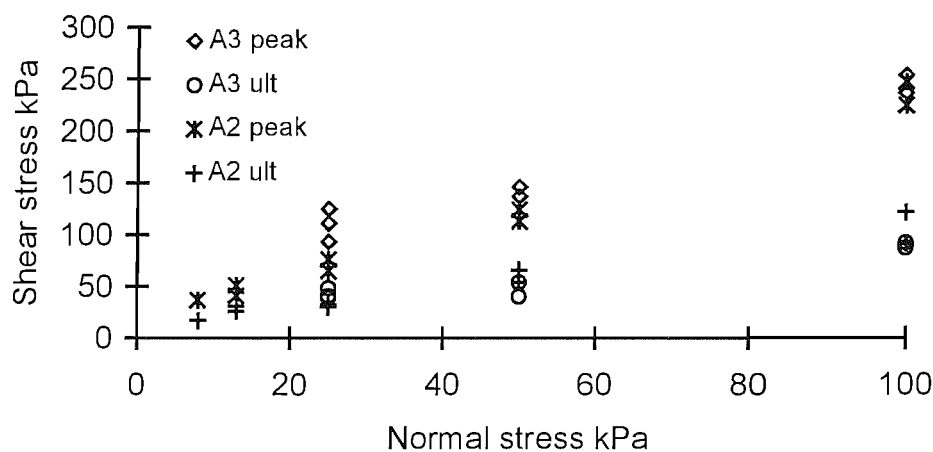


Figure 4.30a Envelope for intact A2 and A3 at normal stresses of 100kPa and below

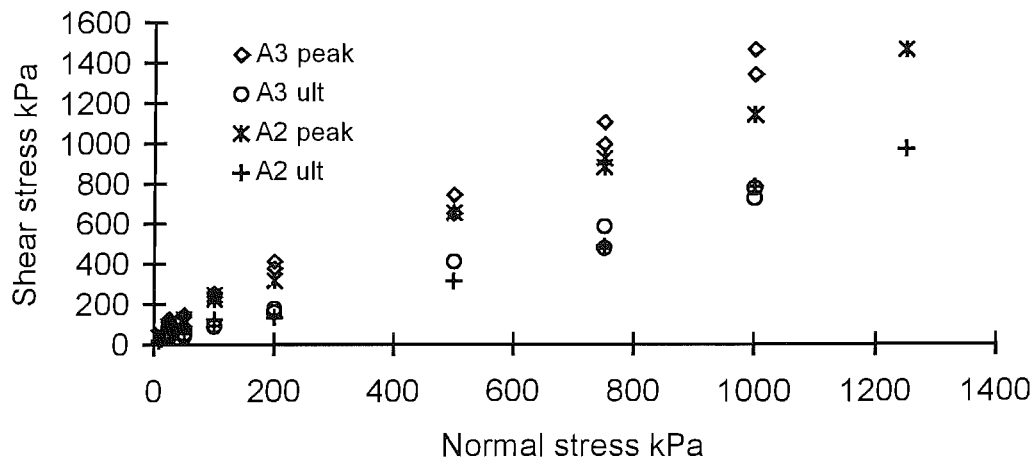


Figure 4.30b Envelope for intact A2 and A3

	σ'_3 kPa	ϕ'_{peak}	c kPa	no. of tests	r^2 value
A2	$8 \leq \sigma'_3 \leq 100$	65°	16	8	0.989
A3	$25 \leq \sigma'_3 \leq 100$	61°	60	7	0.959
A2	$100 \leq \sigma'_3 \leq 1250$	47°	103	8	0.996
A3	$100 \leq \sigma'_3 \leq 1000$	52°	107	10	0.977

Table 4.2 Comparison of A2 and A3 peak friction angles and extrapolated intercepts.

A3 has a larger intercept, extrapolated from data points with $\sigma'_3 \leq 100$, than A2. This is to expected, A3 displayed far higher cohesion in hand sample. No tests were carried out on A3 at 8 and 13 kPa, this was unfortunate as results from this range would have displayed the larger intercept with less extrapolation. At 100kPa A2 shows a larger and more defined change of ϕ'_{peak} than A3.

A2 and A3 have close c values extrapolated from data points above 100kPa; whether this has any relevance is not clear. A3 has a larger ϕ'_{peak} than A2 from $100 \leq \sigma'_3 \leq 1000$ kPa, only one test for A3 was carried out at a normal load above this

range and it gave a similar value as A2 with a normal load of 10MPa. The A3 peak envelope must therefore drop to meet that of A2 at this load.

A3 displays a very linear ϕ'_{ult} over the tested range (37° , $r^2 = 0.9881$). The drop seen in A2 ϕ'_{ult} between 100 and 750kPa did not occur with A3. A possible explanation is that with A3 no gap exists in the mechanisms that elevate the ϕ'_{ult} of intact material above that of the disaggregated material. These were postulated to be backward facing steps at low loads and grain crushing at higher loads.

4.6 Direct shear - conclusions

1. Using a proving ring when testing locked sands in direct shear will not give reliable information on their ultimate strength envelope.
2. The sample preparation method utilising a pluviated edge has been found successful in fitting intact samples of locked sand into the direct shearbox.
3. A locked sand with no cement and a locked sand with a small amount of cement have been shown, when tested in direct shear, to produce a strongly bilinear peak failure envelope with the change in angle at 100kPa. At normal loads below 100kPa ϕ'_{peak} was over 60° , dropping to approximately 50° at loads between 100kPa and 1000kPa. The envelopes are then concave down with a ϕ'_{peak} angle of 38° at 10MPa.
4. When tested in direct shear a locked sand has been shown to display three distinct types of failure at different normal loads.
5. Stress induced structures, resembling columns with their long axis orientated in the direction of the principal stress, were produced during direct shear *at low normal loads ($<100\text{kPa}$)*. These were preserved as a stepped failure surface with the steps in the opposite direction to those displayed in soil dilation models.
6. Dilation at the boundaries of these low normal load tests cannot be accounted for by dilation in the shear zone alone. Areas must have been produced that were less dense than (ie on the wet side of) the critical state void ratio. These areas could have been between rotating columns or created by continuing shear against the stepped shear surface.
7. *At normal loads between 750kPa and 5MPa* the locked sand failed with a near instantaneous loss of strength from peak to ultimate. This was accompanied by

grain crushing and a flatter shear surface. The interlocked fabric produces instantaneous failure at these pressures, which is influenced by apparatus stiffness.

8. The peak strength was not suppressed *at 10MPa*; this is in contrast to the behaviour reported for poorly interlocked cemented sands which become frictional materials at high normal loads. It appears that sands with no grain bonding, but with a large amount of fabric strength, behave in a brittle, rock like manner during direct shear at high normal loads. This is observed as a narrow shear zone with plumose structures and crushed grains.
9. Over the whole range of normal loads used in this study (between 8kPa and 10MPa) the same thickness shear band was produced: equivalent to four times the D_{50} . This is very narrow compared to published results for the rupture zone in sands, and narrower than the reported figures for sandstones.
10. The ultimate intact strength has been found to be higher than the pluviated ultimate strength throughout the range of normal stresses tested. This is considered due to; the formation of steps facing against the shear direction at low normal loads, and grain crushing at high normal loads. The A2 results displayed a gap between these two mechanisms from 200 to 750kPa where ϕ'_{ult} intact was only 1-2 degrees above ϕ'_{ult} pluviated.
11. Unlike the weak sandstones reported in the literature, the wet tests show no evidence that the presence of water weakens A3 if a confining pressure is applied during wetting. Fabric structure in quartz sands, if not disturbed, is not influenced by the presence of water.

CHAPTER 5: TRIAXIAL TESTS

5.1 Methods

5.1.1 The hard shell

Producing 2:1 38mm diameter samples from A3 was found to be impossible without the use of a hard shell. It was assumed that leaving this in place would have had a large effect on the outcome of a test. Using the triaxial apparatus allowed the hard shell to be removed by flushing with water after a confining pressure had been applied. The cell confining pressure held the sample intact and an applied vacuum prevented the development of slaking forces (see wetting section). The method required that the sample was tested wet. It may have been possible to dry the sample by application of a vacuum or compressed air after flushing but this was not attempted.

The softening effect of water on the hard shell was tested by placing 10mm x 10mm x 20mm hairsprayed samples into still water and monitoring the change in strength. This was tested by pushing a probe into the samples at intervals. Full weakening and collapse occurred after one minute. Some adhesion remained between grains that had been heavily sprayed but this was removed by the gentlest of probe movements; it was not possible to move these aggregations of weakly adhering grains without them coming apart. The conclusion drawn was that the remains of the hairspray, after 10 minutes flushing, would have no significant effect on the triaxial test results.

5.1.2 Sample preparation

Forming 36mm diameter by 76mm long intact cylindrical samples of A3 was made possible by keeping the majority of the surface encased in hairspray. The following method proved reliable.

- I. The first three stages followed those of shearbox sample preparation - all preparation was carried out on a glass plate. This produced a prism 10mm larger than required.
- II. One end was ground flat on the glass plate, sprayed and placed on a 38mm platen.
- III. The prism was filed down using 80 grade abrasive cloth stuck to a right angle wooden block; only 1/8 of the emerging cylinder was exposed at a time. A set square was used to check for right angle between the sample and the glass plate.
- IV. The newly exposed areas were sprayed.
- V. Stages 3 & 4 were repeated until the cylinder was completed.
- VI. The height was adjusted with the wooden block and the top end of the sample made flat and parallel to the glass plate. This was checked by placing a platen on the top of the sample and a 300mm straight edge on this. Measurement between the ends of the straight edge and the glass plate were taken; these were kept within 2mm of each other, giving a tolerance on the sample ends of 0.24mm or 0.36°.

Pells and Ferry (1983) found that the ISRM and other authorities had unnecessarily stringent recommendations for the dimensional tolerances of UCS samples. They suggested that for rocks having uniaxial strengths of 50MPa or less there was no statistically significant difference (in UCS tests) if the specimen ends were non-parallel by as much as 2°. What was found to be very important was the roughness of the ends - especially any doming. When forming A2 and A3 to a particular dimension their surfaces are removed by grain plucking. Their D_{50} size is 0.25mm so any surface formed will have at least this roughness. It is suggested that any quoted dimension tolerances that are smaller than the grain size, of these and similar materials, must be treated with caution. Cuccovillo and Coop (1997) quote tolerances of plus or minus 0.01mm for a material with similar grain size (0.25mm), but used gypsum cement to fit the sample to the top and bottom platens.

5.1.3 Testing method

A standard triaxial apparatus was used with load measured by a load cell and volume change measured by a 10ml burette.

1. A 38mm diameter sample was held together by a hard shell whilst placing it in the triaxial cell.
2. Confining pressure was applied
3. A vacuum was applied to the sample via the top platen (fig 5.1).
4. De-aired water was admitted through the bottom platen to wet the sample and flush the hairspray. The water moved up through the sample in 3 to 5 seconds with a 1m head. Flushing continued for 10minutes, with an excess of 100ml being collected from the return pipe.
5. A drained test at 6×10^{-6} m/s closing gap speed was carried out; equivalent to a strain rate of 0.5%/min for a 76mm sample. Each test took approximately 10mins to complete, and given that the water entered the sample in less than 5 seconds with a 1m head it was considered that fully drained conditions were occurring.

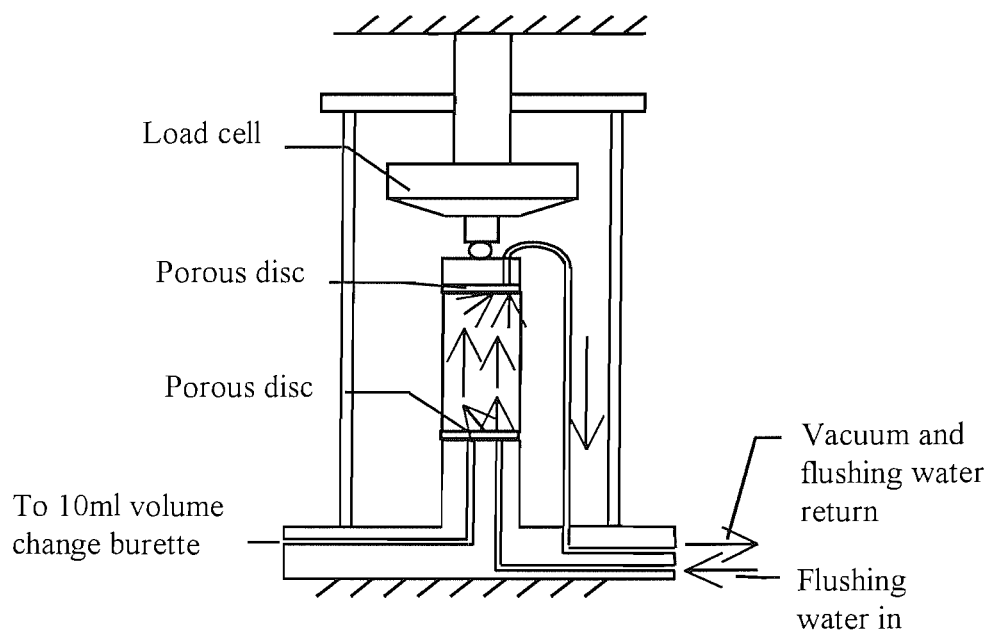


Figure 5.1 Method of applying the vacuum and flushing the sample

5.2 Results

5.2.1 Introduction

In all 15 tests were carried out on samples of A3. Of these one was disregarded due to bad sample preparation, one due to misalignment of the loading frame and two had no results for volume change due to membrane leaks. Testing was at 6, 12, 50, 100, 200 and 300 kPa cell pressures. The confining pressure for the 6 & 12kPa tests was produced by static head, the confining pressure for the other tests was produced by an air water bladder interface. Two tests at 100kPa were on short samples (45 and 50mm) and one test on a long sample (90mm). All other tests were on 76 ± 4 mm samples. Initial results with the 76mm samples showed that the high ϕ' angle of the material may have been preventing a shear plane developing due to the maximum stress ratio occurring steeper than corner to corner. Short samples were tested to see if this effect could be exacerbated and a long sample to see if the effect could be prevented.

5.2.2 Mobilised ϕ' and volumetric strain vs. axial strain plots.

Figure 5.2 shows typical mobilised ϕ' and volumetric strain vs. axial strain graphs for 6, 12, 50, 100, 200, and 300kPa confining pressures. The ϕ'_{mob} figures were calculated using;

$$\sin \phi'_{mob} = (\sigma'_1 - \sigma'_3) / (\sigma'_1 + \sigma'_3) \quad 5.1$$

The ϕ'_{mob} values represent the angle from the origin to a tangent on the stress circle of the More-Coulomb plot for that point of the test. No cohesion intercept is allowed for and the peak ϕ'_{mob} values are therefore larger than those from the Mohr-Coulomb plot derived from the peak states of all the tests where an intercept is present.

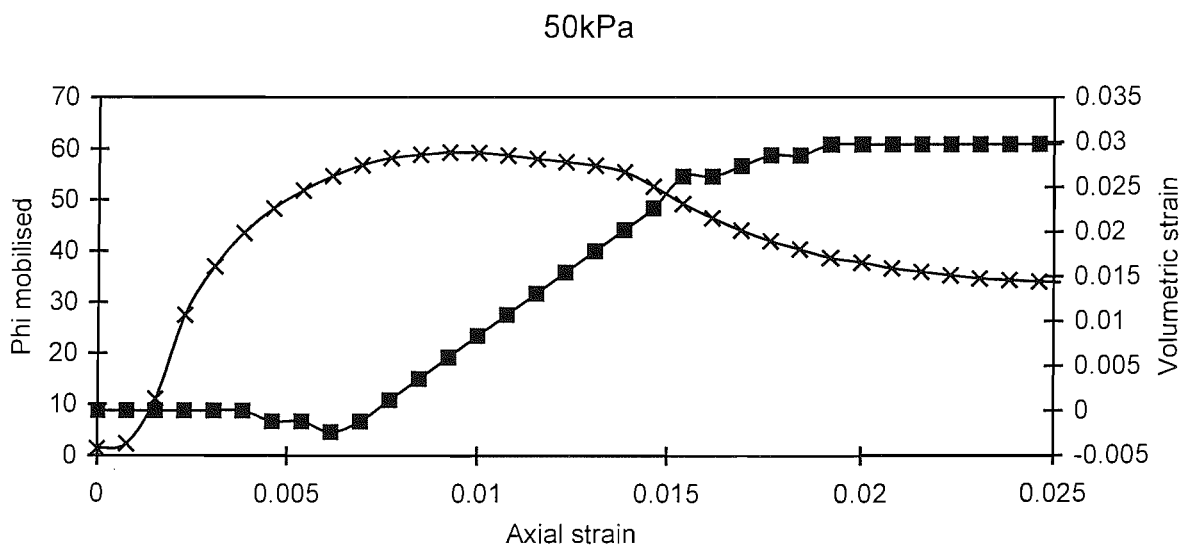
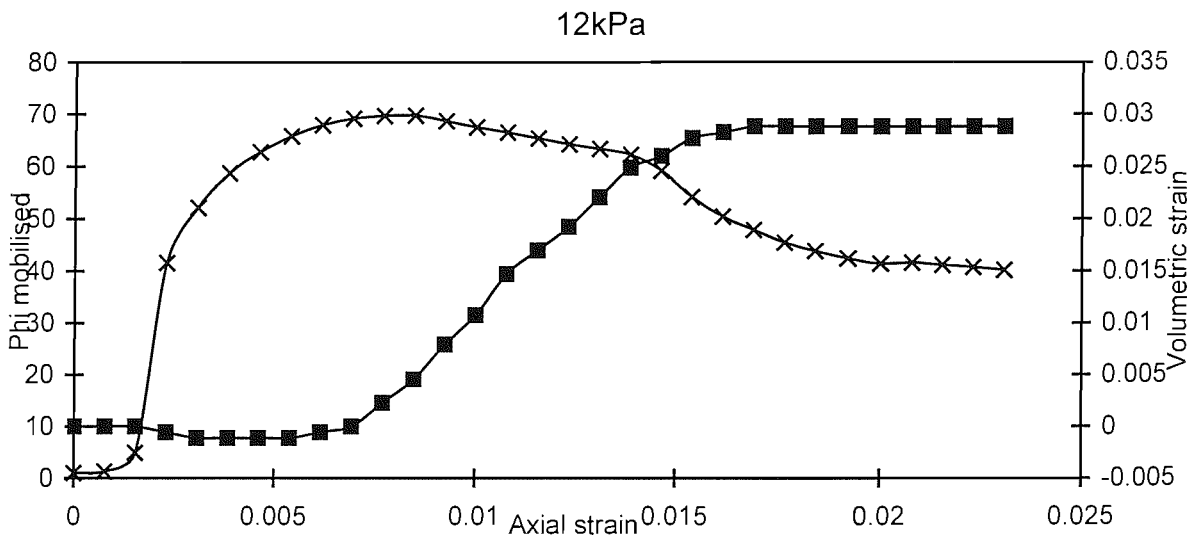
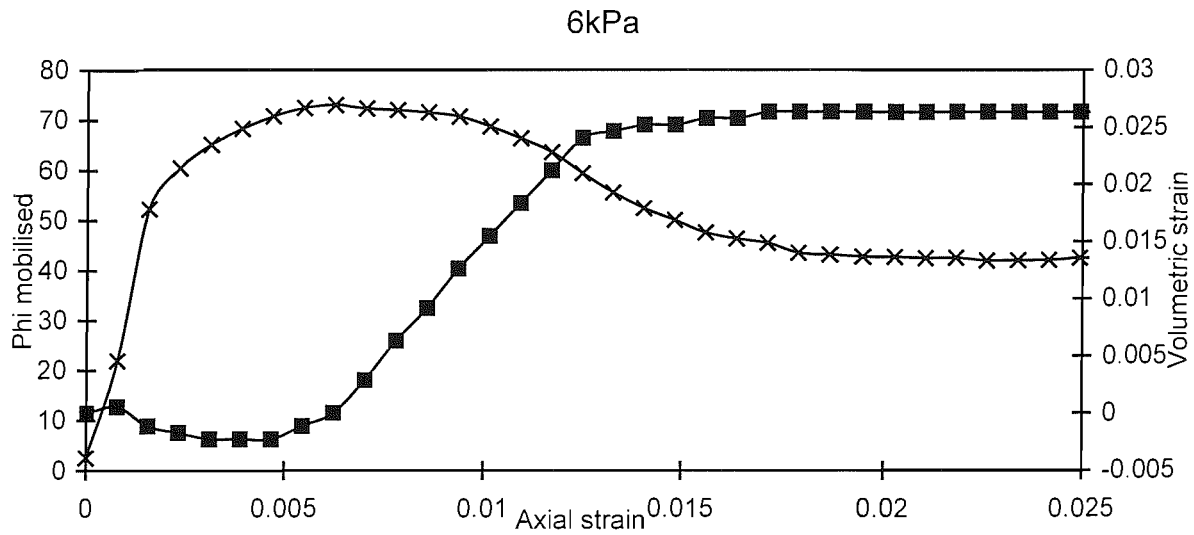


Figure 5.2a Phi mobilised vs axial strain and volumetric strain vs axial strain for confining pressures of 6, 12 and 50kPa

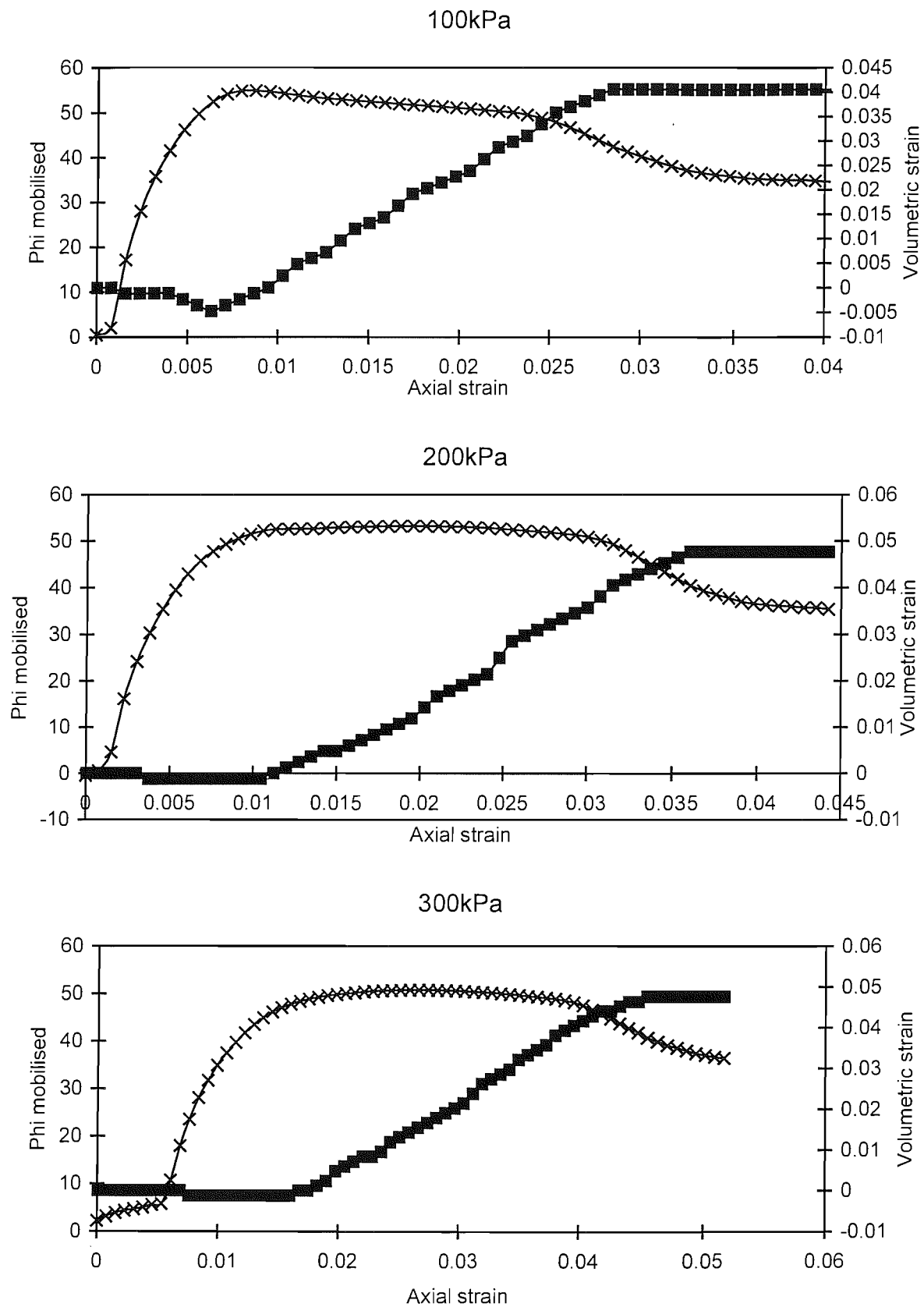


Figure 5.2b Phi mobilised vs axial strain and volumetric strain vs axial strain for confining pressures of 100, 200 and 300kPa

The ϕ'_{mob} values are presented with an area correction but without a membrane correction. The membrane correction changes as the failure mode moves from barrelling to single plane slip. Figures given in B.S. 1377 part 8: 1990 and Head (1986) show a correction of only 0.7 kPa for a strain of 5% for barrelling distortion. Much larger figures are given in Head (1986) for single plane slip; 30kPa at 5% strain from start of slip and 50kPa cell pressure, a factor is also given for the angle of the slip plane. No consensus appears to exist on how much membrane correction to apply and it is assumed here that the membrane confining forces could be ignored due to:

1. The small strains to peak (all less than 3% and at the lower confining pressures less than 1%)
2. The small strains after a single plane slip had commenced (similar to the strains to peak)
3. Lower confining pressures, where the membrane correction would be important, produced lower strains to peak and lower strains to a steady state.

In calculating the axial strain no attempt was made to calibrate the compliance of end platens, the load cell, or the loading frame. This method of calibration is considered to be notoriously inaccurate (Elliot 1993) and would have been required only to find accurately the stiffness of the material, which was tested using local LVDTs during uniaxial tests.

5.2.3 Extended peak and dilation

The most striking feature of the stress strain plots is the presence of an extended peak. Corresponding to the extended peak is dilation occurring at a uniform rate. Both the length of the extended peak and the total volume change increase with confining pressure with a step between 50 and 100kPa. (figure 5.3).

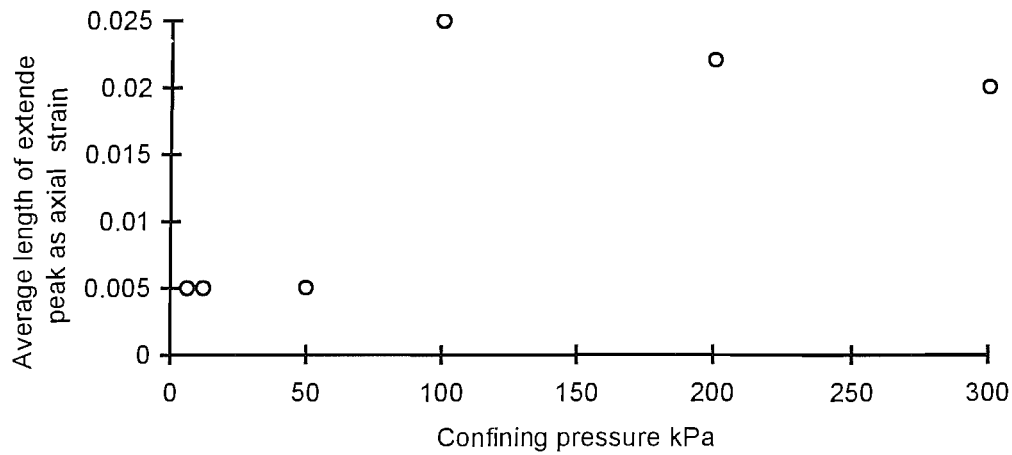


Figure 5.3a The average length of the extended peak (as axial strain) plotted against confining pressure. Note the change between 50 and 100kPa.

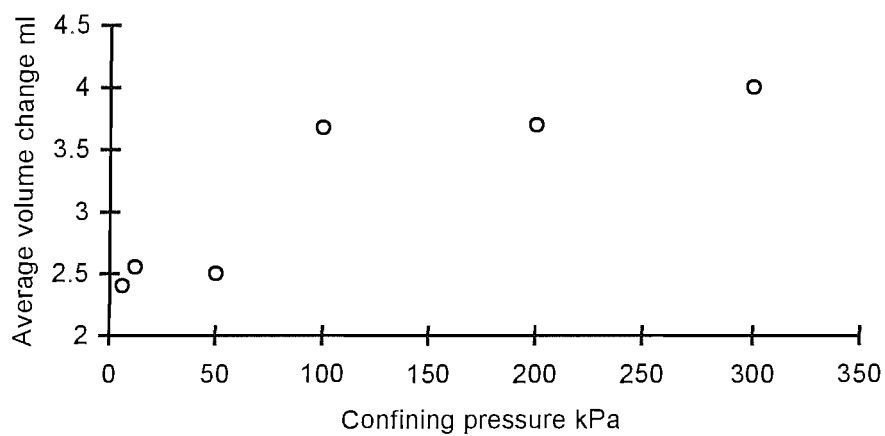


Figure 5.3b The average volume change plotted against confining pressure. Note the change between 50 and 100kPa.

Figure 5.4 shows the length of the extended peak (as strain) plotted against the total volume change. Two data points are shown for the non 2:1 samples; one for strains calculated from the actual length and one for strain calculated from a nominal 76mm. This is explained in the discussion section.

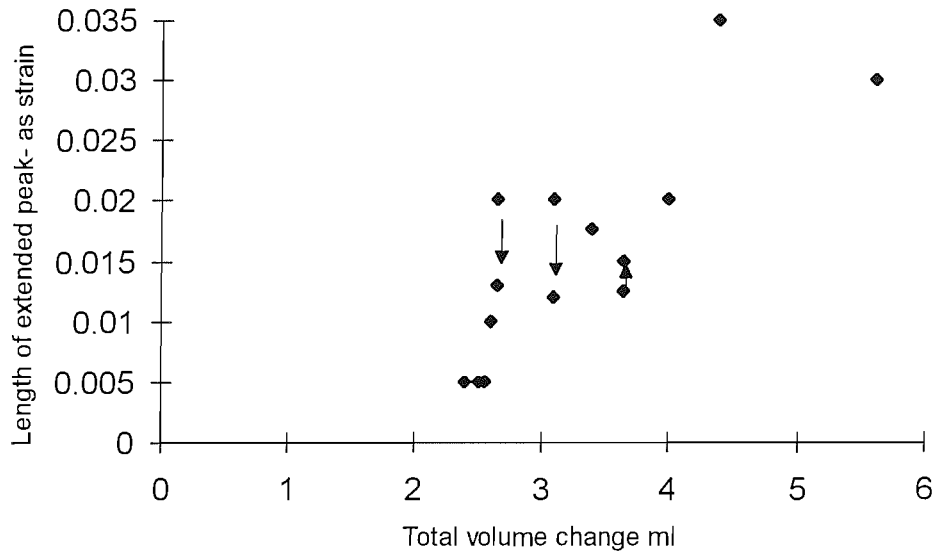


Figure 5.4 The length of the extended peak plotted against the total volume change. The arrows show the two short and the one long sample corrected to a nominal axial strain value using a length of 76mm.

Because the uniform dilation occurred at a fairly steady load the compliance and bedding errors could be discounted. Axial strain (ϵ_a) has therefore been calculated for the period of the extended peak using the jack speed. The dilation angle (ψ) values were originally calculated using the equation for triaxial strain (ψ_t) conditions;

by definition $\sin \psi = \epsilon_{vol} / \gamma$ and $\gamma = \epsilon_a - \epsilon_r$

and for triaxial conditions $\epsilon_{vol} = \epsilon_a + 2\epsilon_r$

$$-\sin \psi_t = 2\epsilon_{vol} / (3\epsilon_a - \epsilon_{vol}) \quad 5.2$$

The ψ_t values calculated from the above equation were, for the lower pressure tests, in excess of 90° and in general were considered to be excessive (figure 5.5). The dilation angle values were recalculated assuming plane strain conditions (ψ_{ps});

for plain strain conditions

$$\epsilon_{vol} = \epsilon_a + \epsilon_r$$

$$-\sin\psi_{ps} = \epsilon_{vol} / (2\epsilon_a - \epsilon_{vol}) \quad 5.3$$

These are shown in figure 5.5. The dilation angle falls with increasing confining pressure.

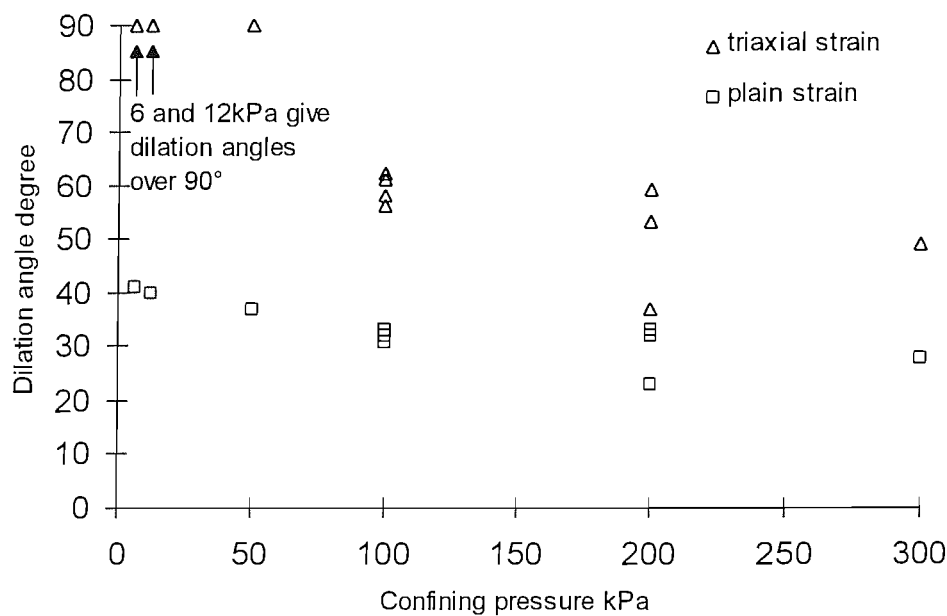


Figure 5.5 The dilation angle calculated for triaxial strain and plain strain plotted against the confining pressure.

5.2.4 Strength envelope

Obtaining the traditional failure envelope on a Mohr-Coulomb plot requires a tangential line to be drawn to the Mohr's circles. This is usually done by eye. If s' , t points are plotted then a series of points is produced and a regression analysis in a standard pc can be used (Parry, 1995). If β' and k' are the angle of slope and the intercept obtained from an s' , t plot then:

$$\tan\beta' = \sin\phi'$$

and

$$k' = c' \cos\phi'$$

Figure 5.6 shows the s', t peak strength plot drawn for all tests. An intercept (c') at 48kPa is present. The envelope is highly linear with $r^2 = 0.9945$ and $\phi'_{\text{peak}} = 50^\circ$. An ultimate strength envelope derived in the same way gave a zero intercept and $\phi'_{\text{ult}} = 35^\circ$.

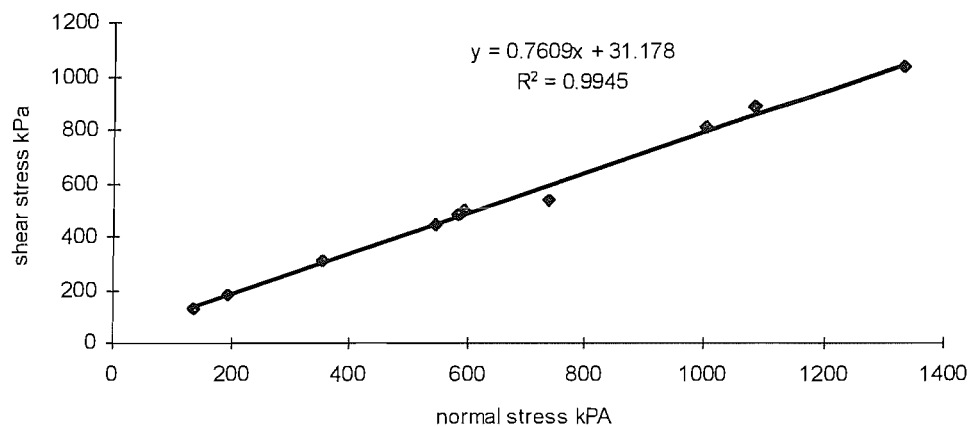


Figure 5.6 Peak strength s', t plot for all the triaxial results

5.2.5 Failure Mode

It was noteworthy that all tests between 50 and 300 kPa produced failure planes orientated between 64° and 60° from the horizontal; in the 2:1 samples the slip plane was corner to corner (figure 5.7a). The low confining pressure tests (6 and 12 kPa) failed as shown in figure 5.7b; the majority of the material was still intact at the end of these tests whereas the higher normal loads left intact material only at each end of the sample. All the tests at the higher confining pressures (100kPa and over) showed an amount of barrelling before a shear plane developed. Figure 5.7c and d shows the shear planes for the long and short samples.

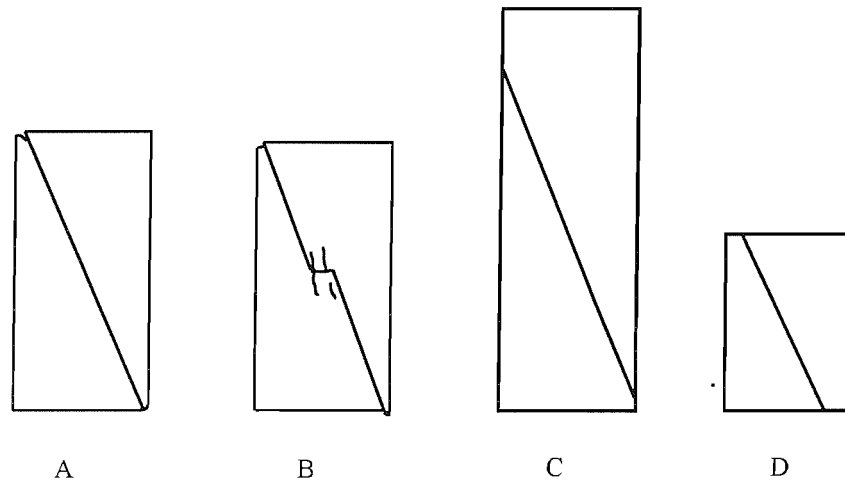


Figure 5.7 Comparison of the shear plane orientation and morphology. A) The shear plane in the 2:1 samples at pressures at 50kPa and over was from corner to corner. B) The shear plane at confining pressures below 50 kPa contained a central step. C) and D) Both the long and short samples produced shear planes at the same angles as the 2:1 samples (60 to 64 degrees).

5.2.6 Long and short samples

Figure 5.8 shows the mobilised friction angle and volumetric strain vs. axial strain graphs for the 45mm, 50mm, and 90mm samples. These samples show similar total dilation, measured as a volume, to the other 100kPa confining pressure tests; volumetric strain figures vary depending upon the length of the sample.

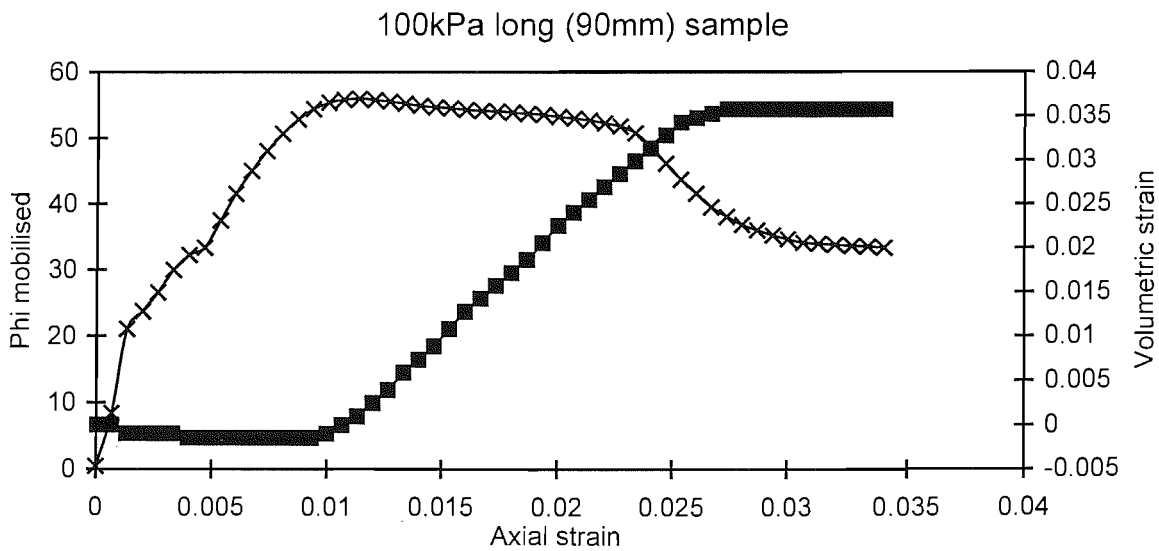
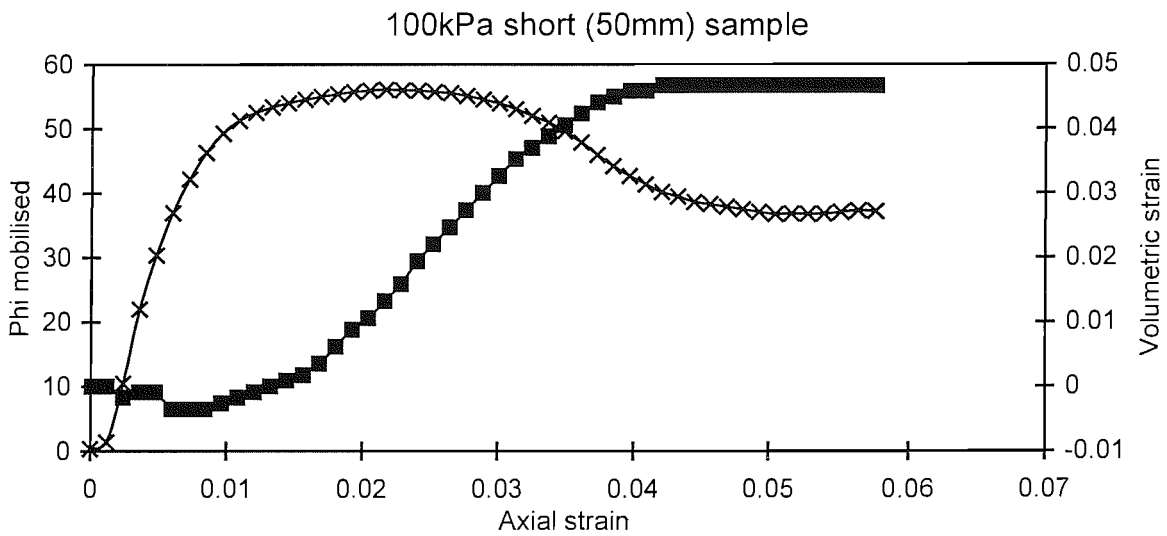
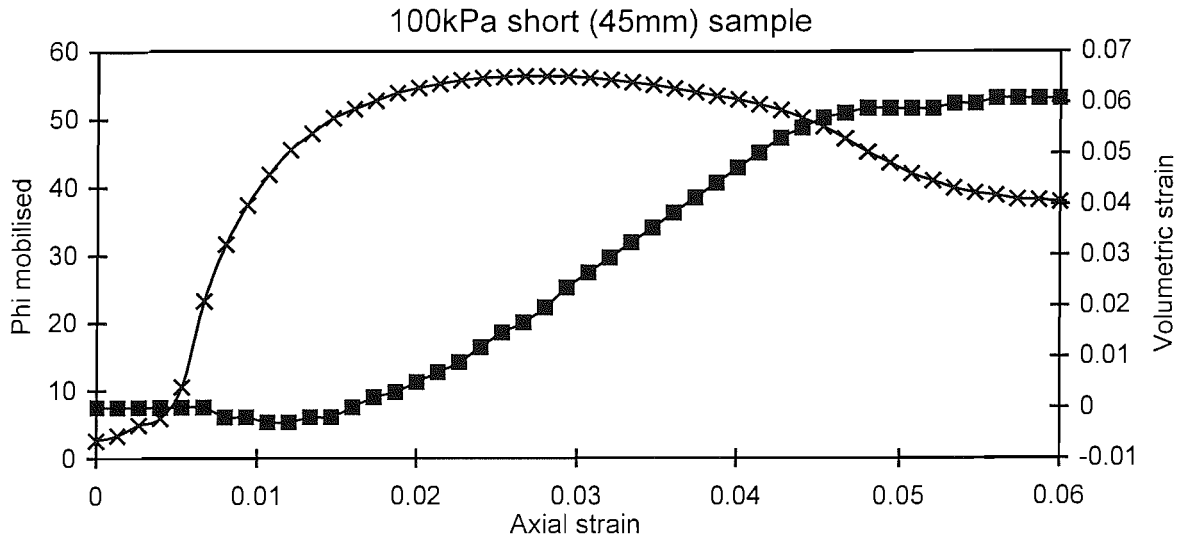


Figure 5.8 Phi mobilised vs axial strain and volumetric strain vs axial strain for the long and short samples

5.3 Observations and discussion

5.3.1 Sample uniformity

The test results show a consistency which is in keeping with the homogeneity of the material but surprising given the difficulties of sample preparation. The constant orientation of the shear plane for all of the tests at 50kPa and over confirms the uniformity and continuity of the A3 test samples.

5.3.2 Extended peak

Present in all the tests was an extended peak. This was initially presumed to be due to the material shearing and softening over large volumes until weak enough for a localised shear plane to develop. The shear plane would only form when the shear resistance of the material was lowered enough to allow a localised shear plane to occur at the steepest kinematically permissible location - i.e. corner to corner. The orientation of the plane of maximum stress ratio (or stress obliquity), as defined by the Mohr- Coulomb model is

$$\theta = 45 + \phi'/2$$

which would have been steeper than corner to corner and therefore prevented the development of a shear plane. The 2:1 samples have a potential corner to corner θ of 63° corresponding to a ϕ' angle of 36° and the observed ultimate ϕ'_{mob} figures are all in the mid to high thirties. This supports the concept that the sample weakened until corner to corner failure was possible.

Three observations are against this theory:

- The short and long tests all showed failure plane angles similar to those of the other 50 to 300 kPa tests. If the development of the localised shear plane was dependent upon it being kinematically possible or 'easier' when orientated corner to corner, then the short samples should have needed much more dilation, and therefore weakening and lowering of θ before localisation occurred, and the long sample should have needed less dilation, weakening and lowering of θ before

localisation. What was observed was that both the long and short samples sheared at approximately the same angle and not corner to corner.

- The total dilation was similar for all sizes of sample tested at 100kPa; i.e. the same amount of weakening was occurring at the same confining pressure regardless of the length of the sample.
- The plot of the length of the extended peak against total volume change (figure 5.4) is roughly linear. The data points for long and short samples lie the furthest away from this line. If they are corrected to a nominal strain derived from a length of 76mm (the length of the other samples) they move closer to this line and lie within the data points of the 2:1 samples. This implies that the total volume change is not dependent upon sample length and the mechanism of failure is also independent of sample length.

The above reasoning suggests that localisation at a steep θ is being prevented; the material undergoes quasi-plastic deformation (with slight strength loss) accompanied by dilation before developing a shear plane at a fixed angle of approximately 63° , and it is chance that the shear plane angle fits corner to corner in a 2:1 sample.

5.3.3 Dilation angles

The uniform ψ angle matching the extended peak implies that a single mechanism of shear is continuing throughout this period. If it is assumed that no macro voids were produced then the amount of material involved can be calculated; given the density of the intact material (1.796Mg/m^3), the particle density (2.638 Mg/m^3), the amount of dilation (2.5cm^3 at the lower confining pressures to 5.6cm^3 at the higher confining pressures) and estimating the void ratio after shear (0.76 - see direct shear section). A volume of 5.6cm^3 will be produced by 28cm^3 dilating uniformly and a volume of 2.5cm^3 will be produced by 13cm^3 dilating uniformly. The volume of the 2:1 samples is 86cm^3 so the figures represent large proportions of the sample volume. Because the void ratio after shear has been estimated as very near to ρ_{\min} this method gives the minimum amount of material involved that could have produced the observed dilation. The only other explanation of the large dilation is

to suggest that parts of the sample were at a lower than critical state density. Oda and Kazama (1998) have reported voids, thought to be caused by rotating or buckling columns in shear zones. These were observed in a sand without the interlocked fabric of A3. It is possible that a smaller volume than predicted above was causing the observed dilation by failing with the formation of rotating columns, which produced voids between them. The interlocked fabric of A3 would certainly enhance the formation of any stress-induced structures.

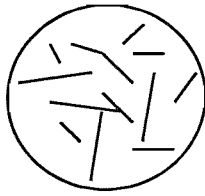
5.3.4 Triaxial strain or plane strain

It is obvious from observations of the development of a corner to corner shear plane that plane strain conditions were occurring toward the end of the test. The dilation rate suggests that plane strain conditions apply during the whole of the extended peak; if triaxial strain calculations are used then the dilation angle for the lower pressure tests goes over 90° ; which is meaningless. A constant dilation rate suggests that one type of failure mechanism occurs throughout the period of constant dilation, i.e. until a shear plane develops. It is concluded that the steepness and the linearity of the dilation show that plane strain failure alone was occurring before and after the shear plane developed.

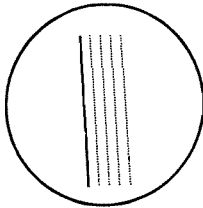
In favour of triaxial strain is the observation that barrelling occurred but this may not have been in all radial directions. Plane strain (elliptical) barrelling, however, observed from most angles, and without localisation, will mimic “proper” triaxial strain barrelling.

5.3.5 Fabric structure and the failure mechanism

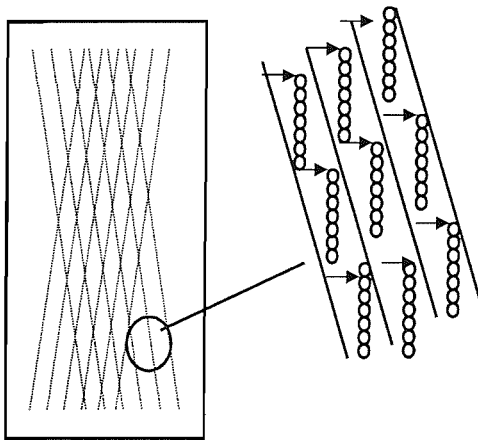
The plane strain conditions, if they are accepted as occurring during the tests, must be due to the presence of fabric structure within the sample. An explanation of how fabric produces plane strain conditions, and prevents localisation in the form of a shear plane, until after an extended peak, is now attempted (figure 5.9):



In a sand without structure, small scale shearing occurs over all of the sample apart from the restrained ends. These protoshears continue at random orientations until localisation, in the form of a rupture, develops.



In A3 this stage must be marked by the shears orientating themselves to a single, or two conjugate, series of parallel planes. It is this orientation that is the mechanism by which fabric structure produces plane strain conditions; the initial small scale shear influences the rest forcing them to conform to the same orientation.



Localisation, in the form of the shear plane seen at the end of the test, is prevented by the formation of stress induced structures which produce large amounts of dilation. These are envisaged to be columns consisting of several grains. They cause it to be energetically more expensive for the shear plane to develop than for another protoshear to initiate at an adjacent location.

Figure 5.9 The influence of fabric structure on the failure mechanism

Non - continuous small scale shearing occurs over the entire sample apart from the restrained ends. In a sand with no structure these protoshears would continue at random orientations (when viewed in plan) until localisation developed. In A3 this stage must be marked by the protoshears orientating themselves to a single, or two opposing, series of parallel planes. It is this orientation that is the mechanism by which fabric structure produces plane strain conditions; the initial small scale shear influences the rest to develop at the same orientation. Localisation, in the form of the shear plane seen at the end of the test, is prevented by the formation of stress induced structures which, if further strained, produce large amounts of dilation for

each increment of axial strain. These are envisaged to be columns consisting of several grains and similar to those reported by Oda and Kazama, (1998). The stress induced structures cause it to be energetically more expensive for the shear plane to develop than for shear to start at another location. It is speculated that this mechanism creates a moving front of dilating sand. The higher confining pressure tests producing a larger total dilation but at a lower dilation angle because a higher confining pressure increases the energy required for dilation. Dilation on a particular plane is restricted but more of the sample undergoes dilation and softening.

It is suggested that the low pressure tests, especially those at 6 and 12kPa, gave a larger dilation angle due to the energy required for volumetric strain being less. This dilation is assumed to be due to movement along the steep protoshears that was prevented by energy considerations in the higher pressure tests. Failure then occurred along these steeper, weakened planes with a central step to make the shear zone kinematically admissible. The central step consisted of small shears parallel to the loading direction which became part of a disaggregated zone after the peak.

If plane strain conditions are accepted then, as outlined above, some form of localisation must have occurred before the shear plane developed; the morphology and scale of this was not directly observed and must form the basis of further work.

5.3.6 Softening, dilation and soil mechanics.

Dilation is now accepted as responsible for the peak strength in structureless sands (Bolton1986). However some of the ϕ'_{mob} vs strain plots (figure 5.2) show that no dilation occurred before the peak had been reached. The dilation continues at the same rate throughout the extended peak. This may be explained by considering the observed dilation as being due to progressive loss of structure and results in loss of the sample's strength towards that of the disaggregated material. A3 is strong by nature of its fabric; its peak strength is not due to dilation.

5.3.7 A3 triaxial behaviour compared to that of rock

The softening behaviour seen in A3 can be considered to be due to substantial modifications that take place in the sample during the extended peak part of the test. In this respect it is similar to a stiff hard rock where a series of fractures develops and propagates as the load approaches the peak. In rock tests, this softening produces heterogeneity and usually the boundary conditions become more important. Fractures parallel to the axis of loading are seen in low confining pressure triaxial tests on rock; at higher pressures these are replaced by an inclined surface of rupture traversing the entire sample (Goodman, 1989).

5.4 Conclusions - triaxial testing

1. The hard shell method of preparation using a coating of hairspray was satisfactory.
2. The failure envelope derived from the triaxial tests is linear with no change at 100kPa as was recorded from the direct shear tests (chapter 4). The triaxial ϕ'_{peak} value of 50° is smaller than the ϕ'_{peak} values recorded for direct shear at normal loads of less than 100kPa (61° for A3 and 65° for A2), but similar to the ϕ'_{peak} values recorded for direct shear at normal loads of more than 100kPa.
3. A3, and presumably other sands without bonding but with a high degree of grain fabric, fail during triaxial testing in a unique manner that is unlike the failure of unstructured dense sands, weakly cemented sands and sandstones.
4. Two morphologies were displayed by the ultimate, narrow shear zone; below 50kPa two steep separate shear planes were connected by a disaggregated zone toward the middle of the sample, at 50kPa and above the final shear zone was a single plane. This was always at an angle of 60° to 64° .

5. An extended peak is present and is matched by dilation. Both the length of the extended peak and the total dilation increases with increasing confining pressure. A step is present in this behaviour: at a confining stress of 100kPa and above much more dilation is observed, but at a lower dilation angle, with more of the sample weakening.
6. Plane, not triaxial, strain conditions were occurring from the beginning of the extended peak even though no restriction in the r_2 direction was applied.
7. The peak strength of this material is due to its fabric structure and not the observed dilation, as shown by many of the tests, which indicate no dilation before the peak strength.

CHAPTER 6: UNIAXIAL TESTS

6.1 Methods

6.1.1 Introduction

Neither the direct shear tests or the triaxial tests gave results on the stiffness of the intact material or the magnitude of strains required to before the fabric was destroyed. Uniaxial testing of A3 was carried out to obtain this information. It was considered that any disturbance to the sample would be highly significant to measurements of stiffness, especially at small strains. Testing air dry was the simplest method since wetting would have added another chance of fabric disturbance and required the application of a confining pressure or a confining pressure and a vacuum.. Testing dry was preferred also because it also approximates more closely to field conditions than wet testing. This however caused a sample preparation problem; it was not possible to produce 2:1 samples without using a hairspray coating and if the sample was to be tested dry then flushing could not be used to remove the hairspray. It was found possible to produce 1:1 (100mm high by 100mm diameter) samples of A3 if extreme care was taken and, in conjunction with lubricated end platens, this was the method chosen. The lubricated ends consisted of a disc of 0.28mm membrane with a layer of silicone grease between it and the platen. Lubricated or free ends and the use of 1:1 specimens are discussed by Head (1986) who also gives extensive references.

It was not possible to produce and test samples of intact A2 by this method.

6.1.2 Sample preparation

1. The first three stages followed those of shearbox sample preparation - all preparation being carried out on a glass plate. This produced a prism 10mm larger than required.
2. One end was ground flat on the glass plate and placed on a 100mm platen,

3. The prism was filed down using 80 grade abrasive cloth stuck to a right angle wooden block. A set square was used to check for right angle between the sample and the glass plate
4. The height was adjusted with the wooden block and the top of the sample made flat and parallel with the glass plate.
5. Tolerances were calculated as for the triaxial tests

Operations three and four required great care to prevent the top edge from breaking off. This method was not able to produce a test sample out of A2; sharp corners could only be produced with A2 if hairspray was used.

6.1.3 Apparatus

The uniaxial apparatus used is shown in figure 6.1. This varied extensively from the usual unconfined compressive strength test apparatus. Two linear variable differential transformers (LVDTs) were used to measure strain over the middle half of the sample. The LVDTs allow strain measurement without bedding errors and the calibration of the rubber membranes, end platens, load cell and loading frame is not required. Local LVDTs were also thought necessary due to the small deflections A3 would produce before failure. Cuccovillo and Coop (1997) whilst investigating pre-failure deformation in structured sands used local LVDTs to measure strains of 0.0001%. They suggested that this accuracy was required because of the stiffness of the sands. Here, strain measurements better than 0.0005% were achieved; this figure was arrived at by observing the range of the data points around a linear section of the stress strain plot.

The LVDTs were fastened to the specimen by gluing their holders to a standard 100mm triaxial rubber membrane (0.28mm), extra support being provided by rubber bands. The confining pressure provided by the membrane and the rubber bands was not considered significant due to the small strains involved (see triaxial section).

This method also had the advantage that the specimen was contained and after failure no cleaning up was required.

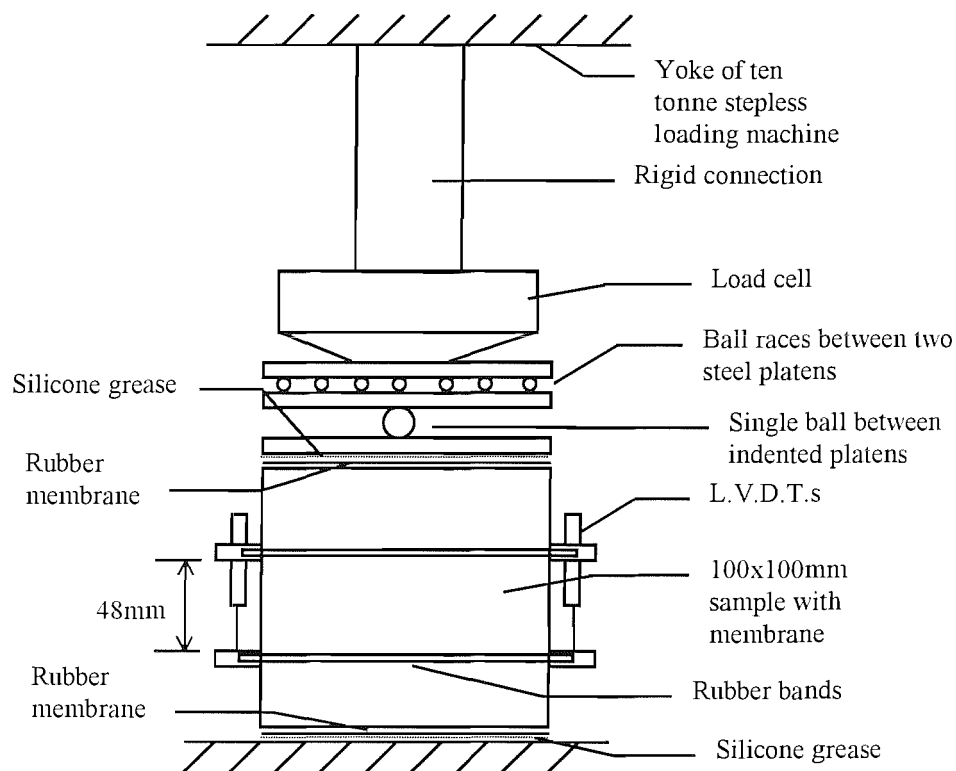


Figure 6.1 The Uniaxial apparatus

Lubricated platens result in the ends of the sample spreading out and therefore may require the use of enlarged end platens. Enlarged platens were not used; they are only considered necessary if strains larger than 10% are to be produced (Head 1986), which is two orders of magnitude greater than those predicted.

A3 specimens could only be prepared to fairly wide dimensional tolerances (see chapter 5); these were within those given by Pells and Ferry (1983) but orders of magnitude greater than those suggested by Elliot (1993) for use without spherical seats. Given the stiffness and brittle behaviour of A3 it was thought necessary to

provide some form of accommodation for non- parallel ends. Debate exists in the rock mechanics literature over whether to allow the top platen unrestricted rotation (Elliot 1993, ISRM 1978). Elliot (1993) considered it reasonable for field tests where accurate grinding of the sample ends may not be possible but warned it may introduce an increasing shear load as its orientation changes. ISRM (1978) guidelines require a spherical seat on the upper end of the specimen, this is lubricated with mineral oil and locks up as the load increases after accommodating any non-parallel in the sample ends. The unconfined compressive strength tests of soil mechanics do not use spherical seats, but the apparatus however allows some accommodation of the top platen (Head 1986). Triaxial soil tests have traditionally utilised a single ball bearing (approximately 10mm in diameter) to transmit the axial load to the top platen; this was readily available and chosen for the A3 uniaxial tests.

Unrestrained lateral movement of the top platen was provided to allow single plane slip (or plane strain) to occur and prevent an increasing shear load due to changes in the orientation of the top platen. It also made setting up easy; the possibility of non - axial loading was prevented. The apparatus, with unrestrained lateral motion above a single ball bearing, allowed only a vertical force to be transmitted through the centre of the top platen. The load cell was tested for non-axial but still vertical loading and at the most extreme possible lateral displacement of 25mm was found to vary by only 3%. The maximum lateral displacement during testing was always orders of magnitude less than 25mm and it was assumed that the load cell readings would not be significantly effected.

The strain rate was dictated by a jack speed of 0.2mm/min (0.2% per min) but all strain calculations used the information from the LVDTs. The time to failure was between 5 and 10 minutes.

6.2 Results

6.2.1 Introduction

Four tests on A3 were carried out designated U2, U3, U4, U5. Only U5 had reload loops. Without the aid of a hard hairspray shell, producing intact samples was at the very limit of what was possible. The main problem was the loss of the top edge of the sample. Even though U4 had a visibly larger cement content (still only trace) than the other uniaxial samples, it was slightly damaged during preparation with a 3mm x 10mm crescent missing from its top corner.

6.2.2 LVDTs

Figure 6.2 shows the stress strain graph for test U3, the strain was calculated directly from the closing gap between the load cell and the jack without any allowance for compliance or bedding errors. The same test is shown in figure 6.3 with the strain calculated from the two LVDTs (acting over the middle half of the sample). Note that the strain to failure is an order of magnitude greater if the closing gap speed is used to calculate the strains. The two plots originating from the two LVDTs diverge and show expansion before and after the peak strength. Similar results were obtained for U2 and U4, an explanation of this is given in the discussion section.

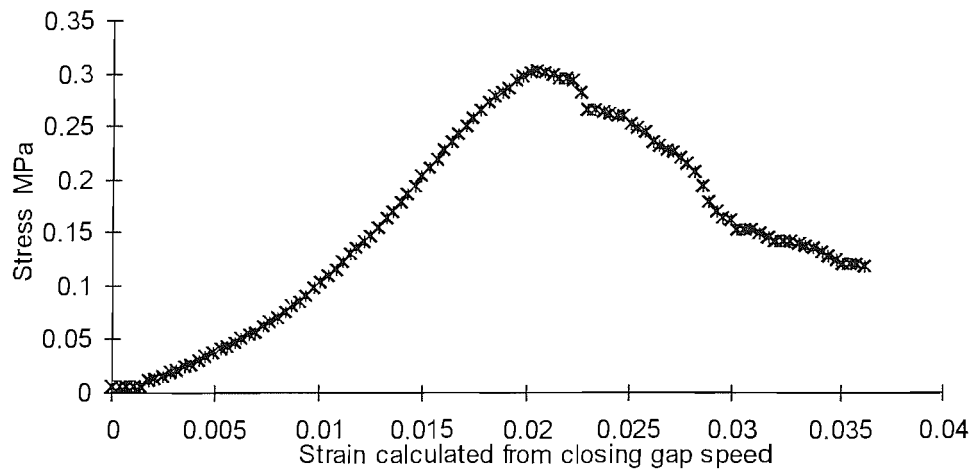


Figure 6.2 Stress strain plot for test U3. The strain is calculated from the closing gap between the platens.

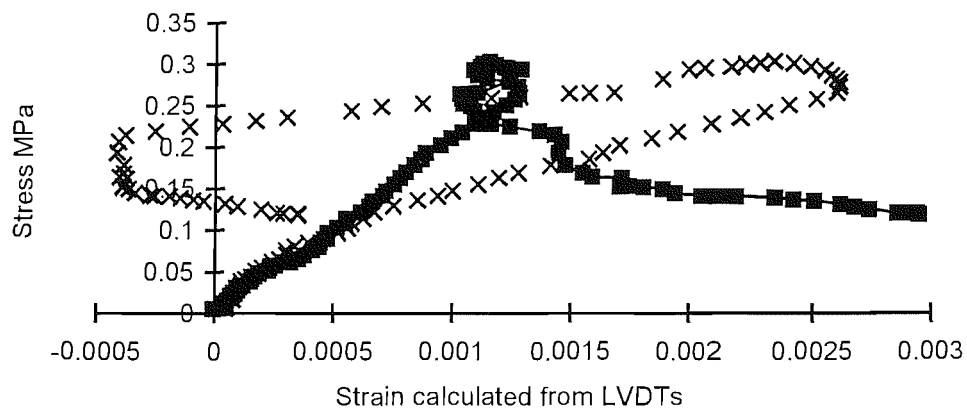


Figure 6.3 Stress strain plot for test U3. The strain is calculated for each of the LVDTs acting over the middle half of the sample.

6.2.3 Stress at failure and failure mode

Although the rubber membrane prevented detailed observation of the failure mechanism during the test it could be carefully removed at the end of the test and the failure surfaces noted. Table 6.1 shows the failure stress and failure mode of all tests. U2 and U3 failed with the formation of six or seven vertical columns of intact

material comprising the total external surface of the sample (figures 6.4 and 6.5), U3 showed a distinct central cone at the bottom of the sample (figure 6.4c), and both had disaggregated material in the centre. U4 failed with a 70° shear plane orientated toward the missing crescent on the top corner of the sample.

Test	Failure stress kPa	Failure mode
U2	486	Vertical split / vertical pillars
U3	303	Central cone / near vertical pillars
U4	265	70° shear plane
U5	291	70° shear plane

Table 6.1 The failure stress and failure mode of all tests

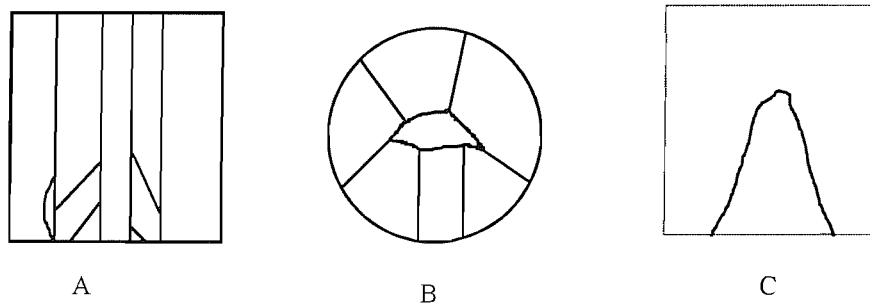


Figure 6.4 Failure mode of U2 and U3. A) Intact vertical columns with 40° to 60° shears between them. B) Plan of A. C) Intact cone left after U3.

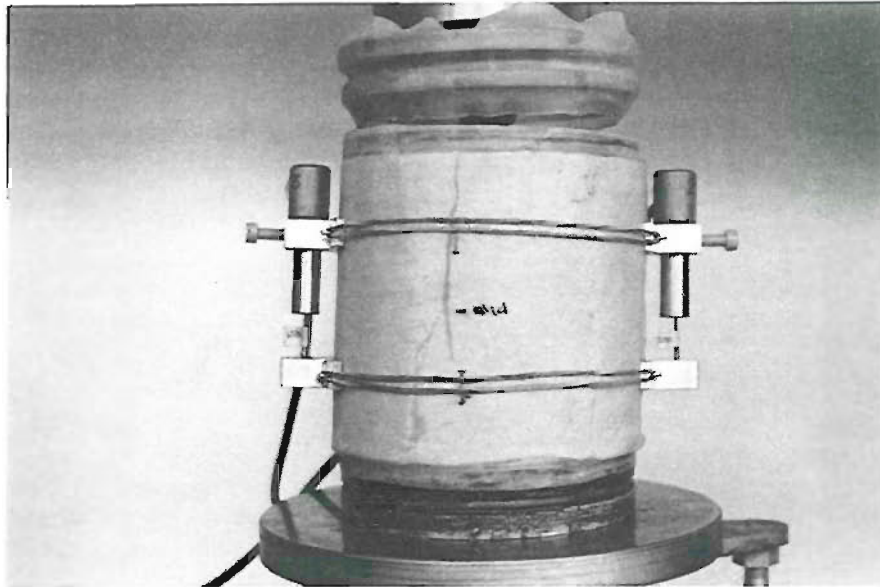


Figure 6.5 Photograph of uniaxial sample U2 toward the end of the test

Figure 6.6 shows a photograph of sample U5 after testing and removing the membrane. The lines on the surface are where grains have fallen away, the angles of these lines are given in figure 6.7. The centre of the sample was extremely fragile and the sample as a whole showed signs of immanent collapse; to prevent collapse whilst photographing and noting details it was hairsprayed. The full force of the spray would have been enough to erode the sample; this was prevented by increasing the distance between the spray and the sample and allowing the spray to fall upon it. The sample appeared totally disaggregated in the centre. Areas of the external surface were weaker than the intact material but the majority of the external surface behaved with intact strength when probed.

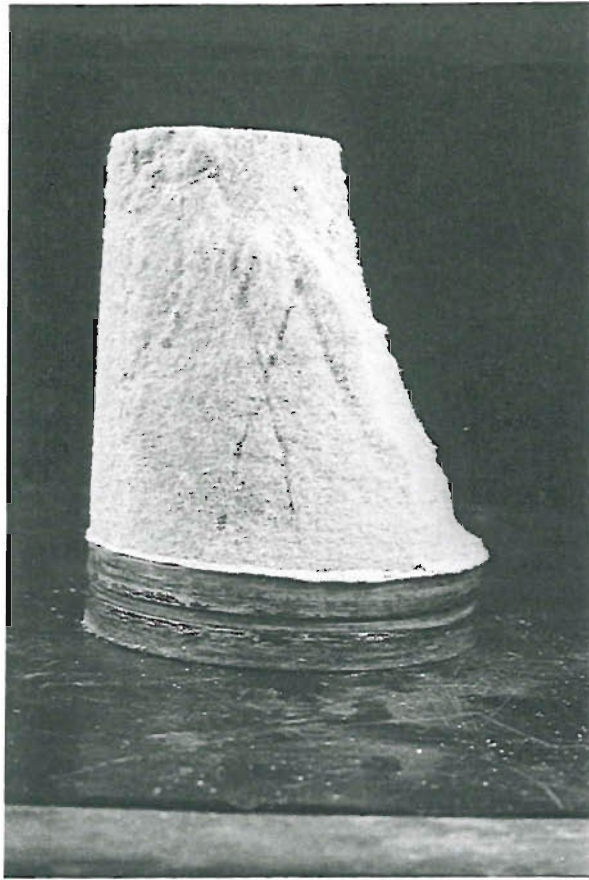


Figure 6.6 Photograph of U5 after removal of the rubber membrane showing lines on the surface of the sample

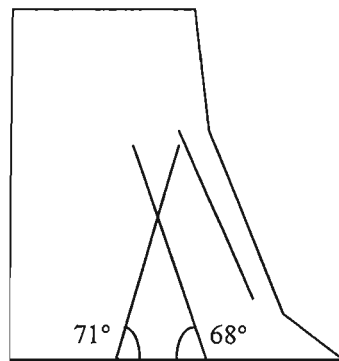


Figure 6.7 Details of the lines on the surface of U5

6.2.4 Stress strain plots

Figure 6.8a,b and c shows the stress strain plots to, and after, failure for tests U2, U3 & U4. The small strain end of the U2 plot is shown in figure 6.9. Table 6.2 gives the values of Young's modulus (E) for linear areas of the plots; these are derived from an average of the two LVDTs.

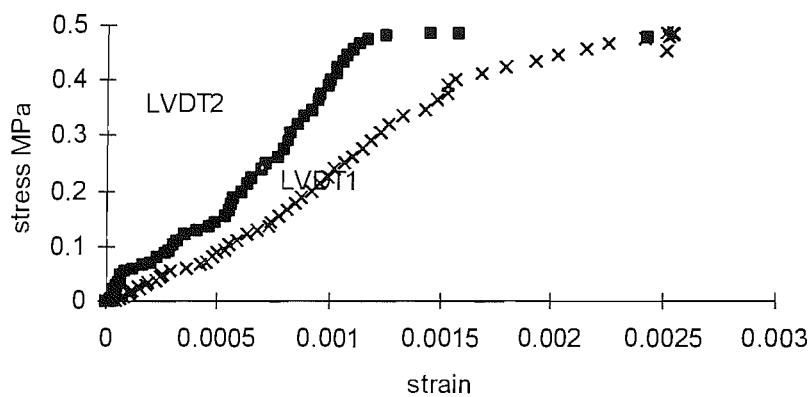


Figure 6.8a Stress strain plot for test U2

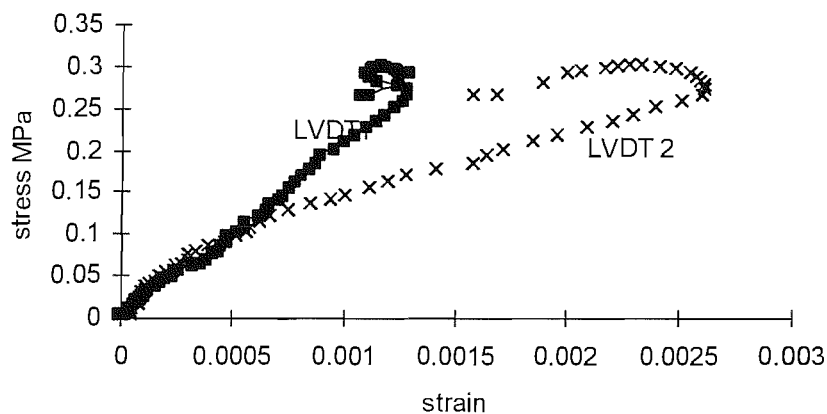


Figure 6.8b Stress strain plot for test U3

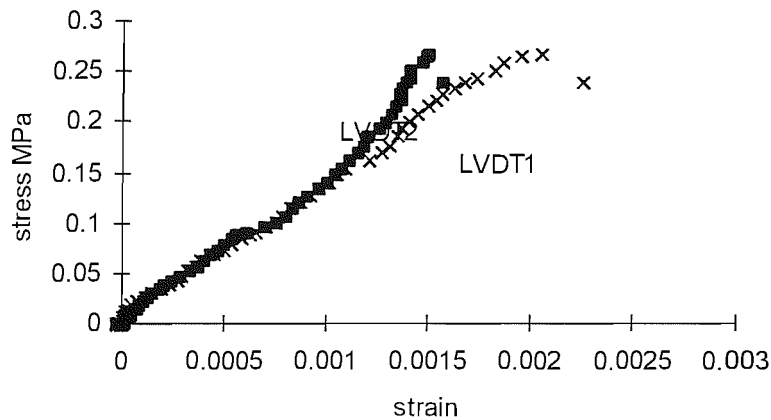


Figure 6.8c Stress strain plot for test U4

6.2.5 Stiffness

Figure 6.9 shows the small strain end of the U2 test stress strain plot. All tests showed an initial linear 'flat' zone with strain increasing with no increase in stress. This zone is only a strain of 2×10^{-5} long with U4 but 4×10^{-5} long with the other tests. Between strains of 4×10^{-5} and 15×10^{-5} U2, U3 and U4 showed a linear increase in stress with strain giving an approximate E values of 400 MPa. Stiffness declined after this, and continued to decline during test U3. Tests U2 and U4 showed an increase in stiffness toward failure. The stress rose in a series of linear steps, increasing in stiffness, with flatter, concave up, sections between them. For U2 and U5 the stiffness before failure was greater than the initial stiffness. Stiffness figures are summarised in table 6.2 The averaged strains to failure for U2, U3 and U4 were very similar; approximately 0.002.

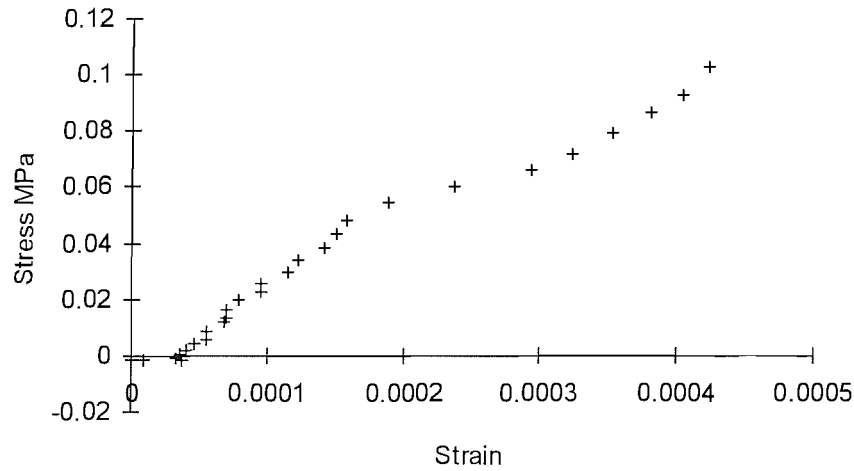


Figure 6.9 The stress strain plot of U2 for small strains showing the initial flat zone followed by a linear zone with $E = 400\text{MPa}$.

Test	Strain range	E (MPa)
U2	below 4×10^{-5}	ap. zero
U2	4×10^{-5} to 15×10^{-5}	396
U2	65×10^{-5} to 103×10^{-5}	395
U2	123×10^{-5} to 128×10^{-5}	780
U3	below 4×10^{-5}	ap. zero
U3	4×10^{-5} to 9×10^{-5}	378
U3	9×10^{-5} to 64×10^{-5}	170
U3	64×10^{-5} to 190×10^{-5}	119
U4	below 2×10^{-5}	ap. zero
U4	2×10^{-5} to 5×10^{-5}	345
U4	15×10^{-5} to 56×10^{-5}	129
U4	121×10^{-5} to 150×10^{-5}	224

Table 6.2 Values of Young's modulus for the linear regions of tests U2, U3 and U4

6.2.6 U5 - reload loops

Figure 6.10 shows the stress strain plot for U5. The loops show little hysteresis and the stress strain curve between loops consists of very linear areas. After the initial stiff zone and subsequent decline there was an increase in stiffness after each loop. The E values for the linear sections of the plot derived from an average of the two LVDTs are displayed in figure 6.11a. The stress strain plots of test U5 show very low stiffness values between the reload loops although the reload loops themselves have gradients similar to those recorded for the steeper areas of the other tests. The strain at failure was 0.005; this is twice the failure strain of the tests without reload loops. Figure 5.11b details the final reload loop showing the strain increasing even though the stress is declining.

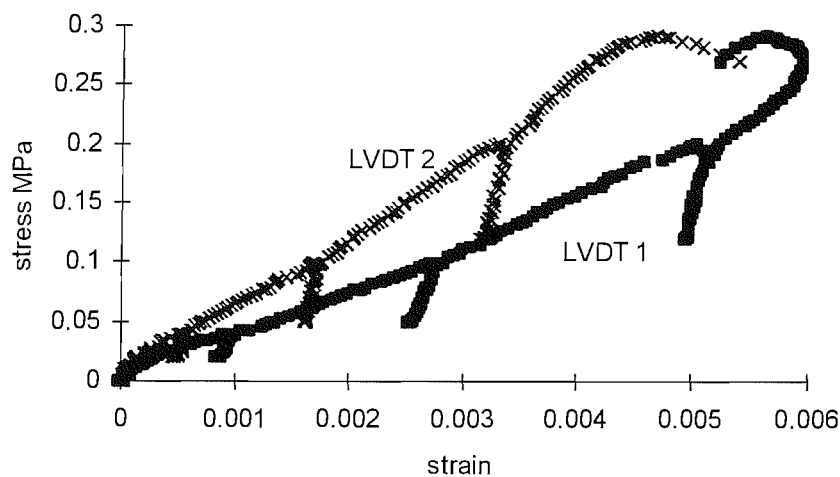


Figure 6.10 The stress strain plot for U5 showing the reload loops

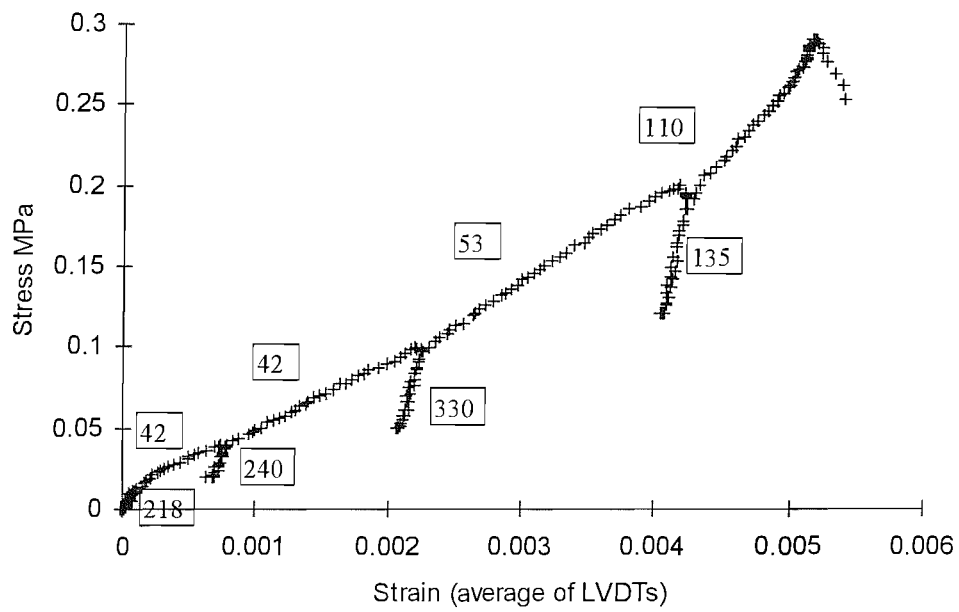


Figure 6.11a The stress strain plot for U5 showing the reload loops. Strain is calculated as an average of the two LVDTs. The boxed numbers are the E values (MPa) for the adjacent linear zone calculated from the average strain

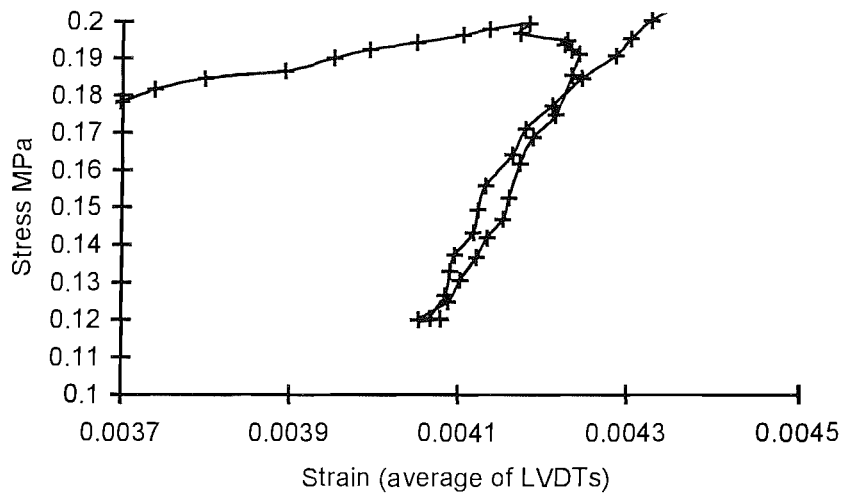


Figure 11b Detail of the stress strain plot for U5 showing the final reload loop with the strain increasing even though the stress is declining.

6.3. Observations and discussion

6.3.1 Local LVDTs and divergence

Local LVDTs were found to give the accurate measurements of stiffness at strains below 0.001 and are an obvious way of circumventing the compliance problems of measurements taken from parts of the apparatus external to the platens. At strains approaching peak stress and beyond the LVDTs recorded widely diverging displacements (figure 6.2) and an average of the two needs to be interpreted with care; certainly toward the end of the tests any E values calculated from an average of the two LVDTs is unlikely to be valid. Divergence due to initial non-axial loading was possibly occurring, although the closeness of the strains recorded by the LVDTs, for tests U3 and U4, at the lower end of the stress strain plots argues against this. Non-symmetrical failure would ultimately result even with perfectly axial initial conditions and this would also produce divergence in the LVDT readings. Test U4 and U5 failed with the formation of a shear plane (figures 6.6 and 6.7), the location of the LVDTs relative to this biaxial feature would have influenced the recorded strains and their divergence and a similar process may have occurred with the other tests.

6.3.2 Local LVDTs and expansion

After the peak the LVDTs recorded expansion by 30 to 125% of their original compression for tests U2, U3 and U4; a full plot of U3 is given in figure 6.3. This expansion began slightly before the peak for U3. These plots bare little resemblance to the plots of stress against jack movement (figure 6.2) where obviously no expansion was recorded. This is explained by the external pillars remaining intact at the end of the test. It is suggested that the strains in the pillars are recoverable and on removal of load they regained their original dimensions. The external pillars were able to shed load before the peak was reached resulting in the LVDTs (which were attached to the pillars) recording expansion even though the stress on the sample as a whole was still increasing. The expansions of over 100% occasionally

recorded by the LVDTs, and the large divergence between the LVDTs at the later stages of the tests, can be explained by the possibility of shear zones forming between the mounting points of the LVDTs. There is also the possibility of barrelling of the sample changing the orientation of the LVDTs and producing a false expansion reading.

6.3.3 Local LVDTs and stiffness

Local LVDTs record the strain occurring at two locations on the outside of the sample. There is no reason to believe that what is happening at the surface is representative of what is occurring over a section through the sample. This is obviously the case when localisation begins but it may also be true earlier. The increased stiffness recorded toward the peak may be due to the part of the sample with the LVDTs attached moving away from the load, its share then being taken by more central material, this then takes all of the applied load and is found totally disaggregated at the end of the test.

6.3.4 Stiffness at small strains

There are two explanations for the lack of stiffness apparent below 0.004% strain:

- The micro-sutured contacts between the grains allow movement. This could be due to sample disturbance or could be present in the insitue material.
- Was not due to sample behaviour but a bedding error within the LVDTs.

This lack of stiffness was not seen to the same extent in U4 which contained a larger amount of cement, and it is possible that any cement would have inhibited the former mechanism. The second explanation is also unlikely due to the identical displacements recorded by the two LVDTs at these small strains. Non - linear behaviour of rock under uniaxial loading has been attributed to the presence of pores or minute cracks (possibly due to sample disturbance) closing on initial

loading (Deere and Miller, 1966). The behaviour could also be thought of as akin to that of a flexible sandstone (itacolumite) where sutured contacts are separated by a thin zone of clay or mica which impart a flexibility to the material (Adams et. al.1984).

6.3.5 Stiffness variation

All the tests show stages with E values above 200 MPa, and a maximum of 800 MPa was recorded for U2. These are many times higher than the figure of 120 MPa given for dense sand (Head 1986). This is to be expected; A3 is much denser than 'dense sand' and it has large, interlocking grain contacts. It is also usual for stiffness to increase with load. What is surprising is that two areas of high stiffness were produced; one at low strains and one before failure. It is possible that these are due to the two scales of interlock; grain boundary interlock (micro-suturing) and interlock of the angular grains themselves. The material is initially very stiff until grain boundary interlock is overcome. Movement can then occur between grains due to slack in interlock between them. This slack is eventually taken up, the grains have to move relative to each other and the sand becomes progressively stiffer.

Other interpretations are possible involving movement of stress induced structures; pillars of intact material collapsing and/or moving away from the stress and shedding their load onto adjacent pillars. The latter fits well with the observed flatter concave sections between the linear (though increasing in stiffness) sections. These flatter concave sections represent the displacement required to mobilise the strength of the adjacent pillars. Increasing stiffness toward the end of a uniaxial test is unusual but has been observed with marble using steel platens and a H/D ratio of 0.25 (Brady and Brown 1993). Marble consists of interlocked carbonate crystals with a bond strength between the crystals less than the crystals strength. The low H/D can be envisaged as not allowing certain failure modes and therefore mobilising the higher strength and stiffness of the interlocked grains.

6.3.6 Peak strengths

Peak strengths were similar except for U2 (table 6.1) which was considerably higher. The failure mechanism for U2 was different from the other tests in that only vertical pillars, with some secondary 45° to 60° shear planes, were formed. It is inferred that this failure mode produces a higher strength.

Although not investigated it is highly likely that the peak strength in an unconfined compression test would be influenced by the sample size; the interlocking mechanism of these materials will certainly require a certain number of grains before it can function.

6.3.7 Failure type

Figure 6.12 shows an idealised model of the failure typified by U3. Cone and socket failure has been observed in brittle materials during uniaxial compression; Nadai (1931) shows photographs of cone development in sandstones. Development of a central crack in uniaxial tests on brittle materials is common but the several pillars surrounding disaggregated material produced by A3 is not generally reported in the literature, although it was recorded by Richards (1992) for locked sands of similar provenance to A3. It is possible that the use of 'soft' platens (silicone grease on rubber) was in part responsible for this behaviour; if the Poissons ratio of the platen is lower than that of the sample then lateral tensile forces can be produced. These tend to pull the sample apart at each end resulting in vertical fractures.

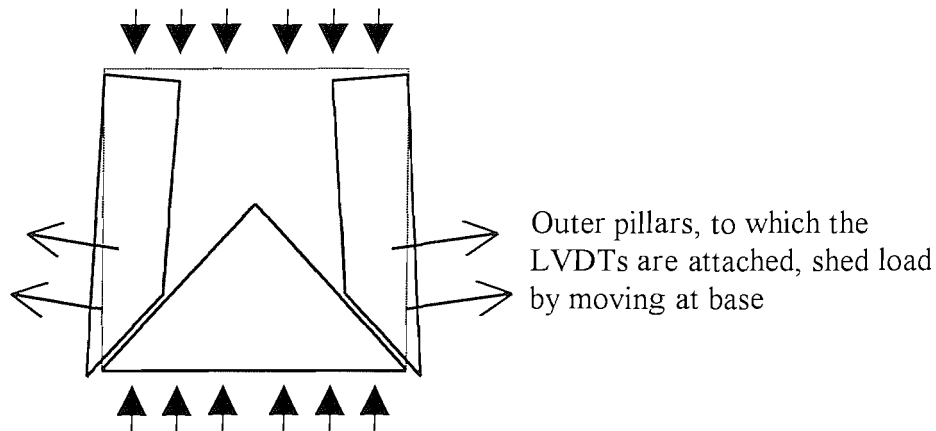


Figure 6.12 Idealised model of failure typified by U3

Why 70° failure planes should develop (U4 and U5), rather than pillars with a central cone or pillars with 40° to 60° shear planes between them, is not clear. It is possible that the occurrence of the different failure types is triggered by small differences in the morphology or structure of the samples, or by small differences in the apparatus, especially in the lubricated ends and the encompassing membrane.

6.3.8 Reload loop test

The remarkable lines on the surface of U5 (figure 6.6 and 6.7) are possibly the surface manifestation of two conjugate sets of shear bands. These, however, were not apparent on the surface of U4. U5 failed at a higher strain to the other tests with a strain to failure of 0.005 compared to 0.002. It is assumed that this difference was due to the reload loops. It is possible that the reload loops allowed time for another failure mechanism to develop by working the material back and forth. This is supported by careful observation of the stress strain curves just before the reload loops (figures 6.10, 6.11a and 6.11b). These show that as the stress was lessened (by reversing the jack) the strain continued briefly to be positive (compressive). This can be attributed to either:

- The LVDTs giving spurious strain readings, possibly due to bending of the pillars on which they were attached. On the initial lessening of the load the pillars straightened resulting in a compressive reading
- A time dependant rearrangement of grains and/or stress induced structures. When the load was initially lessened a rearrangement of grains and/or stress induced structures continued to occur allowing compression even though the stress was lessening.

6.4 Conclusions - uniaxial testing

1. The modified apparatus was successful in obtaining both the strain to failure and the stiffness values.
2. A3 in UCS tests produces a novel type of failure with the outside of the sample remaining intact and the centre disaggregating.
3. Generally A3 shows greater stiffness than conventional dense sand samples with two areas of high stiffness; this behaviour is determined by its fabric structure.
4. Peak strength on monotonic loading is mobilised after small movements (less than 0.2% strain).
5. When tested A3 has a small amount of flexibility; the grain contacts allow a very small movement (less than strains of 0.0002) before any strength is mobilised, and is similar to a flexible sandstone (itacolumite) in this respect. It is possible that the flexibility was imparted by sample disturbance.
6. With these materials the measurement of strain by LVDTs, fastened to the outside of the sample, may not give reliable results due to the outside of the sample behaving differently to the centre.

CHAPTER 7: GENERAL DISCUSSION

7.1 General discussion

7.1.1 Introduction

This section makes a comparison between the results of the various testing methods used. The applicability of Bolton's (1986) relative dilation index is considered and also the concept of structure permitted space (on a voids ratio vs effective stress plot) as proposed by Leroueil and Vaughan (1990). The term *dense fabric structure* is introduced to make the distinction between sands that will display abrupt yield and contractile behaviour, and sands that will not behave in this manner even at the highest envisaged engineering loads. A comparison is made between the behaviour produced by fabric rather than bonded structure and consideration is given to whether the behaviour of a sand with a dense fabric structure assists the concept of a continuous geotechnical spectrum. Conceptual models of dense fabric structure are proposed using brick shapes and spurred disks. Finally it is attempted to extrapolate the findings of this work into the conceptual models of granular materials in general.

7.1.2 Comparison of the results from the different testing methods

The A2 and A3 direct shear results showed a bilinear peak strength envelope that was not seen in the triaxial tests. This is considered due to the initial localisations within the shearbox, formed at normal loads of 100kPa and under, creating intact columns of material which then interacted with the shearbox boundaries. The columns rotate and result in large dilation rates and high peak strength. The boundary in the triaxial test is very different and no structures, at least on a similar scale, are formed. Dilation in the triaxial test does not occur until after the peak and the strength mobilised at peak must be attributed to fabric structure rather than dilation. This is in keeping with the observation that at low normal loads the triaxial ϕ'_{peak} is 11° less than the direct shear ϕ'_{peak} . Triaxial friction angles generally are reported to be 2° to 3° lower than direct shear friction angles (Bolton, 1996). This

is in keeping with the A3 ϕ'_{ult} results which were 37° for the shear box and 35° for triaxial. The larger difference seen with the peak results is considered due to the extra dilation caused by the stress induced structures that form in the direct shear apparatus.

The suggestion that direct shear tests in general may be underestimating the peak ϕ' value due to the horizontal plane not being the plane of maximum stress ratio (see direct shear discussion section 4.4.18 and Jewel and Wroth, 1987) would imply that the direct shear results are being underestimated. It is obvious that in the case of A2 and A3 that no underestimation is taking place and that column formation, whose orientation may be influenced by the horizontal plane not being the plane of maximum stress ratio, produces very large dilations and high peak friction angles.

The triaxial ϕ'_{ult} (37°) is high compared to that of the direct shear at normal loads of 100kPa and above (31°) but small compared to that of direct shear at normal loads of 100kPa and below (50°). This is probably due to the orientation and morphology of the ultimate shear plane. The direct shear apparatus forces this to be on an overall horizontal plane, no matter how tortuous a path due to the original localisations, whereas the triaxial apparatus does not prescribe the angle of the failure plane. With A3 the triaxial ϕ'_{ult} is dependant upon the orientation of the final shear plane; if this is at an angle less steep than that predicted by the Mohr - Coulomb model then the ϕ'_{ult} produced will be greater than that from a direct shear test.

The strength results from the uniaxial tests can be compared to the triaxial and the direct shear tests results using:

$$\sigma_{ucs} = 2c' \cos \phi' / 1 - \sin \phi'$$

Taking the A3 direct shear test values of $\phi' = 61^\circ$ and $c' = 60\text{kPa}$ gives an unconfined compressive strength value of 541kPa, taking A3 triaxial values of $\phi' = 50^\circ$ and $c' = 50\text{kPa}$ gives an unconfined compressive strength value of 263kPa.

These values are within reasonable conformity with the spread of those from the uniaxial tests, which are between 265kPa and 486kPa. It appears that although A3 has been observed behaving in novel ways, and very differently in direct shear compared to triaxial testing, a Mohr-Coulomb analysis of peak strength can be used to compare the results of a test carried out where $\sigma'_3 = 0$. This is in contradiction to the reported behaviour of materials with an interlocked structure such as fissured rock and weak sandstones that need a normal load before the extra strength is mobilised (see section 1.2.9. and 1.2.10). No account, however, has been taken for the difference in size between the testing methods and the uniaxial samples had a larger (100mm) diameter than the triaxial samples(38mm).

7.1.3 Peak strength and dilation

Bolton (1986) described an empirically derived relative dilation index (I_R) defined in terms of relative density (I_D) and effective stress level (p'):

$$I_R = I_D (10 - \ln p') - 1 \quad 7.1$$

This index was found to have a simple correlation with the difference between the maximum ϕ' and the critical state ϕ' values:

$$\phi'_{\max} - \phi'_{cv} = 5 I_R \quad \text{for plane strain} \quad 7.2$$

$$\phi'_{\max} - \phi'_{cv} = 3 I_R \quad \text{for triaxial strain} \quad 7.3$$

The difference $\phi'_{\max} - \phi'_{cv}$ is, according to this analysis, due solely to dilatancy in the dense soil. Bolton suggested that values I_R of above 4 may need corroboration due to the extreme dilatent strength which would be implied. The relationships above were derived by analysing data from 17 investigations, but no sand in these investigations had a relative density above unity. The relative density of A2 is 1.35 which gives an I_R value at low (100kPa) normal stress greater than 6 and is therefore unusable. Not until the normal load reaches 540kPa does the I_R value reach 4.

At the high pressures (10MPa) used to test A2 in the direct shear box the I_R value becomes 0.006 suggesting that at these pressure no significant dilation occurs and $\phi'_{\max} = \phi'_{cv}$. A large peak and dilation, however, were observed and the conclusion has to be drawn that the relative dilation index fails when used for locked sands (which have a D_r greatly in excess of 100) at high pressures.

7.1.4 Dense fabric structure

That A2 and A3 have structure is beyond doubt. The term structured has been used extensively to mean that some form of bonding is present and that a structure permitted space is created on a voids ratio vs effective stress plot. If the stress is increased the material yields abruptly if it is in this space (Leroueil and Vaughan, 1990). The structure of A2 and A3 is due solely to the shape and arrangement of the grains (fabric structure) and produces a very dense packing arrangement of unbonded grains. This may be termed a *dense fabric structure*. Generally the terms dense and loose are dependent on the pressures encountered but here the term dense will be used to denote an unbonded material with fabric structure that will not simulate loose soil behaviour at the highest envisaged engineering pressures.

This dense fabric structure has produced novel results in strength tests when compared to other structured soils such as those where bonding is present. The yield of A2 and A3 at low pressures is not abrupt. Localisation begins before peak on planes that are not at the same orientation as the final shear plane in the direct shear box. In the triaxial apparatus localisation begins after peak but is presumed to consist of parallel protoshears that form a moving front of dilating sand. The final shear surface forms within these after considerable weakening; displayed as an extended peak followed by failure to a steady ultimate strength value.

7.1.5 Locked - bonded

Cemented sands are widely reported to display brittle behaviour at low pressures and ductile behaviour at higher pressures (Clough et al, 1981; Coop and Atkinson, 1993). At low pressures the cementation is more significant than the frictional component of strength. As pressures increase the bonding provided by the cement is overcome and the mobilised friction becomes more important. The fines produced by the broken cement may, however, produce a stronger frictional material.

A2 has no cement and A3 has negligible cement, their strength comes from an interlocked grain fabric and not from grain bonding. In the direct shear apparatus this produces different types of failure at different normal loads. Although A2 and A3 have less of a peak at high/medium normal loads it shows “brittle” behaviour with sudden loss of strength (ie. a vertical line on a τ vs ϵ plot). It is suggested that this is due to the shedding of load from one breaking asperity to another, resulting in instantaneous failure. Stored elastic energy within the sample, and possibly the apparatus, then produces the accompanying dilation. At low normal loads instantaneous failure does not happen, the forces available are not great enough to break the grains and failure occurs by rotation and slipping of grains. The force supported by an individual grain is released slowly onto the surrounding ones as its shear resistance is overcome due to movement and geometry change. The geometry change may be in the form of individual grain movements or of stress induced structures supporting the principal stress.

The direct shear tests show that sands with no grain bonding, but with a large amount of fabric strength, behave in a rock like manner (with brittle failure and plumose structures) during direct shear at high normal loads, and at low normal loads superficially like a highly dilatant soil but with the development of columns supporting the principal stress. This is almost the opposite to purely cemented sands and raises the question of how the mechanisms given above influence behaviour of

sands that have a fabric component of strength and some bonding strength. These make up the bulk of transitional arenaceous materials between sand and sandstone and have been the most studied. It is possible that bonding may hide or even remove the effects of dense fabric structure; for example any tensile strength could prevent the formation of columns in the direct shear test.

Figure 7.1 compares the τ_{peak} vs σ'_n direct shear test plots for two idealised sands, one with bonded structure (taken from Head, 1982, p527) and one with dense fabric structure. The cohesive intercept where a bonded structure is present is due to adhesion between grains. The small cohesive intercept for the sand with idealised dense fabric structure is due to fabric cohesion and no adhesion exists between individual grains.

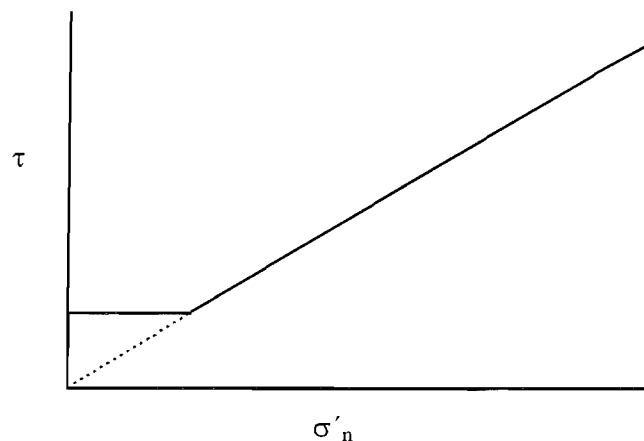


Figure 71a Strength envelope for a weakly cemented sand with low interlocking

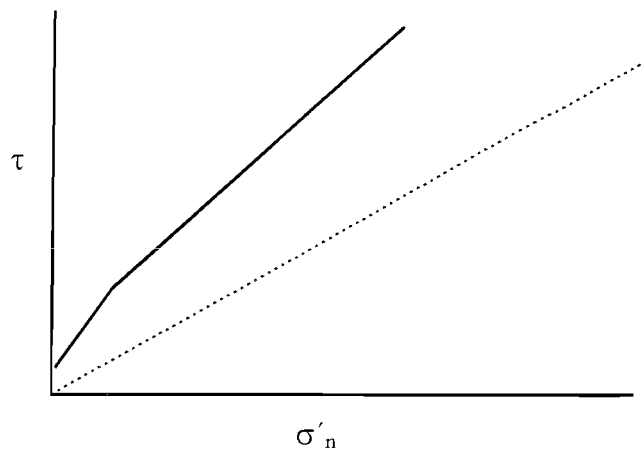


Figure 7.1b Strength envelope for a sand with dense fabric structure but no bonding

7.1.6 A continuous geotechnical spectrum?

Many authors now argue that soft rocks are part of a continuous geotechnical spectrum. Recent publications have suggested that even hard rock can be incorporated into the critical state model to produce a spectrum from soft clay to hardest granite (Novello & Johnston 1995). Traditionally, however, rocks and soils have been treated very differently, rock mass strength having been the study of discontinua i.e. the weaknesses between blocks of intact material, whereas soils have been considered a continuum. Rock mechanics emphasises the variability of the material; qualitative assessment is often needed and the mathematics often becomes complex with many unknown variables. Soil mechanics, by treating the soil as a continuum, produces quantitative and precise analytical solutions.

This study has described two arenaceous materials that fit uneasily into either of the soil or rock categories. A2 and A3 are isotropic and homogeneous leading to the conclusion that producing constitutive equations should be possible. However, they have a highly interlocked dense grain fabric, which enables them to develop structures that resist the applied load during shearing. It is suggested that these structures and their failure mechanisms are test dependent and dominate locked sand behaviour at low normal loads. At higher loads the behaviour of locked sands changes and becomes more rock like. Incorporating rock into the critical state framework utilises the brittle/ductile transition with increasing pressure as being similar to the dilatant/contractile behaviour of soil (Novello & Johnston 1995). The locked sands studied here do not show either of these characteristics at the pressures tested and have to be considered as materials with totally novel behaviour. It is possible that at loads greatly in excess of 10MPa, brittleness will be suppressed and ductile behaviour dominate due to grain crushing bypassing the interlocking mechanism. Tests at these pressures will however be of very limited consequence to engineering design.

7.2 Modelling and implications

7.2.1 Conceptual / physical modelling of dense fabric structure.

Figure 7.2 shows how the grain fabric of a soil may be modelled on a pile or a stack of bricks. A pile of bricks will act in a similar way to any angular particulate material and traditional soil models can be used to interpret its behaviour. If a wall is built out of stacked, but uncemented bricks it will not produce lateral pressure on loading and cannot be modelled as a soil. Note that the stack may be at a high void ratio (7.2c) and still display behaviour that does not fit into a soil model. The material of 7.2c might, depending upon the strength of the bricks, cut through a normal consolidation line for the material of 7.2a. The material of 7.2b has dense fabric structure, the material of 7.2c has loose fabric structure and at high loads has the potential to yield abruptly.

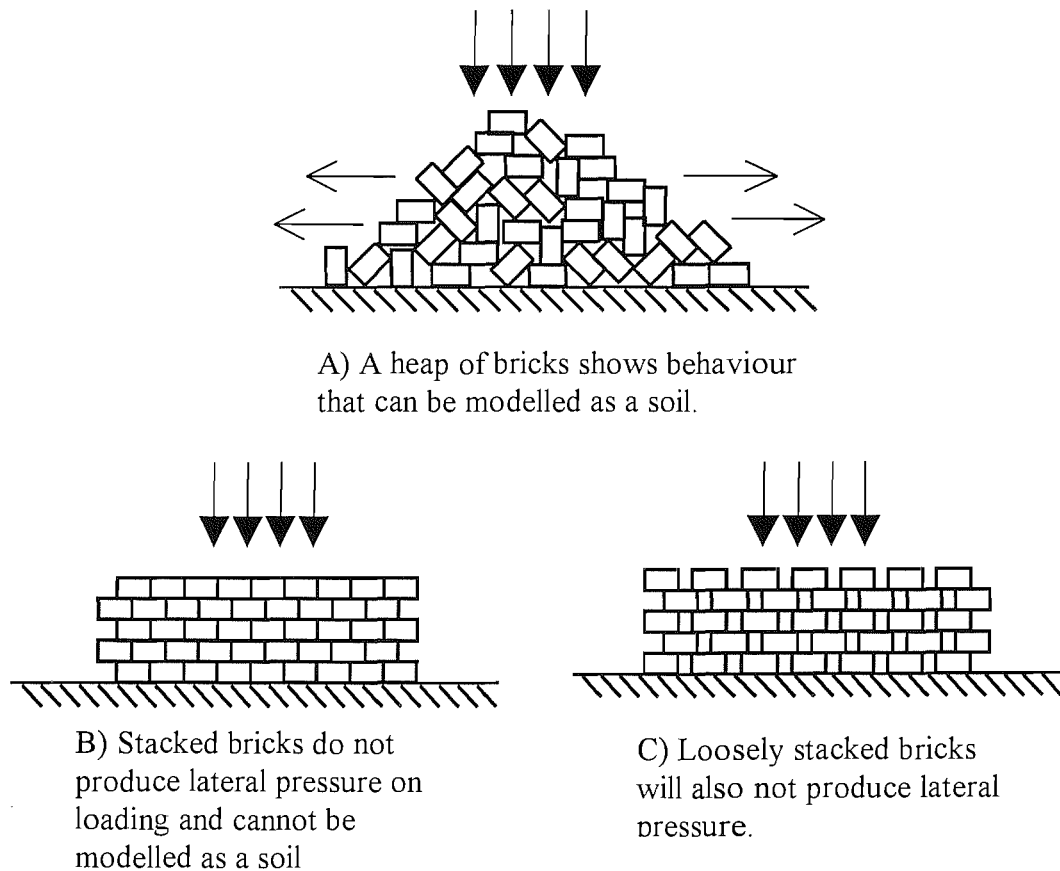


Figure 7.2 Conceptual modelling of grain fabric using stacked and heaped bricks

Many authors report experiments using shaped discs or rods, in a two dimensional loading frame, to model soil behaviour (see references in Oda and Kazama, 1998). Shapes can be proposed that assist in conceptualising the behaviour of locked sand (figure 7.3) and these could actually be constructed and tested. These are different to the usual circular or ovoid discs/rods in that they have asperities or spurs that interlock. No tensile strength is produced but it is kinematically inadmissible for the discs to move, when loaded in unconfined compressive stress, without the spurs being broken. Spurs at lesser angles would allow movement and presumably produce stress induced structures such as those seen in jointed rock models (see direct shear discussion) and oval disc models (Oda and Kazama, 1998). The spurred discs are not isotropic; to produce isotropy the discs would have to be serrated over their whole edge and be randomly packed.

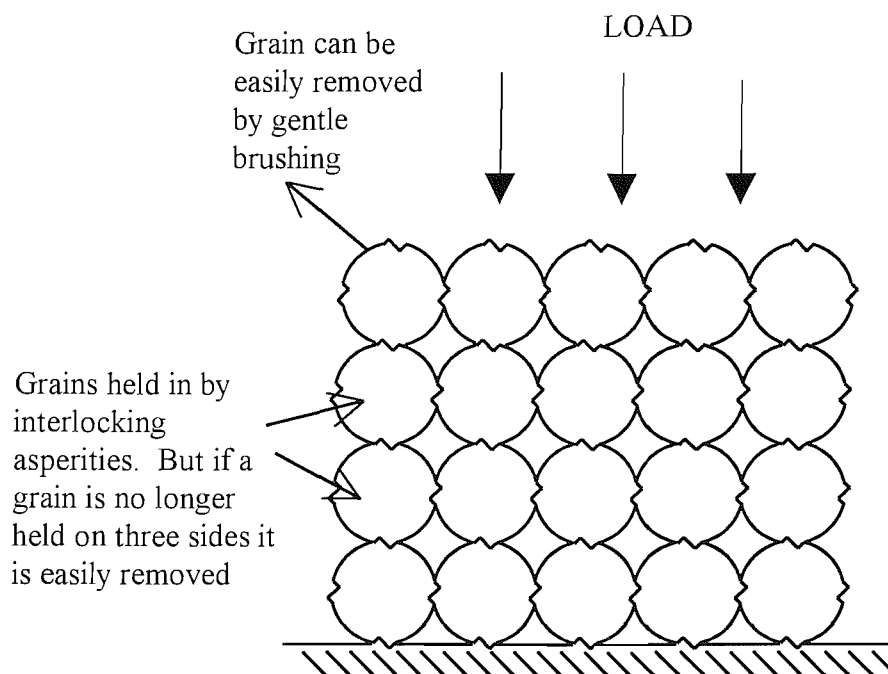


Figure 7.3 Two dimensional modelling of a locked sand. The basic unit is a disc or rod with interlocking spurs that lock into the those of adjacent discs. The spurs have ramps at 45° . The discs represent individual grains of sand. Note that it is kinematically impossible for disc movement to occur due to shear load unless asperities are sheared off. However the model produces no tensile strength and discs located at the top corners of the block can be removed by the smallest of forces.

7.2.2 Implications for soil models

This section attempts to extrapolate the results of this work - involving the yielding of a sand with a highly interlocked fabric - into the conceptual models of general soil mechanics.

Terzaghi and Peck (1948) suggested that the weakening from the peak to ultimate strength with continued strain is associated with a progressive disintegration of the structure of the soil. More recently the peak has been explained by the energy required for dilation resulting in the empirical equation (Bolton, 1986):

$$\phi'_{\text{peak}} = 0.8\psi + \phi'_{\text{cs}}$$

and other theoretical formulas that closely fit the experimental data (see Rowe, 1962, and other references in Bolton, 1986). Dilation has been considered to be a result of sliding taking place on planes at an angle to the overall shear direction (Newland and Allely, 1957), (figure 7.4a). Although dilation correlates with the extra strength of dense sands and the energy arguments are irrefutable, it is suggested here that dilation is a boundary manifestation of a failure mechanism that must occur not only with locked sands but also with dense sands in general.

It is obvious that dilation is not responsible for the strength of rocks. Also it has been observed during this research that dilation in sands with a dense fabric structure, but no grain bonding, does not necessarily match the peak strength according to the above equation. The direct shear results of A2 and A3 at normal stresses of between 750kPa and 5MPa showed that dilation and strength decline occur simultaneously and instantaneously. The triaxial tests also showed that dilation does not correspond to the peak in the way the conventional theory would suggest.

It is possible to envisage a material that was not dense but had an interlocked fabric that gave it strength above that of the disaggregated material. The “stick and ball” models of atoms, for example, if given a cubic arrangement would not dilate to failure but would still show strength above that of the disaggregated sticks and balls. A sand, however, can only exhibit fabric structure in proportion to its density. This is simply due to its component parts being nearly spherical; the only way they can fit together in an interlocked manner is by being arranged very close to each other. The interlocked fabric, which is present to an extent in all dense sands, results in it being difficult for grains to change their arrangement relative to their immediate neighbours, and stress induced structures are produced on loading. The greater the interlock the larger the magnitude and effect of these structures.

It is suggested that the behaviour of dense sand, with dilation matching the peak, is due to the rotation (and collapse) of many small stress induced structures, each giving rise to a small dilation and loss of strength (fig 7.4c). Measured at the test boundaries this appears as smooth curves representing dilation and strength loss to an ultimate steady value. Evidence for the existence of columnar structures, such as these in rupture zones in sands, has been put forward by Oda and Kazama (1998), and concentrations of stress into columns has been seen in 3D particle flow code modelling of direct shear box tests (R. Harkness pers. comm.) and in the many disc experiments using two dimensional loading frames (Oda and Kazama, 1998).

Evidence from this and other studies strongly suggests that in general ϕ'_{peak} is greater than ϕ'_{cv} because granular materials produce stress induced structures that support the shear stress and is not due to consideration of friction and dilation alone. Extrapolating this concept further it can be tentatively proposed that ϕ'_{cv} is greater than ϕ'_u (the friction angle of grains on a flat plate of the same material) because of the formation of stress induced structures, in the form of columns of grains. A steady volume is created by the columns collapsing into macrovoids created as the columns rotate.

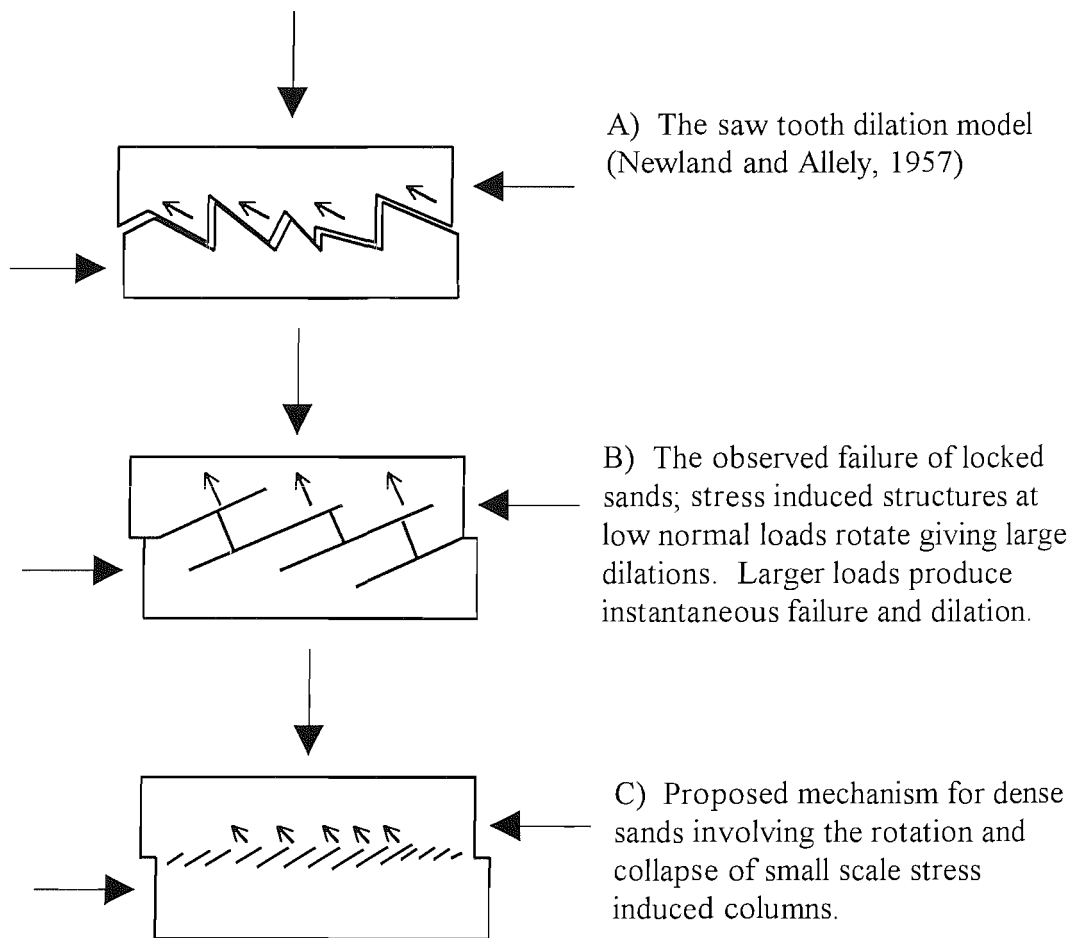


Figure 7.4 Conceptualisation of dilation and peak strength as being due to the rotation and collapse of stress induced structures.

CHAPTER 8: CONCLUSIONS AND RECOMMENDATIONS FOR FURTHER WORK

8.1 Conclusions

8.1.1 Sampling improvements

Block sampling techniques for locked sands with very little cohesion have been greatly improved. Two types of saw have been designed and built. These have greatly increased the speed at which intact blocks of locked but unbonded sand can be extracted. They have also been found useful in sampling bonded sands.

The successful use of a hard shell created by spraying the sample with hairspray has allowed small intact samples to be made for testing. This is especially important in the production of 2:1 triaxial samples where the hard shell can be removed by flushing before the test commences.

8.1.2 Disaggregated sample preparation

An improved method of producing high density reconstituted samples to allow comparison with the intact material has been developed. A greater understanding of the processes occurring during slow pouring (pluviation) has been obtained with observation of an energetic layer of sand consisting of grains moving with large horizontal velocities. This layer is always present when high densities are reached quickly and results in a peak in the density versus depositional intensity relation.

8.1.3 Strength testing

When strength tested locked sands have been shown to behave in a unique manner; they cannot be placed into either the soil or rock conceptual frameworks and behave in an almost opposite manner to weakly cemented but poorly locked sands. They

form stress induced structures which cause unique interactions with the test boundary, and ultimately localise into a very narrow shear band.

When tested in direct shear the locked sands produce a strongly bilinear peak failure envelope, with the change in angle at 100kPa, followed by a concave down zone extending to the limit of the tested range. At normal loads below 100kPa ϕ'_{peak} is over 60°, dropping to approximately 50° at loads between 100kPa and 1000kPa. The envelope is then concave down with a ϕ'_{peak} angle of 38° at 10MPa; the peak strength is not suppressed. This is in contrast to the behaviour reported for poorly interlocked cemented sands which become frictional materials at high normal loads. These three zones within the failure envelope correspond to three distinct types of failure at different normal loads:

- Stress induced structures, resembling columns with their long axis orientated in the direction of the principal stress, were produced during direct shear *at low normal loads (<100kPa)*. These were preserved as a stepped failure surface with the steps in the opposite direction to those displayed in soil dilation models. Dilation at the boundaries of these low normal load tests cannot be accounted for by dilation in the shear zone alone. Areas must have been produced that were less dense than (ie on the wet side of) the critical state void ratio. These areas could have been between rotating columns or created by continuing shear against the stepped shear surface.
- *At normal loads between 750kPa and 5MPa* the locked sands failed with a near instantaneous loss of strength from peak to ultimate. This was accompanied by grain crushing and a flatter shear surface. The interlocked fabric produces instantaneous failure at these pressures, which is influenced by apparatus stiffness.
- The peak strength was not suppressed *at 10MPa*; this is in contrast to the behaviour reported for poorly interlocked cemented sands which become frictional materials at high normal loads. It appears that sands with no grain

bonding, but with a large amount of fabric strength, behave in a brittle, rock like manner during direct shear at high normal loads. This is observed as a narrow shear zone with plumose structures and crushed grains.

The failure envelope derived from the triaxial tests is linear with no change at 100kPa as was recorded from the direct shear tests. The triaxial ϕ'_{peak} value of 50° is smaller than the ϕ'_{peak} values recorded for direct shear at normal loads of less than 100kPa (61° for A3 and 65° for A2), but similar to the ϕ'_{peak} values recorded for direct shear at normal loads of more than 100kPa. The failure mode observed during triaxial testing was unlike those of unstructured dense sands, weakly cemented sands or sandstones, and as with the direct shear tests there is a distinct change in behaviour above a certain normal load. An extended peak is present and is matched by dilation. Both the length of the extended peak and the total dilation increases with increasing confining pressure. A step is present in this behaviour: at a confining stress of 100kPa and above much more dilation is observed, but at a lower dilation angle, with more of the sample weakening. Two morphologies were displayed by the ultimate, narrow shear zone; below 50kPa two steep separate shear planes were connected by a disaggregated zone toward the middle of the sample, at 50kPa and above the final shear zone was a single plane. This was always at an angle of 60° to 64° . Analysis of the dilation angles suggests that plane, not triaxial, strain conditions were occurring from the beginning of the extended peak, even though no restriction in the r_2 direction was applied.

The differences between the observed behaviour in the two forms of test (direct shear and triaxial) are due to the boundary interactions of the stress induced structures and the final orientation of the shear plane compared to the applied stresses. The results from both testing methods indicated that the peak strength of these materials is due to their fabric structure. Dilation occurred after the peak as a consequence of the disintegration of the soils structure. In this respect they behave in a similar way to a rock where dilation occurs after failure.

The A3 uniaxial results shows that an interlocked fabric produces greater stiffness than that of merely dense sand, and that peak strengths are mobilised after very small movements (less than 0.2% strain). Some flexibility was recorded at strains of less than 0.004%; which may be due to disturbance and not a feature of the insitue material.

8.1.4 Stability of locked sands

The strength parameters ϕ'_{peak} and c' derived from conventional tests on intact material show that the Park Pit quarry walls are within a factor of safety of 2. It has been strongly argued that negative pore water pressure has no significant effect on the strength of these sands. What gives them strength is cohesion due to an interlocking fabric (fabric cohesion) and a high friction angle. The high friction angle is due to the high density and grain contact morphology preventing grain rotation and producing stress induced structures.

Only a very small confining pressure is needed to prevent fabric disturbance on wetting. The surface layer of Park Pit is sealed with a cemented crust of optically opaque minerals. This prevents cyclical erosion due to wetting and drying and maintains the surface layer in a strong intact form.

8.1.5 Modelling and Implications

Conceptual models of dense fabric structure and fabric structure in general have been proposed, and which can explain the observed behaviour. The results of this work have been extrapolated into the conceptual models of general soil mechanics resulting in the statement: ' ϕ'_{peak} is greater than ϕ'_{cv} because granular materials form stress induced structures that support the shear stress and not due solely to consideration of forces produced by friction and dilation'. The denser, and therefore the more interlocked, the granular material is the more pronounced are the stress induced structures.

8.2 Recommendations for further work

8.2.1 Strength testing

The large number of previously unseen behaviour modes that occurred during the strength testing programme have produced many questions and further research must address these. It is envisaged that further strength testing should pursue both of the following directions:

- To continue testing materials on the sand/sandstone border. These require investigation in their own right but investigating them will also shed light on what effect an interlocked fabric has on all geomaterials.
- To investigate dense fabric structure using whatever materials are thought to be suitable to give a spectrum of materials with varying amounts of dense fabric structure.

A great amount of effort is spent designing and building novel testing apparatus but the mode of failure of all geomaterials will be influenced to some degree by the testing method used. Any 'new' geomaterial should therefore be tested, firstly and extensively, using all appropriate standard testing methods. Only after this should apparatus and methods be designed with the purpose of either:

- Forcing the new material to behave in a manner that has already been observed and interpreted in other materials.
- Investigating further a novel mode of failure seen in the standard tests where these tests did not allow the material to fully develop the novel mode of failure or lacked detailed measurement of it.

The direct shearbox tests on intact A2 and A3 were fairly extensive, covering a wide range of normal loads. It is suggested that little could be gained by increasing the level of instrumentation of future direct shear tests except for the accurate measurement of linear strain to obtain dilation angles. These could then be

compared to the results for disaggregated A2 and A3 and published results. Some evidence of sensitivity to strain rate was found in the direct shear testing program and this could also be investigated. Improved capture of the changes in fabric during shearing by better impregnation and thin section methods would be helpful. Direct shear tests on pre-formed flat and stepped failure surfaces, in a similar manner to the experiments of Patton (1966), would produce information on what was causing the high values of ϕ'_{peak} and especially ϕ'_{ult} .

The triaxial tests were very limited and any future testing program should initially concentrate on better instrumented triaxial tests. A suggested programme is outlined below:

1. Stress path triaxial tests using a 100mm cell at pressures of 25 to 1000kPa to allow a yield surface to be constructed and different phases to be identified. Measurements of radial strain to be made on three diameters in one plane to ascertain if plain strain or triaxial conditions are occurring as the test proceeds.
2. Triaxial tests at pressures between 1MPa and 10MPa to ascertain if the failure modes seen in direct shear at these pressures is present
3. Test the material using a biaxial apparatus to investigate the stress induced structures that were observed in direct shear at low loads.
4. Further develop the thin section methods of investigating how the fabric changes during strain and how the strain induced structures are formed. This is envisaged to require the use of an interim cementing agent, or a resin highly diluted with a solvent, flushed through the sample whilst the stresses are still in place.

It is proposed that to investigate fabric structure both different testing methods and several materials with varying amounts of interlocked fabric should be used. Of especial interest is the 'granulated' marble of Rosengren and Jaeger (1968); with a porosity of only 4% this would be a good end member in an array of materials with varying amounts of interlocked fabric.

8.2.2 Sampling

The hard shell method was highly successful, but hairspray cannot be used to produce the hard shell unless the conditions are dry and this precludes its use in the field. Another medium must be found that will set on damp sand. This could be used to cover the field sample leaving an exposed face for the moisture to escape. In the laboratory the water soluble hairspray would then be used whilst the sample was being reduced in size to fit the relevant test. Using the above method could result in sand with very small cohesion (from bonded or fabric structure) being successfully sampled.

8.2.3 Pluviation

Several undergraduate projects have been carried out at Southampton University Geotechnical Laboratories to further investigate the formation of dense sand samples. These have incorporated both vibration and the mixing of sizes. A paper has been accepted (ASTM) entitled 'Determining the maximum density of sands by pluviation'. This work is continuing and it is intended to find ways of preparing the highest possible degree of interlocked fabric in remoulded sands.

8.2.4 Formation of the interlocked fabric

The thin section photograph figure 3.15 of A2 shows two grains with an interpenetrating and micro-sutured contact. This contact was exceptional in that these features were easily visible at the magnifications available (x400) using an optical microscope. Higher magnifications are needed if the sutured contacts and the strangely shaped grains are to be studied. The use of a scanning electron microscope, transmitting electron microscope and high magnification cathodoluminescence will allow both the morphology and the mineralogy of the contacts to be explored and give information on the method by which the grain contacts and the strangely shaped grains have formed. Currently the two conflicting theories are those of pressure solution and solid diffusion.

Grain fracturing at contacts in Reigate Silver Sand is another problem that requires explanation. It is suggested that these occurred during the geological ageing of RSS due to compactional processes. Detailed point counting of thin sections orientated both parallel and perpendicular to bedding would possibly verify this.

8.2.5 The dark crust

The proposed mechanism of formation of the dark crust seen on the walls of Reigate Park Pit could be verified by observing a newly opened wall over several days or weeks. Standard petrographic techniques such as x-ray diffraction and the transmitting electron microscope would identify the mineralogy of the crust and hopefully its provenance.

8.2.6 Modelling

Modelling using a two dimensional frame and disks is discussed in the modelling section 7.1.7. The usual format of these; either circular or ovoid disks, could be closely followed except the discs would be given some form of interlocking asperities. Numerical modelling using a particle flow code with spurred discs is also possible with PC level computing power.

The equations initially developed by Ladanyi and Archambault (1972) to predict the shear strength of closely jointed rock masses produce a bilinear failure envelope. These merit further investigation as to their applicability to sands with a dense fabric structure, an example of which has been seen to show a very marked bilinear failure envelope in direct shear.

REFERENCES

- Adams, A.E., Mackenzie, W.S. and Guilford, C. (1987). *Atlas of Sedimentary Rocks under the microscope*. Longman, Harlow. 104pp.
- Anon. (1981). *Code of practice for Site Investigations, British Standard BS5930:1981*. British Standards Institution, London.
- Anon. (1990). *British Standard methods of test for soils for engineering purposes, British Standard BS1377:1990*. British Standards Institution, London.
- Authur, J.R.F. and Menzies, B. K. (1972). Inherent anisotropy in a sand. *Geotechnique*, **22**, 115-128.
- Bagnold, R. A. (1941). *The physics of blown sand and desert dunes*. Methuen, London.
- Barnes, D.J. & Dusseault, M.B. (1982). The influence of diagenetic fabric on oilsands behaviour. *Canadian Journal of Earth sciences* **19**, 804-18.
- Barton, M.E. (1974). Soft Sandstones: geotechnical properties and sensitivity to moisture changes. *Proceedings 2nd International Congress of the International Association of Engineering Geology*, Sao Paulo, Brazil, **1(IV)**, 7.1-7.6.
- Barton, M. E. (1993). Cohesive sands: The natural transition from sands to sandstones. *Geotechnical engineering of hard soils-soft rocks*, Anagnostopoulos et. al. (eds). Balkema, Rotterdam.
- Barton, M. E. and Cresswell A. W. (1998). Slope stability in a sand/sandstone borderline material. *The geotechnics of hard soils-soft rocks*, Evangelista and Picarelli (eds). Balkema, Rotterdam.
- Barton, M.E., Mockett, L.D. & Palmer, S.N. (1993). An engineering geological classification of the soil/rock borderline materials between sands and sandstones. *In: Cripps, J.C., Coulthard, J.M., Culshaw, M.G., Forester, A., Hencher, S.R. & Moon, C.F. (eds.) The Engineering Geology of Weak Rock*. Engineering Geology Special Publication no. 8, 115-123. Balkema, Rotterdam.
- Barton, M.E. & Palmer, S.N. (1989). The relative density of geologically aged, British fine and fine-medium sands. *Quarterly Journal of Engineering Geology*, **22**, 49-58.
- Barton, M.E. & Palmer, S.N. (1990). The geotechnical investigation of geologically aged, uncemented sands by block sampling. *Proceedings of the 6th Congress of the International Association of Engineering Geology*, Amsterdam. 1, 281-8.

- Barton, M.E., Palmer, S.N. & Wong, Y.L. (1986). A geological investigation of two Hampshire Tertiary Sand Beds: are they locked sands? *Quarterly Journal Engineering Geology* **19**, 399-412.
- Barton, M. E. and Cresswell A. (1988). Slope stability in a sand / sandstone borderline material. *The Geotechnics of Hard Soils - Soft Rocks*, Evangelista and Picarelli (eds). Balkema, Rotterdam.
- Barton, N. and Choubey, V. (1977). Shear strength of rock joints in theory and practice. *Rock Mechanics*, **10**, 1-54.
- Blyth, F.G.H. and de Freitas, M.H. (1984). *A Geology for Engineers*, 7th edition. Edward Arnold, London.
- Bolton, M. D. (1986). The strength and dilatency of sands. *Geotechnique* **39**, No.1 65-78.
- Bolton, M. D. (1991). *A Guide to Soil Mechanics*, 2nd edition.. Macmillan.
- Bowden, F. P. and Tabor, D.(1967). *The friction and lubrication of solids*. Oxford University Press.
- Brady, B.H.G & Brown, E.T. (1993). *Rock Mechanics for Underground Mining*, 2nd edition. Chapman & Hall, London.
- Butterfield, R. and Andrawes, K. Z.(1970). An air activated sand spreader for forming uniform sand beds. *Geotechnique*, **20**, 92-100.
- Casey, R., (1961). The stratigraphical palaeontology of the lower Greensand. *Palaeontology*, **3**, 487-621.
- Clarkson, E. N. K. (1986). *Invertebrate Palaeontology and Evolution*. 2nd ed. Harper Collins.
- Clough, G. W., Sitar, N., Bachus, R. C. and Rad, N. S. (1981). Cemented sands under static loading. *Journal, Geotechnical Engineering Division (Proceedings, American Soc. Of Civil Engineers)* **107**, 799-817.
- Colback, P.S.B. & Wiid, B.L.(1965). The influence of moisture content on the compressive strength of rocks. *Proceedings of the Rock Mechanics Symposium, Toronto* 65-83.
- Coop, M. R. and Atkinson, J. H. (1993). The mechanics of cemented carbonate sands. *Geotechnique* **43**, No.1, 53-67
- Cresswell, A. and Barton, M. E. (1999) determining the Maximum Density of Sands by Pluviation. *Geotechnical Testing Journal, ASTM, december 1999*.

- Cuccovillo, T and Coop, M. R. (1997). The measurement of local axial strains in triaxial tests using LVDTs. *Geotechnique* **47**, No.1, 167-171
- Cuccovillo, T and Coop, M. R. (1997). Yielding and pre-failure deformation of structured sands. *Geotechnique* **47**, No.3, 491-508
- Cuccovillo, T and Coop, M. R. On the mechanics of structured sands - submitted 1999.
- de Freitas, M.H. (1993). Weak arenaceous materials. *In*: Cripps, J.C., Coulthard, J.M., Culshaw, M.G., Forester, A., Hencher, S.R. & Moon, C.F. (eds.) *The Engineering Geology of Weak Rock*. Engineering Geology Special Publication no. 8, 115-123. Balkema, Rotterdam.
- Deere, D. U. & Miller, R. P. (1966). Engineering classification and index properties of intact rock. *Technical Report No AFWL-TR-65-166*, Air Force Weapons Laboratory, Kirkland Air Base, New Mexico.
- Denekamp, S.A. and Tsur-Lavie, Y. (1981). The study of relative density in some dune and beach sands. *Engineering Geology*, **17**, 159-173.
- Denisov, N. Y. and Reltov, B. F. (1961). The influence of certain processes on the strength of soils. *Proceedings 5th International Conference on Soil Mechanics and Foundation Engineering*, vol 1, 75-78.
- Dobereiner, L. & de Freitas, M.H. (1986). Geotechnical properties of weak sandstones. *Geotechnique*, **36**, 79-94.
- Dusseault, M.B. & Morgenstern, N.R. (1979). Locked sands. *Quarterly Journal Engineering Geology* **12**, 117-131.
- Einstein, H. H., Nelson, R. A., Bruhn, R. W., Hirschfield, R. C. (1970). Model studies of jointed rock behaviour. *Proc. 11th Symp. Rock Mec.* AIME, New York.
- Elliott, G.M. (1993). Triaxial Testing for Rock Strength. *In*: Hudson, J.A. (ed.) *Comprehensive Rock Engineering; Principles, Practice & Projects*, **3**, 87-104.
- Enrenberg, S. N. (1989). Assessing the relative importance of compaction processes and cementation to reduction of porosity in sandstones: discussion: compaction and porosity evolution of Pliocene sandstones, Ventura Basin, California: discussion. *The American Association of Petroleum Geologists bulletin*, **73**, No. 10
- Goodman, R. E. (1989). *Introduction to Rock Mechanics*. Wiley.
- Hasizadeh, J. and Law, R. D. (1991). Water weakening of sandstone and quartzite deformed at various stress and strain rates. *Int. J. Rock Mec. Min. Sci. & Geo. Abs.*. Vol. **28** No. 5, 431-439.

Hawkins, A.B. & McConnell, B.J. (1992). Sensitivity of sandstone strength and deformability to changes in moisture content. *Quarterly Journal of Engineering Geology*, **25**, 115-130.

Head, K.H. (1980). *Manual of soil laboratory testing*. Pentech, London.

Hodgson, J. M. (ed.) (1976) *Soil Survey Field Handbook*, Technical Mongraph 5, Soil Survey of Great Britain, Harpenden.

Hoek, E. (1983). Strength of jointed rock masses. *Geotechnique*, **33**, 187-223.

Hoek, E. & Bray, J.W. (1981). *Rock Slope Engineering*, 3rd edition. Institution of Mining and Metallurgy, London.

Hoek, E. & Brown, E.T. (1982). *Underground Excavations in Rock*, revised 1st edition. Institution of Mining and Metallurgy, London.

Houseknecht, D.W. (1988). Intergranular pressure solution in four quartzose sandstones. *Jnl. Sed. Pet.*, **58**, 228-246.

Houseknecht, D.W. (1987). Assessing the relative importance of compaction processes and cementation to reduction of porosity in sandstones. *American Ass'n. of Petroleum Geologists Bulletin* **71**, 633-642.

Houseknecht, D.W. (1989). Assessing the relative importance of compaction processes and cementation to reduction of porosity in sandstones: Reply. *American Ass'n. of Petroleum Geologists Bulletin* **73**, 1277-1279.

International Society for Rock Mechanics. (1981). Suggested Methods for Determining the Uniaxial Compressive Strength and Deformability of Rock Materials. In: Brown, E.T. (ed.) *Rock Characterization Testing and Monitoring, ISRM Suggested Methods*. Part 2 Laboratory and Field Testing, 111-116. Pergamon Press, Oxford.

Jewell, R. A. and Wroth, C. P. (1987). Direct shear tests on reinforced sands. *Geotechnique*, **37**, 53-68.

Johnston, I.W. & Novello, E.A. (1994). Soil mechanics, rock mechanics and soft rock technology. *Proceedings of the Institution of Civil Engineers, Geotechnical Engineering*, **107**, 3-9.

Kolbuszewski, J. (1948). An experimental study of the maximum and minimum porosities of sands. *Proc. 2nd Int. Con. Soil Mech.* **1**, 158-165.

Ladanyi, B. and Archambault, G. (1970). Simulation of shear behaviour of a jointed rock mass. *Proceedings of the 11th symposium rock mechanics*. A.I.M.E. New York.

- Lee, K. L. (1977). Adhesion bonds in sands at high pressure. *J. Geotech. Eng. Div., Am. Soc. Civ. Engs.* **103**, GT8, 908-1013.
- Leroueil, S. & Vaughan, P.R. (1990). The general and congruent effects of structure in natural soils and weak rocks. *Geotechnique*, **40**, 467-488.
- Lundegard, P. D. (1992). Sandstone porosity loss - a "big picture" view of the importance of compaction. *J. of Sed. Pet.*, vol 62, 250-260.
- MacKenzie, W.S. & Guilford, C. (1980). *Atlas of rock-forming minerals in thin section*. Longman, UK.
- Mazzullo, M. & Magenheimer, S. (1987). The original shapes of quartz sand grains. *J. of Sed. Pet.*, vol **57**, 479-487.
- Mandl, G., de Jong, L. N. J. and Maltha, A. (1977). Shear Zones in granular material. *Rock Mechanics*, **9**, 95-144.
- Mcbride, E.F. (1989). Quartz cement in sandstones: a review. *Earth Science Reviews* (Elsevier) **26**, 69-112.
- Mesri, G.; Feng, T. W. & Benak, J.M. (1990). Post densification penetration resistance of clean sands. *Journal of Geotechnical Engineering*, **116**, 1095-1115.
- Mitchell, J.K. (1976). *Fundamentals of soil behaviour*. John Wiley & Sons. London
- Mitchell, J.K. & Solymar, Z. V. (1984). Time dependant strength gain in freshly deposited or densified sand. *Journal of Geotechnical Engineering*, (Proceedings, American Society of Civil Engineers) **110**, 1559-1575.
- Muhlhaus, H. B. and Vardoulakis, I. (1987). The thickness of shear bands in granular materials. *Geotechnique*, **37**, No. 3, 271-283.
- Nadai, A. (1931). *Plasticity*. McGraw-Hill, London.
- Newland, P. L. and Allely, B. H. (1957). Volume changes in drained triaxial tests on granular materials. *Geotechnique*, **7**, 17-34.
- Novello, E.A. & Johnston, I.W. (1995). Geotechnical materials and the critical state. *Geotechnique*, **45**, 223-235.
- Oda, & Kazama, H. (1998). *Geotechnique*, **48**, No. 4, 465-481.
- Ord, A., Vardoulakis, I., and Kajewski, R. (1991). Shear Band Formation in Gosford Sandstone. *Int. J. Rock Mech. Min. Sci. & Geomech. Abstr.*, **28**, No. 5, 397-409.

- Palmer, S. M. and Barton, M. E. (1986). Avoiding microfabric disruption during the impregnation of friable, uncemented sands with dyed epoxy. *Journal of sedimentary petrology*, Vol **56** No. 4, 556-557.
- Palmer, S. M. and Barton, M. E. (1987). Porosity reduction, microfabric and lithification in U. K. uncemented sands. In: Marshall, J. D. (ed) *Diagenesis of sedimentary sequences*. Geological Society Special Publication No. **36**, 29-40.
- Pate, C. R. (1989). Assessing the relative importance of compaction processes and cementation to reduction of porosity in sandstones: discussion. *The American Association of Petroleum Geologists bulletin*, **73**, No. 10.
- Patton, F.D. (1966). Multiple modes of shear failure in rock. *Proceedings of the 1st International Congress on Rock Mechanics, Lisbon*, **1**, 509-513.
- Pells, P.J.N. (1993). Uniaxial Strength Testing. In: Hudson, J.A. (ed.) *Comprehensive Rock Engineering; Principles, Practice & Projects*, **3**, 67- 85.
- Pells, P.J.N. & Ferry, M.J. (1983). Needless stringency in sample preparation standards for laboratory testing of weak rocks. *Proceedings of the 5th International Congress on Rock Mechanics, Melbourne*, **A**, 203-207.
- Powrie, W. (1997). *Soil mechanics; concepts and applications*. Chapman and Hall.
- Pryor, W. A. (1973). Permeability-Porosity patterns and variations in some Holocene Sand Bodies. *The American Association of Petroleum Geologists bulletin*, **57**.
- Raynor, D. H. (1981). *The Stratigraphy of the British Isles*. Cambridge.
- Richards, N. P. (1992). *The engineering geology of the Lower Greensand of South-East England with particular reference to the microfabric, geotechnical index properties and shear strength characteristics*. PhD thesis , University of Southampton.
- Richards, N. P. and Barton, M. E. (1999). The Folkestone Bed Sands: microfabric and strength. *Quarterly Journal of Engineering Geology*, **32**.
- Roscoe, K. H. (1970). The influence of strains in soil mechanics. *Geotechnique*, **20**, No. 2, 129-170.
- Roscoe, K. H., Schofield, A. N. and Wroth, C. P. (1958). On the yielding of soils. *Geotechnique*, **8**, No. 1, 22-52.
- Rowe, P. W. (1962). The stress-dilatency relation for static equilibrium of an assembly of particles in contact. *Proc. Roy. Soc. A* **269**, 500-527.

- Schmertmann, F.H. (1991). The mechanical ageing of soils. *Journal of Geotechnical Engineering A.S.C.E.* **117**, 1285-1330.
- Schneider, H.J. (1978). The laboratory direct shear test - an analysis and geotechnical evaluation. *Bulletin of the International Association of Engineering Geology*, **18**, 121-126.
- Schofield, A. N. (1988). Mohr Coulomb error correction. *Ground engineering. August 1988*
- Sitar, N. (1983). Slope stability in coarse sediments. In Yong, R.N. (ed) *Geological Environment and Soil Properties. A.S.C.E. Special Publication 7*, 82-98.
- Stephenson, L. P., Plumley, W.J. and Palciauskas, V.V. (1992). A model for sandstone compaction by grain interpenetration. *Journal of Sedimentary Petrology* **62**, 11-22.
- Taylor, J.M. (1959). Pore-space reduction in sandstones. *Bulletin American Ass'n Petroleum Geologists* **34**, 701-716.
- Terzaghi, K. & Peck, R.B. (1948). *Soil Mechanics in Engineering Practice*. 1st Edition, John Wiley & Sons, New York.
- Tucker, M. (1991). *Sedimentary Petrology*, 2nd edition. Blackwell Scientific Publications, Oxford.
- Vesic, A. S., and Clough, G. W. (1968). Behaviour of granular materials under high stress. *Proc. Am. Soc. Civil Eng.*, **94** SM3, 661-686
- Walker, B, P. and T. Whitaker, (1967). An apparatus for forming uniform beds of sand for model foundation tests. *Geotechnique*, **17**, 161-167.
- Walter, J. E., Hight, W. H., and Vallee, R. P. (1982). Determining maximum void ratio of uniform cohesionless soils. *Transportation Research Record*, **879**, 42-51.
- West, G. (1994). The effect of suction on the strength of rock. *Quarterly Journal of Engineering Geology*, **27**, 51-56.
- Whitten, D.G.A. & Brooks, J.R.V. 1972. *The Penguin Dictionary of Geology*. Penguin Books
- Williams L. A. Parks, G. A. and Crerar, D. A. (1985). Silica diagenesis, 1. Solubility controls. *Journal of Sedimentary Petrology*, **55**, No 3, 301-311.
- Williams L. A. and Crerar, D. A. (1985). Silica diagenesis, 2. General mechanisms. *Journal of Sedimentary Petrology*, **55**, No 3, 313-321.